

PERFORMANCE OF ZINC-RICH EPOXY PRIMERS CONTAINING CARBON
NANOTUBES ON THE CORROSION PROTECTION OF CARBON STEEL IN
SIMULATED CONCRETE PORE ENVIRONMENTS

A Thesis

by

YENNY PAOLA CUBIDES GONZALEZ

Submitted to the Office of Graduate and Professional Studies of
Texas A&M University
in partial fulfillment of the requirements for the degree of

MASTER OF SCIENCE

Chair of Committee,	Homero Castaneda
Committee Members,	Patrick Shamberger
	Jodie Lutkenhaus
Head of Department,	Ibrahim Karaman

August 2016

Major Subject: Materials Science and Engineering

Copyright 2016 Yenny Paola Cubides Gonzalez

ABSTRACT

The performance of zinc-rich epoxy primers containing carbon nanotubes (CNT-ZRPs) on the corrosion protection of carbon steel in simulated concrete pore solutions contaminated with chloride ions was investigated. The research project was divided in two main sections; in the first part of this project, the author studied the influence of zinc content on the corrosion protection mechanism of carbon nanotubes/zinc rich epoxy primers on carbon steel under exposure to a simulated concrete pore solution. Based on the zinc content, three mechanisms of corrosion protection were identified. The CNT-ZRP with 60 wt.% Zn exhibited good barrier protection during the entire immersion period as a result of the highly cross-linked character of the epoxy binder. In contrast, the CNT-ZRP with 70 wt.% Zn afforded short-term sacrificial protection to the metallic substrate followed by intermediate barrier protection. Furthermore, it was found that the presence of CNTs in the coating system with 70 wt.% Zn, enhanced the electrical contact between the zinc particles and the carbon steel surface, allowing to provide sacrificial protection to the steel substrate. In addition, CNTs increased the barrier properties of the coating, suggesting that CNTs blocked micropores and defects in the material, hindering the diffusion of electrolyte throughout the coating. Finally, an extended galvanic protection was provided for the CNT-ZRP with 80 wt.% Zn. Insoluble zinc corrosion products were found inside the material and at the coating surface, as a result of the galvanic protection process and a self-corrosion process of the zinc

particles. These mechanisms of corrosion protection were characterized quantitatively by electrochemical techniques such as open circuit potential (OCP), electrochemical impedance spectroscopy (EIS), and localized electrochemical impedance spectroscopy (LEIS) and high-resolution techniques such as scanning electron microscopy (SEM) coupled with energy dispersive X-ray spectroscopy (EDS) and X-ray photoelectron spectroscopy (XPS).

In the second part of the research project, the influence of chloride concentration in the simulated concrete pore solution on the corrosion performance of these coating systems was investigated. The corrosion protection mechanisms for the different coating systems were similar to the ones described above, however, the effect of different chloride concentrations in the simulated concrete pore solution was noticeable; it was found that concrete pore environments with low chloride concentration allowed passivation of the carbon steel surface and formation of solid zinc corrosion products. In contrast, simulated concrete pore solutions with high chloride concentration led to breakdown of the passive layer, blister formation, and dissolution of zinc corrosion products previously formed during the sacrificial protection process.

DEDICATION

I dedicate this thesis to my family and my boyfriend. I love you all.

ACKNOWLEDGEMENTS

I would like to thank my committee chair, Dr. Castaneda, and my committee members, Dr. Shamberger, and Dr. Lutkenhaus, for their guidance and support throughout the course of this research.

A special acknowledgement also goes to my research groups at the University of Akron and at Texas A&M University for their valuable remarks and constructive discussions that allowed me to understand in detail the fundamental insights of this research project. I want to extend my gratitude to the CERL- U.S. Department of Defense Office of Corrosion Policy and Oversight for their financial support, and Tesla Nanocoatings Inc. for their special contribution in the coating preparation.

I also want to express my deepest gratitude to my boyfriend for his continuous support and encouragement since the time I decided to go to the graduate school. Thanks for your patience, for your immense knowledge that you have always shared with me, and for all the confidence that you continuously put on me even in the moments that I didn't have faith in myself. This accomplishment would not have been possible without you.

Finally, thanks to my mother, father, brother, and my best friend, Nina Marcela Perez, for their love, encouragement, and unconditional support to accomplish all my professional achievements. I feel fortunate and blessed to have such an amazing family.

NOMENCLATURE

ZRP	Zinc-rich epoxy primer
CNT-ZRP	Carbon nanotube/Zinc-rich epoxy primer
CNTs	Carbon nanotubes
PVC	Pigment volume concentration
CPVC	Critical pigment volume concentration
SCP	Simulated concrete pore solution
$[\text{Cl}^-]/[\text{OH}^-]$	Chloride-to-hydroxide ratio
SCE	Saturated calomel electrode
OCP	Open circuit potential
EIS	Electrochemical impedance spectroscopy
LEIS	Localized electrochemical impedance spectroscopy
SEM	Scanning electron microscopy
EDS	Energy dispersive X-ray spectroscopy
XPS	X-ray photoelectron spectroscopy
CPE	Constant phase element
Y_0	Admittance
R_c	Coating resistance
$C_{c,\text{eff}}$	Effective capacitance of the coating
R_{ct}	Charge transfer resistance

C_{dl}	Capacitance of the double layer
W_s	Warburg impedance
L	Inductance
R_L	Resistance of the adsorption process
C_{ox}	Capacitance of the layer of zinc corrosion products
R_{ox}	Resistance of the layer of zinc corrosion products

TABLE OF CONTENTS

	Page
ABSTRACT	ii
DEDICATION	iv
ACKNOWLEDGEMENTS	v
NOMENCLATURE.....	vi
TABLE OF CONTENTS	viii
LIST OF FIGURES.....	xi
LIST OF TABLES	xvi
CHAPTER I INTRODUCTION AND LITERATURE REVIEW	1
Corrosion mechanism of reinforcing steel in concrete.....	f
Initiation of corrosion	5
Propagation of corrosion	6
Consequences of the corrosion process.....	7
Chloride-induced corrosion in reinforced concrete.....	7
Chloride threshold value	7
Pitting corrosion	8
Electrochemical aspects in reinforced concrete	10
Anodic polarization curve	10
Electrochemical impedance spectroscopy to study the electrochemical behavior of reinforcing steel in simulated concrete pore solutions.....	13
Zinc-rich epoxy primers	15
Mechanism of corrosion protection of zinc-rich epoxy primers	15
Conductive particles to improve the performance of zinc-rich epoxy primers	18
Electrochemical impedance spectroscopy (EIS)	19
Fundamentals of EIS	19
EIS interpretation	23
Application of EIS to organic coatings	26
CHAPTER II EXPERIMENTAL DESIGN.....	32

Experimental procedure to study the influence of zinc content on the corrosion protection mechanism of carbon nanotubes/zinc rich epoxy primers on carbon steel under exposure to a simulated concrete pore solution	33
Electrolyte solution.....	33
Coating samples	34
Electrochemical measurements	35
Local electrochemical impedance spectroscopy (LEIS)	36
Morphology characterization	37
X-ray photoelectron spectroscopy (XPS).....	37
Experimental procedure to study the influence of chloride concentration on the corrosion performance of carbon nanotubes/zinc rich epoxy primers on carbon steel under exposure to simulated concrete pore environments	38
Electrolyte solution.....	38
Coating samples	39
Electrochemical measurements	39
Fog chamber measurements	39
Morphology studies.....	40

CHAPTER III INFLUENCE OF ZINC CONTENT ON THE CORROSION PROTECTION MECHANISM OF CARBON NANOTUBES/ZINC RICH EPOXY PRIMERS ON CARBON STEEL UNDER EXPOSURE TO A SIMULATED CONCRETE PORE SOLUTION.....41

Open circuit potential (OCP)	41
Electrochemical impedance spectroscopy (EIS).....	44
CNT-60ZRP	44
CNT-70ZRP	46
CNT-80ZRP	48
CNT-90ZRP	51
Equivalent electrical circuits	53
Local electrochemical impedance spectroscopy (LEIS)	67
Morphology characterization	69
X-ray photoelectron spectroscopy (XPS).....	75

CHAPTER IV INFLUENCE OF CHLORIDE CONCENTRATION ON THE CORROSION PERFORMANCE OF CARBON NANOTUBES/ZINC RICH EPOXY PRIMERS ON CARBON STEEL UNDER EXPOSURE TO SIMULATED CONCRETE PORE ENVIRONMENTS84

Open circuit potential (OCP)	84
CNT-60ZRP	84
CNT-70ZRP	86
CNT-80ZRP	88
Electrochemical impedance spectroscopy (EIS).....	91

CNT-60ZRP	91
CNT-70ZRP	93
CNT-80ZRP	98
Equivalent electrical circuits	102
CNT-60ZRP	102
CNT-70ZRP	104
CNT-80ZRP	108
Salt spray fog chamber	112
Morphology studies	114
 CHAPTER V CONCLUSIONS	 123
 REFERENCES	 126
 APPENDIX A SUPPLEMENTAL MATERIAL FOR CHAPTER III	 141
Electrochemical behavior of CNT-90ZRP	141

LIST OF FIGURES

	Page
Figure 1. Corrosion degradation process of reinforced concrete. Adapted from Tuutti's corrosion model [33].	5
Figure 2. Schematic representation of the pitting corrosion process of reinforcing steel in concrete. Adapted from [30].	10
Figure 3. Potentiodynamic polarization curve of carbon steel immersed in simulated concrete pore solutions.	12
Figure 4. EIS results of carbon steel samples after exposure for 24 hours to simulated concrete pore solutions: a) Nyquist representation, and b) Bode representation.	14
Figure 5. Corrosion protection mechanism of zinc-rich epoxy coatings.	16
Figure 6. Sinusoidal potential and current signals. Adapted from [58].	21
Figure 7. Impedance complex plane. Adapted from [64].	22
Figure 8. EIS representations: a) Nyquist plot, and b) Bode plot. Adapted from [64].	23
Figure 9. Arrangement of electrical elements: a) in series; and b) in parallel. Adapted from [64].	26
Figure 10. Example of EIS spectra for a polymer-coated steel sample exposed to an aggressive medium for 200 days: a) Nyquist plot, and b) Bode plot.	27
Figure 11. Equivalent electrical circuits to describe the stages in the degradation mechanism of polymer-coated steel substrates under exposure to corrosive media: a) diffusion of electrolyte throughout the coating, b) charge transfer process, and c) diffusion-controlled process.	29
Figure 12. OCP evolution for CNT-ZRPs with different zinc contents immersed in a simulated concrete pore solution with a $[\text{Cl}^-]/[\text{OH}^-]$ ratio of 1 during 150 days.	42

Figure 13. Electrochemical impedance spectra of CNT-60ZRP immersed in a simulated concrete pore solution with a $[Cl^-]/[OH^-]$ ratio of 1 during 150 days: a) Nyquist diagram and b) Bode diagram.	45
Figure 14. Electrochemical impedance spectra of CNT-70ZRP immersed in a simulated concrete pore solution with a $[Cl^-]/[OH^-]$ ratio of 1 during 150 days: a) Nyquist diagram, and b) Bode diagram.	48
Figure 15. Electrochemical impedance spectra of CNT-80ZRP immersed in a simulated concrete pore solution with a $[Cl^-]/[OH^-]$ ratio of 1 during 150 days: a) Nyquist diagram, b) modulus of impedance, and c) phase angle.....	49
Figure 16. Electrochemical impedance spectra of CNT-90ZRP immersed in a simulated concrete pore solution with a $[Cl^-]/[OH^-]$ ratio of 1 during 150 days: a) Nyquist diagram, b) modulus of impedance, and c) phase angle.....	53
Figure 17. Equivalent electrical circuit describing the impedance spectra of CNT-60ZRP immersed in a simulated concrete pore solution with a $[Cl^-]/[OH^-]$ ratio of 1 for 150 days.....	54
Figure 18. Equivalent circuit elements for CNT-60ZRP immersed in a simulated concrete pore solution with a $[Cl^-]/[OH^-]$ ratio of 1 for 150 days: a) coating resistance, and b) coating capacitance.	55
Figure 19. Equivalent electrical circuits describing the impedance spectra of CNT-70ZRP immersed in simulated concrete pore solution with a $[Cl^-]/[OH^-]$ ratio of 1 for 150 days.....	57
Figure 20. Equivalent circuit elements for CNT-70ZRP immersed in a simulated concrete pore solution with a $[Cl^-]/[OH^-]$ ratio of 1 for 150 days: a) coating resistance, b) coating capacitance, c) charge transfer resistance, and d) double layer capacitance.....	59
Figure 21. Equivalent electrical circuits describing the impedance spectra of CNT-80ZRP and CNT-90ZRP immersed in a simulated concrete pore solution with a $[Cl^-]/[OH^-]$ ratio of 1 for 150 days.	62
Figure 22. Equivalent circuit elements for CNT-80ZRP and CNT-90ZRP immersed in a simulated concrete pore solution with a $[Cl^-]/[OH^-]$ ratio of 1 for 150 days: a) CNT-80ZRP, and b) CNT-90ZRP	64
Figure 23. Evolution of coating resistance (R_c) for the different CNT-ZRP systems immersed in a simulated concrete pore solution with a $[Cl^-]/[OH^-]$ ratio of 1 for 150 days.	66

Figure 24. Local electrochemical impedance spectroscopy (LEIS) results for a scratched CNT-90ZRP sample immersed in 0.005M NaCl during 48 hours. a) LEIS spectra at 5h, 10h, and 35h after immersion b) 3D microscope images of the sample before and after exposure.....	68
Figure 25. Cross-section and coating surface images for CNT-60ZRP exposed to the simulated concrete pore solution: a) cross-section of the intact coating, b) cross-section of the coating exposed for 90 days, and c) surface-view of the coating exposed for 90 days.	69
Figure 26. Cross-section and coating surface images for CNT-70ZRP exposed to the simulated concrete pore solution at different immersion times: a) cross-section of intact coating, b) cross-section after 5 days of immersion, c) cross-section after 90 days of immersion, d) surface-view after 90 days of immersion, e) surface-view of CNT-free 70ZRP after 90 days of immersion, and f) cross-section of CNT-free 70ZRP after 90 days of immersion.....	72
Figure 27. Cross-section and coating surface images for CNT-80ZRP exposed to the simulated concrete pore solution at different immersion times: a) cross-section of intact coating, b) cross-section after 20 days of immersion, c) cross-section after 90 days of immersion, and d) surface-view after 90 days of immersion.....	74
Figure 28. Cross-section and coating surface images for CNT-90ZRP exposed to the simulated concrete pore solution at different immersion times: a) cross-section of intact coating, b) cross-section after 20 days of immersion, c) cross-section after 90 days of immersion, and d) surface-view after 90 days of immersion.....	75
Figure 29. XPS spectra for CNT-60ZRP before and after exposure to SCP during 90 days: a) survey spectrum, b) C 1s high-resolution spectrum before immersion, and c) C 1s high-resolution spectrum after immersion.....	78
Figure 30. XPS spectra for CNT-70ZRP after exposure to the simulated concrete pore solution during 90 days: a) survey spectrum, b) speciation diagram of Zn, c) C 1s high resolution spectrum, d) C 1s high resolution spectrum, and e) Zn 2p _{3/2} high resolution spectrum.	81
Figure 31. XPS spectra for CNT-80ZRP after exposure to simulated concrete solution during 90 days: a) survey spectrum, and b) Zn 2p _{3/2} high-resolution spectrum.....	82
Figure 32. Chemical compositions for the different CNT-ZRP formulations based on high-resolution spectra for a) O 1s, and b) Zn 2p _{3/2}	83

Figure 33. OCP measurements of CNT-60ZRP immersed in simulated concrete pore solutions with different chloride-to-hydroxide ratios for 150 days.	86
Figure 34. OCP measurements of CNT-70ZRP immersed in simulated concrete pore solutions with different chloride-to-hydroxide ratios for 150 days.	88
Figure 35. OCP measurements of CNT-80ZRP immersed in simulated concrete pore solution at different chloride-to-hydroxide ratios for 150 days.	90
Figure 36. Impedance spectra of CNT-60ZRP immersed in simulated concrete pore solutions with different chloride-to-hydroxide ratios for 150 days: a) blank solution, b) 0.1 [Cl ⁻]/[OH ⁻], and c) 10 [Cl ⁻]/[OH ⁻].	92
Figure 37. Impedance spectra of CNT-70ZRP immersed in simulated concrete pore solutions with different chloride-to-hydroxide ratios for 150 days: a) blank solution b) 0.1 [Cl ⁻]/[OH ⁻], and c) 10 [Cl ⁻]/[OH ⁻].	94
Figure 38. Impedance spectra of CNT-80ZRP immersed in simulated concrete pore solutions with different chloride-to-hydroxide ratios for 150 days: a) blank solution b) 0.1 [Cl ⁻]/[OH ⁻], and c) 10 [Cl ⁻]/[OH ⁻].	99
Figure 39. Equivalent circuit elements for CNT-60ZRP immersed in simulated concrete pore solutions with different chloride-to-hydroxide ratios for 150 days: a) coating resistance, and b) coating capacitance.	104
Figure 40. Equivalent circuit elements for CNT-70ZRP immersed in simulated concrete pore solutions with different chloride-to-hydroxide ratios for 150 days: a) coating resistance, b) coating capacitance, c) charge transfer resistance, and d) double layer capacitance.	106
Figure 41. Equivalent circuit elements for CNT-80ZRP immersed in simulated concrete pore solutions with different chloride-to-hydroxide ratios for 150 days: a) coating resistance b) coating capacitance, c) charge transfer resistance, and d) resistance of the oxide layer.	110
Figure 42. Photographs of CNT-ZRP samples (intact and scribed surface) after different exposure times to salt spray fog chamber.	114
Figure 43. Visual appearances of the surface of CNT-ZRPs after exposure for 150 days to simulated concrete pore solutions with different chloride-to-hydroxide ratios.	116
Figure 44. SEM micrographs of CNT-60ZRP after immersion for 150 days in the blank solution.	117

Figure 45. SEM micrographs of CNT-70ZRP after immersion for 150 days in a) blank solution, and b) simulated concrete pore solution with a chloride-hydroxide ratio of 10.	118
Figure 46. SEM micrographs of CNT-80ZRP after immersion for 150 days in a) blank solution, and b) simulated concrete pore solution with a chloride-hydroxide ratio of 10.	120
Figure 47. Cross-section analyses of CNT-80ZRP after immersion for 150 days in simulated concrete pore solution with a chloride-to-hydroxide ratio of 10: a) cross-section SEM micrograph b) line scan analyses.....	121
Figure 48. OCP measurements of CNT-90ZRP immersed in simulated concrete pore solution with different chloride-to-hydroxide ratios for 150 days.....	141
Figure 49. Impedance spectra of CNT-90ZRP immersed in simulated concrete pore solutions with different chloride-to-hydroxide ratios for 150 days: a) blank solution b) 0.1 [Cl ⁻]/[OH ⁻], and c) 10 [Cl ⁻]/[OH ⁻].....	141

LIST OF TABLES

	Page
Table 1. Electrical elements and their corresponding impedance functions [64].	23
Table 2. Chemical composition of simulated concrete pore solution with a chloride-to-hydroxide ratio of 1.	34
Table 3. Specifications of the different coating systems.	35
Table 4. Chemical composition of simulated concrete pore solutions with different [Cl ⁻]/[OH ⁻] ratios.	39
Table 5. EDS results (atomic percent) at indicated locations in the SEM images for the different CNT-ZRP systems immersed in the simulated concrete pore solution.	70
Table 6. Chemical compositions for the different CNT-ZRPs based on high-resolution spectra for C 1s, O 1s, and Zn 2p _{3/2}	76

CHAPTER I

INTRODUCTION AND LITERATURE REVIEW*

Reinforced concrete structures exhibit high corrosion resistance due to their highly alkaline conditions (pH 12.5–13). Carbon steel can be used for rebar since it forms a passive oxide layer consisting of iron oxide ($\gamma\text{-Fe}_2\text{O}_3$) and magnetite (Fe_3O_4), which prevents and controls the corrosion-induced deterioration [1-4]. Economic advantages are also an important characteristic of ferrous alloys since they represent cost-effective solutions. Nevertheless, carbon steels are susceptible to halides in electrolyte solutions such as chloride ions, the presence of these species can influence the breakdown of the passive layer and the appearance of localized attack [4-7]. After corrosion or activation processes, the damage to concrete structures can be more severe when corrosion products induce high mechanical stresses that cause the formation of cracks in the concrete surface that may lead to the collapse of the structure [8, 9].

Several coating systems have been studied to control or mitigate rebar deterioration due to corrosion processes, including inorganic, organic, and hybrid protective coatings [10-14]. Zinc-rich epoxy primers (ZRPs) have been applied since the 1930s due to their anti-corrosion properties [15]. These composite materials exhibit two

* Part of this chapter is reprinted from Corrosion Science, vol. 109, Y Cubides, H. Castaneda, Corrosion protection mechanisms of carbon nanotube and zinc-rich epoxy primers on carbon steel in simulated concrete pore solutions in the presence of chloride ions, 145-161, Copyright (2016), with permission from Elsevier.

protection mechanisms when an electrolyte penetrates into the organic binder. First, ZRPs provide cathodic protection by acting as sacrificial anodes when they are in electronic contact with the carbon steel surface [17]. Once cathodic protection is no longer active, ZRPs start to provide barrier protection due to the characteristic nature of the epoxy binder and the formation of zinc corrosion products on both the carbon steel surface and within the binder. These corrosion products fill in pores and reduce the amount of electrolyte that reaches the steel surface [18].

Nevertheless, it has been reported that high zinc content (> 90 wt% Zn) is not sufficient to ensure cathodic protection for a long time, especially for zinc particles with spherical geometry where there is only a single contact between two adjacent particles [16]. In such conditions, self-corrosion of zinc particles due to the presence of oxygen and water will lead to rapid loss of the electrical connection among themselves and with the carbon steel surface [16]. In addition, a high amount of zinc particles can reduce the adhesion to the metal substrate and create difficulties in spraying due to high viscosity and poor dispersion [17]. Therefore, studies have been performed to develop ZRPs with high electrical conductivity but with lower amounts of zinc particles [18-20].

An attractive option for improving ZRP performance is associated with the presence of carbon nanotubes (CNTs) integrated within the binder. CNTs provide excellent mechanical and electrical properties, large surface area, high thermal stability, and chemical inertness [20-22]. CNTs can interconnect the zinc particles and provide higher electrical conductivity allowing that the percolation threshold can be reached with a lower zinc concentration compared with the traditional zinc-rich epoxy primer

(90 wt% Zn content) [20]. Different works have shown effective improvement in the corrosion protection of composite coatings using CNTs by distributing the electrical current to prevent localized attack in the metal surface. In addition, CNTs can provide barrier protection to composite coatings as pore fillers within the epoxy coating [23-25]. Although research has shown positive results to the addition of CNTs, some counter effects in the coating performance have been also reported due to the formation of microgalvanic cells between CNTs and metal compounds resulting in the acceleration of the oxygen reduction reaction [26]; this counter effect makes relevant investigating the effect of CNTs on the zinc rich primers.

The purpose of this work is to investigate the electrochemical behavior of CNT-ZRPs on carbon steel in simulated concrete pore solutions in the presence of chloride ions. The zinc content in the carbon nanotube/zinc-rich epoxy primers and the chloride concentration in the simulated concrete pore solution were the primary variables used for this study. The mechanisms of corrosion protection of the CNT-ZRPs with different zinc contents and their corrosion performance in simulated concrete pore environments with different chloride concentrations were investigated using electrochemical techniques such as open circuit potential (OCP), electrochemical impedance spectroscopy (EIS), and localized electrochemical impedance spectroscopy (LEIS). Based on the electrochemical behavior, coating degradation mechanisms were proposed considering the barrier properties of the epoxy binder, the sacrificial protection of the zinc particles, and the presence of carbon nanotubes. Finally, in order to support the electrochemical findings, scanning electron microscopy (SEM) coupled with energy dispersive X-ray

spectroscopy (EDS) and X-ray photoelectron spectroscopy (XPS) were performed to evaluate the morphology of the coating systems and electrochemical transformations after the exposure tests.

Corrosion mechanism of reinforcing steel in concrete

Reinforcing steel embedded in concrete is passivated as a result of the high alkaline environment of concrete pore solutions (pH values between 12.5 and 13). The oxide/hydroxide protective passive film isolates the reinforcing steel from the environment and prevents further dissolution of the metal substrate as long as it remains intact. It has been reported that this protective passive film consists of an inner layer of magnetite (Fe_3O_4) and an outer layer of ferric oxides such as maghemite ($\gamma\text{-Fe}_2\text{O}_3$) and hematite ($\alpha\text{-Fe}_2\text{O}_3$), which is formed by thermodynamic instability of magnetite in the presence of oxygen [27, 28]. Additional exposure of the inner layer to oxygen and moisture leads to the growth of the ferric oxide layer and the formation of oxyhydroxides including goethite ($\alpha\text{-FeOOH}$), akagoneite ($\beta\text{-FeOOH}$) and lepidocrocite ($\gamma\text{-FeOOH}$) [29-31].

The lifetime of reinforced concrete structures can be compromised by the initiation and propagation of corrosion processes on the reinforcing steel; it is well-known that carbonation and the presence of chloride ions represent the most common factors to initiate corrosion degradation processes [9, 32]. Based on the Tuutti's corrosion model [33], the corrosion-induced deterioration of reinforced concrete can be described in two primary stages: depassivation or initiation time, and propagation time. Figure 1 shows a schematic representation of these stages; the initiation time (T_i)

corresponds to the period from construction of the concrete structure to initiation of corrosion processes at the reinforcing steel. The propagation stage starts with the breakdown of the passive layer as a result of the accumulation of chloride ions on the steel substrate. This stage is subdivided in two periods; the time to cracking (T_c) and the time for development of spalls (T_s) at which the maintenance-free service life (T_{mf}) is reached.

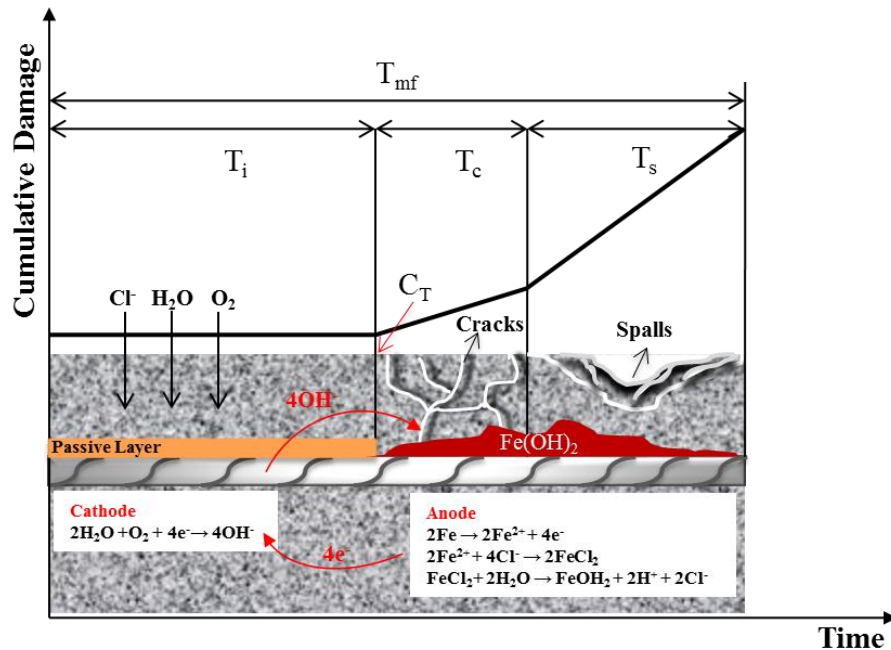


Figure 1. Corrosion degradation process of reinforced concrete. Adapted from Tuutti's corrosion model [33].

Initiation of corrosion

The corrosion initiation starts with the diffusion of aggressive species (chlorides, CO_2 , O_2 , etc.) through the concrete structure. In corrosion of reinforcing steel driven by

chloride ions, once their concentration reaches a critical value at the steel surface, a local breakdown of the passive layer occurs and an electrochemical cell is formed; anodic and cathodic sites are created at the reinforcing steel surface and they electrically interconnect through the steel itself. Concrete pores serve as reservoirs for the electrolytic medium in which chloride ions can be accumulated allowing their direct contact with the metal surface. It has been reported that the extent of the initiation time is highly influenced by the concrete quality, depth of the concrete cover, exposure conditions, the diffusion rate of the aggressive species, and the critical chloride concentration required for the depassivation of the reinforcing steel [30, 34].

Propagation of corrosion

The propagation stage starts with the initiation of corrosion in the reinforcing steel surface as a result of the breakdown of the passive layer and accumulation of aggressive species such as water, oxygen, and chloride ions. The corrosion rate during the propagation stage depends on moisture content, oxygen concentration, temperature, and pH on the concrete pores [34]. As a consequence of this corrosion process, voluminous iron corrosion products start to develop at the reinforcing steel surface, reaching volumes of 2 to 6 times greater than the original species (depending of the chemical composition and hydration degree) which creates tensile stresses inside the concrete structure that eventually results in structural damages such as cracking, spalling or entire delamination of the concrete surface [9, 30, 35].

Consequences of the corrosion process

The loss of concrete due to cracking and spalling of the concrete cover may carry significant consequences in the lifetime of the concrete structure [30]: 1) the load bearing capacity of the concrete structure can be significantly reduced due to the less amount of concrete supporting the structure, 2) the presence of cracks create more diffusional pathways for the penetration of aggressive species leading to an accelerated corrosion process, and 3) the corrosion process induced by chloride ions (pitting corrosion) weakens the reinforcing steel due to reduction of its cross sectional area that results in detrimental of its mechanical properties such as load carrying capacity and fatigue strength.

Chloride-induced corrosion in reinforced concrete

Chloride threshold value

Corrosion of reinforcing steel induced by chloride ions corresponds to one of the most common and severe mechanisms of degradation observed in reinforced concrete structures [30, 36]. Initiation of chloride-induced corrosion starts only when a critical chloride concentration or chloride threshold value (C_T) has been reached on the steel surface. This chloride threshold value has been scientifically defined as the minimum chloride content that is needed for the depassivation of the reinforcing steel. From an engineering perspective, this value has been associated with the chloride content to recognize visible damage of the concrete structure [36]. Numerous studies have been performed to find this value and to establish the parameters that can influence this result

[36-40]. Angst et al. [36] provided an excellent compilation with the influencing parameters that affect the value of C_T :

- Steel/concrete interface
- Concentration of hydroxyl ions in the concrete pore solution (pH)
- Electrochemical potential of the steel
- Cement type
- Surface condition of the steel
- Moisture content
- Oxygen availability at the steel surface
- Electrical resistivity of the concrete
- Degree of hydration
- Chemical composition of the steel
- Temperature
- Chloride nature

They also highlighted that the most predominant factors that influence the value of C_T corresponds to the condition of the steel/concrete interface, the pH of the concrete pore, and the electrochemical potential of the reinforcing steel.

Pitting corrosion

The mechanism of corrosion of reinforcing steel induced by chloride ions corresponds to a localized attack called pitting corrosion. Figure 2 shows a schematic representation of this process; the active zones (pits) corresponds to the areas where breakdown of the passive layer occurred and iron dissolution reaction takes place:



The surrounding areas that are still protected by the passive layer provided the cathodic sites for the oxygen reduction reaction:



The ferrous ions (Fe^{2+}) and the hydroxyl ions (OH^{-}) react to form ferrous hydroxide, which subsequently reacts with oxygen and water to produce ferric hydroxide [41, 42]:

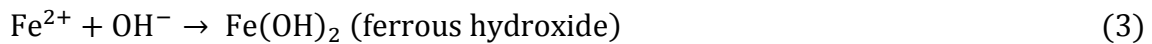


Figure 2 also shows that once the pitting corrosion process starts, an aggressive environment is developed inside the pit as a result of the following reactions [41]:



From equation (6), it can be seen that iron chloride is dissolved and acidity inside the pit increases due to the hydrolysis reaction of iron chloride (FeCl_2), which can induce the migration of more chloride ions (negatively charged ions) towards the pit. As a result of these reactions, an accelerated corrosion process known as the autocatalytic mechanism of pitting corrosion is established; this mechanism can be very serious since high corrosion rates, as high as 1 mm/year, can be developed [30]. As it was mentioned in the consequences of corrosion in reinforcing steel, pitting corrosion can dramatically reduce the cross-sectional area of the steel, compromising its mechanical properties.

Additionally, this corrosion process is difficult to detect by visual inspection since there is not manifestation on the concrete surface such as cracking or spalling.

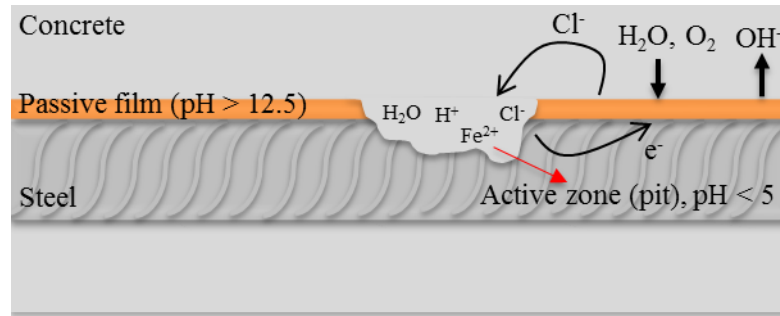


Figure 2. Schematic representation of the pitting corrosion process of reinforcing steel in concrete. Adapted from [30].

Electrochemical aspects in reinforced concrete

Anodic polarization curve

The electrochemical behavior of reinforcing steel in concrete can be described by potentiodynamic polarization curves that correlate the electrochemical potential with the current density. This is a destructive technique and therefore, it cannot be performed in real concrete structures. Additionally, it is more difficult to perform these polarization curves in steel embedded in concrete than in liquid electrolytes due to the large ohmic drop in the concrete, thus simulated concrete pore (SCP) solutions are usually used to conduct these measurements. Figure 3 shows a potentiodynamic polarization curve for a carbon steel sample exposed to a simulated concrete pore solution (0.08M KOH, 0.02M NaOH, and 0.001M Ca(OH)₂, pH =12.98). Figure 3 shows a well-defined passive region (i.e., anodic current density does not significantly change with potential) in the potential range between -0.2 V vs. SCE and 0.6 V vs. SCE with a low anodic current density of less than 10^{-6} A/cm² (1 μ A/cm²). This behavior is characteristic of reinforcing steels that are covered with a protective passive film, and it has been estimated that steels with this

low current density develop propagation periods of more than 20 years before cracking and spalling of the concrete cover occur [43]. The potential range below the passivity region, between the open circuit potential ($E_{\text{corr}} \sim -0.38$ V vs. SCE) and -0.2 V vs. SCE, is called activation region because corrosion processes can occur at the steel surface.

Above the passivity region, anodic current density increases as a result of the oxygen evolution reaction [30]:



This region is known as transpassivity, in which the oxygen evolution corresponds to the anodic reaction, and therefore there is not dissolution of steel or breakdown of the passive layer. However, if this condition remains, the presence of H^+ ions can neutralize the concrete pore solution leading to the depassivation of the steel surface and the initiation of corrosion processes.

Figure 3 also shows the potentiodynamic polarization curve for a carbon steel sample immersed in a simulated concrete pore solution with the same composition as described above but with the presence of 3.5% NaCl. A significant change can be observed in the electrochemical behavior of steel by the influence of chloride ions. The passivity region is significantly reduced (between -0.3 V vs. SCE and -0.1 V vs. SCE) and it can be seen that once the upper potential limit of the passivity region is reached, the anodic current density increases dramatically. This potential is known as breakdown potential or pitting potential (E_{pit}). Pitting potential values decrease with the chloride concentration and it has been defined from values of $+0.6$ V vs. SCE that corresponds to chloride-free solutions to values below -0.5 V vs. SCE for concrete pore solutions with

high chloride content [30]. Besides the appearance of a breakdown potential, the potentiodynamic curve for the steel immersed in the chloride-contaminated solution also shows differences in the corrosion potential and the anodic current density compared to the steel sample immersed in the chloride-free solution. The corrosion potential shifts to more cathodic potentials ($E_{\text{corr}} \sim -0.42$ V vs. SCE) and the anodic current density increases in one order of magnitude ($i \sim 10^{-5}$ A/cm²). This behavior is observed as a result of the pitting corrosion process in which chloride ions destroy the passive layer and induce corrosion processes on the steel surface [44].

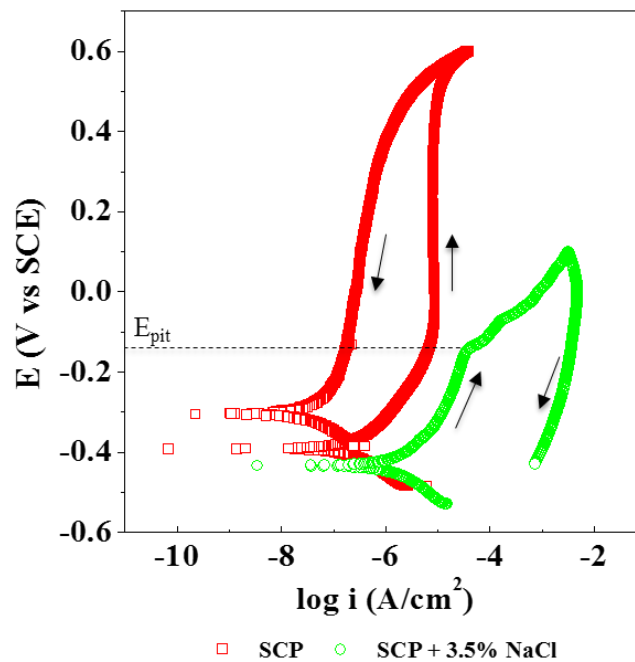


Figure 3. Potentiodynamic polarization curve of carbon steel immersed in simulated concrete pore solutions.

Electrochemical impedance spectroscopy to study the electrochemical behavior of reinforcing steel in simulated concrete pore solutions

Electrochemical impedance spectroscopy (EIS) represents another technique that can be used to describe the electrochemical behavior of reinforcing steel in concrete. This is a nondestructive technique and therefore can be used for studying real concrete structures and to follow the evolution of corrosion degradation processes [45, 46]. Figure 4a shows the Nyquist representations of carbon steel samples after exposure for 24 hours to the electrolyte solutions described above. For the carbon steel substrate immersed in the chloride-free simulated concrete pore solution, a large capacitive loop is observed in the entire frequency range which is associated to the presence of the protective passive film at the steel surface [45]. On the other hand, two time constants are recognized for the carbon steel substrate exposed to the chloride-contaminated simulated concrete pore solution; the time constant at high frequency corresponds to the contribution of the passive layer and the time constant at low frequency describes the presence of charge transfer processes at the steel substrate, which means a local breakdown of the passive layer is taking place. From the Bode representation (Figure 4b) it can be observed that the impedance magnitude at 0.01 Hz, which is associated to the total resistance of the system, is more than one order of magnitude higher for the carbon steel immersed in the chloride-free solution compared to the steel immersed in the electrolyte solution containing chloride ions. The lower impedance magnitude observed for the steel exposed to chloride ions can be explained due to the breakdown of its passive layer and the development of corrosion processes at the metal/electrolyte interface. Figure 4b also

shows that the impedance magnitude at the highest frequency, associated with the resistance of the electrolyte medium, is lower for the steel sample immersed in the solution with chloride ions, meaning that the presence of these ions reduce the resistivity of the concrete pore solution. Finally, the phase angle curve confirms the presence of one time constant (at 1 Hz) for the steel substrate immersed in the chloride-free solution and the development of two time constants (at 10 Hz and 0.01 Hz) for the steel immersed in the chloride-contaminated solution. More details related to the fundamentals and interpretation of EIS will be provided in the last section of this chapter.

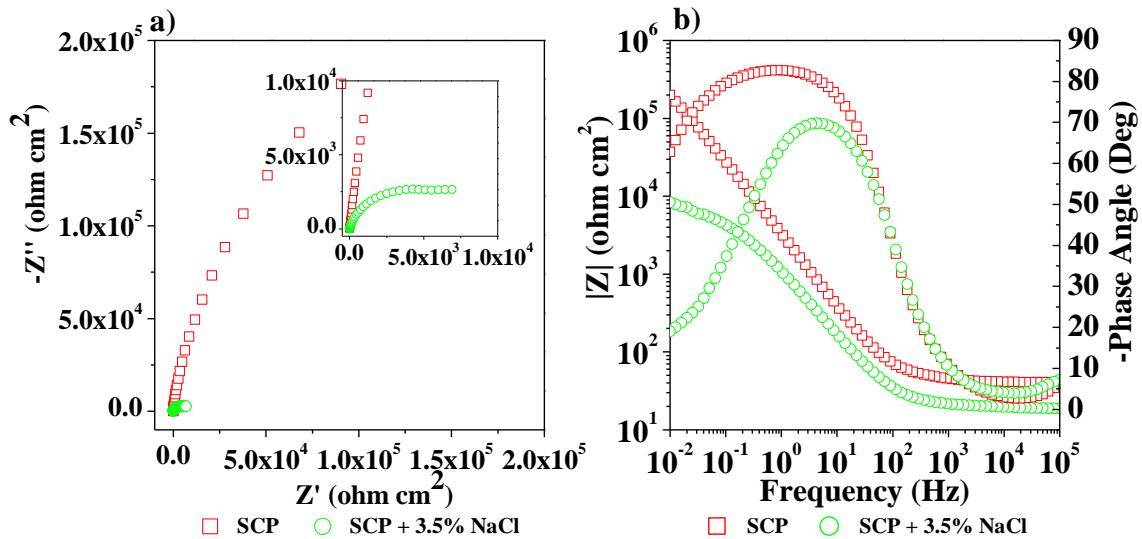


Figure 4. EIS results of carbon steel samples after exposure for 24 hours to simulated concrete pore solutions: a) Nyquist representation, and b) Bode representation.

Zinc-rich epoxy primers

Mechanism of corrosion protection of zinc-rich epoxy primers

Zinc-rich epoxy primers (ZRP) have been extensively used to protect carbon steel substrates from corrosion degradation [47]. They are commonly used as primers in combination with organic topcoats to provide longer corrosion protection and weathering resistance. The mechanism of corrosion protection of ZRP is significantly different to the barrier protection mechanism provided for traditional organic coatings, in which a physical barrier isolating the metal substrate from the environment is the only form of corrosion protection. This barrier protection mechanism is usually referred as a passive corrosion control [48] since the coating system is not involve in electrochemical (or chemical) reactions and once the electrolyte starts to diffuse though the organic material, there is no other form to prevent corrosion on the metal substrate. In contrast, ZRP provide an active corrosion protection (galvanic protection) to the carbon steel substrate due to the preferential dissolution of zinc in the presence of oxygen and moisture. In addition, ZRP can also provide barrier protection due to the presence of the epoxy binder and inhibition of the oxygen reduction reaction at the metal substrate. This inhibition process can be observed as a result of two effects [47]: 1) Electrochemical reactions between oxygen and the zinc particles that were not involved in the cathodic protection process, that reduces the amount of oxygen reaching the metallic substrate and 2) presence of zinc corrosion products at the carbon steel surface as a result of the galvanic protection process, that provide an additional barrier layer to diffusion of oxygen.

The mechanism of corrosion protection of ZRPs is summarized in Figure 5. The first stage corresponds to an intact condition in which the epoxy binder isolates the carbon steel substrate from the environment and represents a physical barrier for the diffusion of aggressive species. A second stage is developed once the electrolyte diffuses through the ZRP and the zinc particles are able to provide galvanic protection to the metallic substrate. Finally, after the cathodic protection is no longer effective, the third stage corresponds to a long-term barrier protection period that is provided due to [47]: 1) the presence of zinc corrosion products on the carbon steel surface that reduces the amount of ionic species reaching the metallic substrate and 2) the formation of zinc corrosion products in the coating system that block ionic pathways for the diffusion of aggressive species across the material.

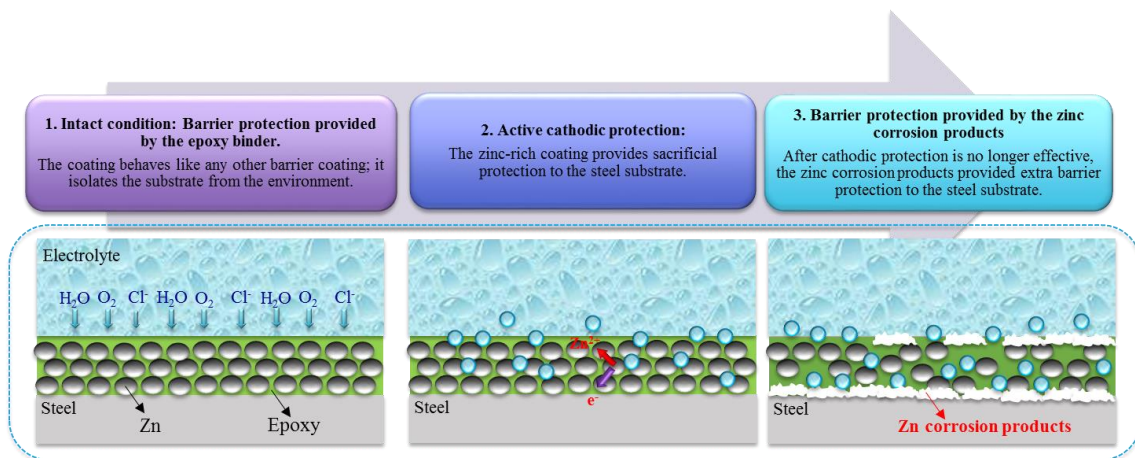


Figure 5. Corrosion protection mechanism of zinc-rich epoxy coatings.

During the second stage shown in Figure 5, ZRPs must satisfied three conditions in order to provide an effective galvanic protection to the steel substrate [47]:

- 1) The zinc particles must be electrically connected with each other in order to provide a conductive network for the electronic transfer between the zinc particles and the carbon steel substrate.
- 2) The zinc particles must be in electrical contact with the carbon steel substrate.
- 3) The ZRP must be wetted by an electrolyte to induce electrochemical reactions between the zinc particles and oxygen leading to the formation of solid corrosion products that protect the steel.

The last condition is relatively easy to satisfy once the coated steel substrate is exposed to an aggressive environment such as seawater. On the other hand, the first two conditions are more difficult to accomplish since they are related to the design, preparation, and application of the paint to the metallic substrate. These conditions imply that a large load of zinc particles must be added to the epoxy binder in order to guarantee the continuous electrical pathways between the zinc particles and the metal substrate for the cathodic protection process to take place. Several studies have reported that the zinc content must be higher than 90 wt% Zn to provide sacrificial protection to bare steel [19, 49-52], however, different parameters can influence the amount of zinc needed for cathodic protection such as, the particle size since small particles can provide more specific area for electrochemical reactions than larger particles [16], particle morphology which is related to the particle-to-particle contact [53, 54], and the presence of additives

that can influence the activity or the extent of the galvanic protection process [18, 48, 50, 55].

Conductive particles to improve the performance of zinc-rich epoxy primers

Conductive particles have been proposed to improve the galvanic effect of the zinc particles and to reduce the required zinc content that can compromise the physico-mechanical properties of the epoxy binder such as adhesion, flexibility, and impact resistance [56]. Marchebois et al. [52] studied the presence of carbon black in zinc-rich powder coatings; they found that cathodic protection was provided by coating systems with 50 wt% Zn and 5 wt% carbon black when the samples were immersed in artificial seawater. This behavior was explained by the presence of carbon pigments, which can increase electrical conductivity and porosity within the epoxy coating, allowing for a higher penetration of electrolyte and subsequently a higher activation of the zinc particles; nevertheless, some drawbacks were found due to issues with powder homogeneity and powder application. Other authors have proposed hybrid coatings that use intrinsically conductive pigments such as polyaniline (PANI) and polypyrrole (PPy). Meroufel et al. [55] proposed using hydrochloride polyaniline (PANI-Cl) in order to increase the conductivity of the epoxy binder. Low percolation was obtained with PANI hybrid coatings, which means that PANI pigments did not improve the electrical properties of the epoxy binder; furthermore, the activation of the zinc particles was higher in ZRPs without PANI pigments. However, cathodic protection was extended to 100 days of immersion due to low percolation and porosity. In addition, the retention of zinc corrosion products within the binder provided excellent barrier protection. Gergely

et al. [18] studied the effect of PPy-deposited nano-size alumina particles (PDAPs) in zinc-rich paint formulations; they found a moderate galvanic function with an appreciable improvement in barrier protection. In addition, they also reported that the presence of PDAPs increased adhesion of the hybrid coating to the metal substrate and decreased degradation of the epoxy binder.

Electrochemical impedance spectroscopy (EIS)

Fundamentals of EIS

Electrochemical impedance spectroscopy (EIS) has been extensively used to investigate corrosion processes, coatings and paints, membranes in living cells, fuel cells, chemical sensors, supercapacitors, batteries, and others [57]. EIS represents a powerful and nondestructive method to characterize intrinsic material properties such as electrical conductivity, dielectric constant, and mobility of charges, but also properties related to interfacial phenomena including adsorption, reaction rate constants, double layer capacitances, and diffusion coefficients of species at the interface [57].

EIS is usually performed by applying a small sinusoidal potential signal $V(t)$ (i.e., excitation amplitude between 5 mV to 10 mV) to a particular system and then measuring the sinusoidal current response $I(t)$ with the same frequency but shifted in phase with respect to the excitation signal (see Figure 6). These time-domain signals are transferred to the frequency domain by using the Fourier transform and the relationship between the perturbation potential signal and the response current signal in the frequency domain corresponds to the AC impedance of the system:

$$Z(\omega) = \frac{F[V(t)]}{F[I(t)]} = \frac{V(\omega)}{I(\omega)} \quad (8)$$

It is important to mention that EIS can be only applied when the system under study satisfied the conditions of linearity, causality, stability, and finiteness [58-60]. A system behaves linearly when the current output signal is proportional to the voltage input signal. Causality means that the AC current response is only caused by the AC voltage perturbation and it is not the result of instrument artifacts or external noise [58]. The system must be stable during the acquisition time of EIS data, meaning that the system must return to its original condition once the perturbation is removed. Finally, impedance must be a continuous and finite function in the entire frequency range. Kramers-Kronig (K-K) transforms has been used to validate EIS data [61-63]. This method uses mathematical relations to transform the measured real component into the imaginary component and vice versa, the calculated imaginary component should reproduce the measured imaginary component and vice versa, if measured real and imaginary components do not satisfy the K-K transforms, the measured data violate one of the conditions (linearity, causality, and stability) and therefore it cannot be considered as EIS data.

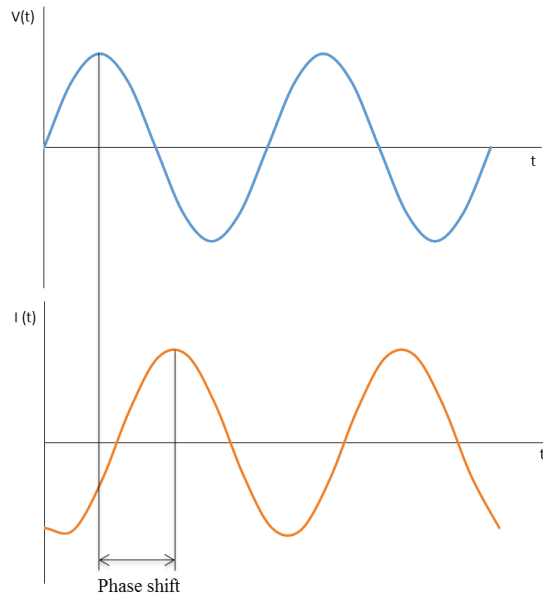


Figure 6. Sinusoidal potential and current signals. Adapted from [58].

Based on equation (8), impedance can be seen as the resistance of a system to the flow of an AC current, however, impedance differs from the electrical resistance described in the Ohm's law because it takes into account a frequency dependence. By definition, the impedance response corresponds to a complex quantity [57]:

$$Z(\omega) = Z'(\omega) + jZ''(\omega) \quad (9)$$

Where, $j = \sqrt{-1}$, $Z'(\omega)$ represents the real component, and $Z''(\omega)$ corresponds to the imaginary component. In polar form, the impedance can be also be written as:

$$Z(\omega) = |Z|\exp(j\varphi) = |Z|(\cos(\varphi) + j\sin(\varphi)) \quad (10)$$

Where $|Z|$ represents the magnitude of the impedance or the impedance modulus and φ corresponds to the phase angle. From Figure 7, impedance magnitude can be expressed as follows:

$$|Z(\omega)| = \sqrt{Z'(\omega)^2 + Z''(\omega)^2} \quad (11)$$

And phase angle can be written as:

$$\varphi(\omega) = \tan^{-1}\left(\frac{Z''(\omega)}{Z'(\omega)}\right) \quad (12)$$

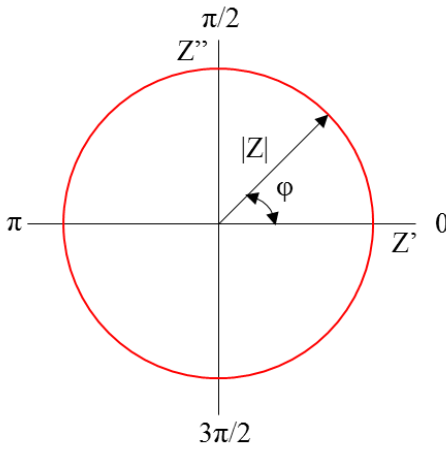


Figure 7. Impedance complex plane. Adapted from [64].

Based on the parameters described in the complex plane, EIS can be graphically represented in two common formats: 1) the complex impedance plane representation that is usually called Nyquist plot in which the negative imaginary impedance component ($-Z''(\omega)$) is plotted against the real impedance component ($Z'(\omega)$) at each specific frequency and 2) the Bode plot, in which the impedance magnitude and the phase angle are plotted as a function of frequency. These two representations are shown in Figure 8.

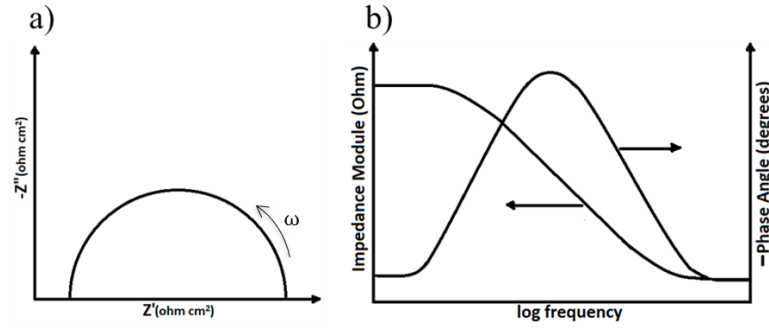

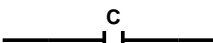
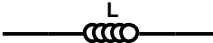


Figure 8. EIS representations: a) Nyquist plot, and b) Bode plot. Adapted from [64].

EIS interpretation

EIS spectra are commonly interpreted by using equivalent electrical circuits that usually contain electrical elements such as resistors, capacitors, and inductors. The proper equivalent circuit to describe the impedance response should be selected based on the best fitting with the EIS data and the best physical interpretation of each of the electrical elements according to the phenomenon under study [58]. Table 1 shows these electrical elements with their corresponding voltage/current relationships and their impedance functions:

Table 1. Electrical elements and their corresponding impedance functions [64].

Electrical element	Voltage/current relation	Impedance
Resistor	 $V = IR$	$Z = R$
Capacitor	 $I = C \frac{dV}{dt}$	$Z = \frac{1}{j\omega C}$
Inductor	 $V = L \frac{dI}{dt}$	$Z = j\omega L$

From Table 1, it can be observed that the impedance of a resistor is independent of frequency and it only has contribution from the real impedance component, since there is no imaginary impedance component, the phase angle is zero and therefore, the AC current that passes through a resistor is in phase with the AC voltage [58]. In contrast, the impedance of capacitors and inductors show frequency dependence and they only have contribution from imaginary impedance component, which means that the current is out of phase 90° with respect to the voltage [58]. From Table 1, it is also observed that the impedance of a capacitor decreases and the impedance of an inductor increases as the frequency is increased.

In addition to resistors, capacitors and inductors, which are usually called ideal or passive circuit elements [58, 64], non-ideal circuit elements have been proposed to study real systems with more complex phenomena. Constant phase element (CPE) has been defined to account for deviations from ideal capacitive behavior due to surface heterogeneities, porosity, non-uniform potential and current distribution, presence of electroactive species, and presence of crystal phases and grain boundaries [58]. The impedance of a CPE is given by:

$$Z_{\text{CPE}} = \frac{1}{Y_0(j\omega)^\alpha} \quad (13)$$

Where, Y_0 corresponds to an effective CPE coefficient and α represents an empirical exponent without a clear physical interpretation [58]. These CPE parameters α and Y_0 are independent of frequency and for a pure capacitor, $\alpha = 1$ and Y_0 corresponds to the capacitance [65].

The Warburg impedance corresponds to another non-ideal circuit element that describes the diffusion process of reacting species at the metal/electrolyte interface. This diffusion process is developed due to previous charger transfer or adsorption processes that create concentration gradients of electroactive species between the bulk of the electrolyte and the interface [58]. In the Nyquist representation, Warburg impedance is shown as a diagonal line with a slope of 45° and in the Bode plot, it exhibits a phase angle of 45°[58]. The expression for an infinite Warburg impedance (i.e., the thickness of the diffusion layer is infinite) is given by [58]:

$$Z_W = \sigma(\omega)^{-1/2}(1 - j) \quad (14)$$

Where σ is the Warburg coefficient which is described as:

$$\sigma = \frac{RT}{n^2 F^2 A \sqrt{2}} \left(\frac{1}{C_O^* \sqrt{D_O}} + \frac{1}{C_R^* \sqrt{D_R}} \right) \quad (15)$$

With

D_O : Diffusion coefficient of the oxidant

D_R : Diffusion coefficient of the reductant

A: Surface area of the electrode

n: Number of electrons involved

For a bounded diffusion layer, the Warburg impedance is modified by:

$$Z_O = \sigma(\omega)^{-1/2}(1 - j) \tanh \left[\delta \left(\frac{j\omega}{D} \right) \right] \quad (16)$$

Where δ represents the thickness of the Nernst diffusion layer and D corresponds to the effective diffusion coefficient of the different diffusing species.

The impedance expressions for all electrical elements described above are used to calculate the total impedance response (transfer function) of the electrical circuit. For electrical elements arranged in a series configuration (see Figure 9a), the total impedance can be calculated from:

$$Z = Z_1 + Z_2 \quad (17)$$

And for electrical elements in parallel (see Figure 9b), the total impedance is given by:

$$Z = \left[\frac{1}{Z_1} + \frac{1}{Z_2} \right]^{-1} \quad (18)$$

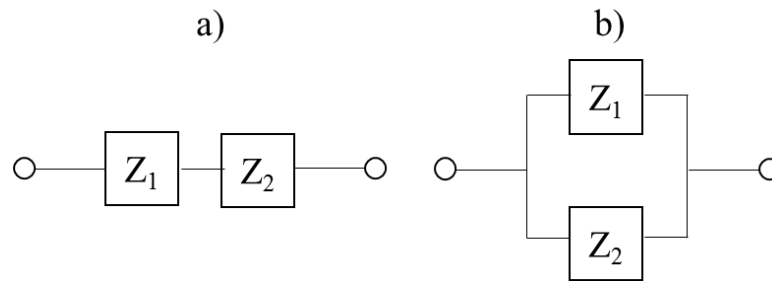


Figure 9. Arrangement of electrical elements: a) in series; and b) in parallel. Adapted from [64].

Application of EIS to organic coatings

EIS has been extensively used to study the coating degradation and the extent of corrosion in polymer-coated metallic substrates due to the exposure to aggressive environments [60, 66, 67]. Figure 10 shows an example of typical Nyquist and Bode plots that represents the electrochemical behavior of a polymer-coated steel sample exposed to a corrosive medium for 200 days.

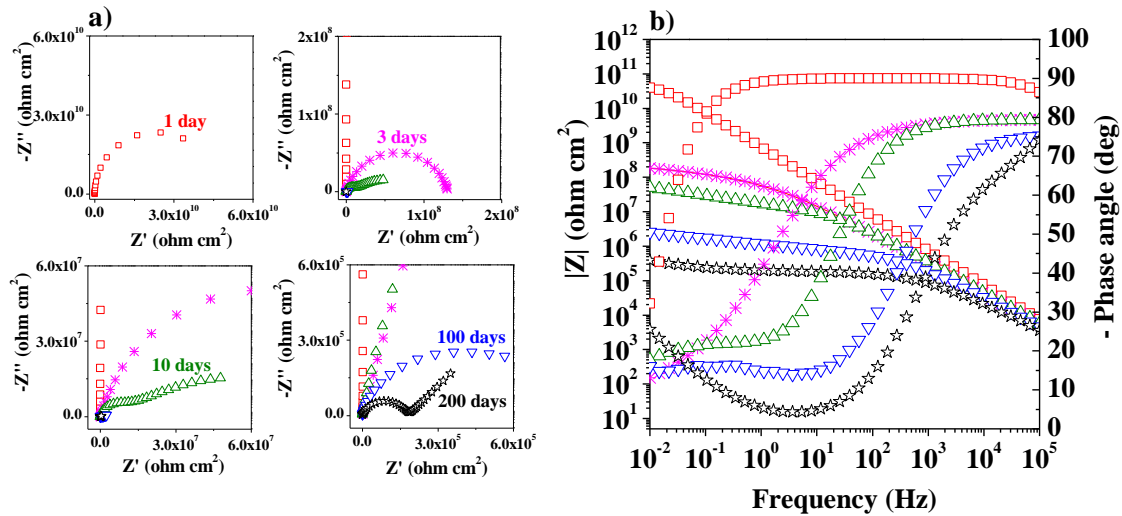


Figure 10. Example of EIS spectra for a polymer-coated steel sample exposed to an aggressive medium for 200 days: a) Nyquist plot, and b) Bode plot.

The evolution of the impedance response shown in Figure 10 is characteristic of the organic coatings (polymers) that only provided barrier protection to the steel substrate. The impedance response in the first day of immersion represents the intact condition in which the permeation of water through the organic coating is negligible. The intact condition shows a large semicircle in the Nyquist representation, a straight line with slope of -1 in the impedance magnitude curve, and a phase angle of 90° during almost all the frequency range. This behavior is usually called capacitive behavior because is similar to the impedance response of a pure capacitor meaning that the organic coating represents a dielectric material that separates the steel substrate from the environment [67].

After the first day of immersion, the degradation of the coating system can be described in three stages: Diffusion of electrolyte, charge transfer process, and diffusion-

controlled process [67]. The impedance response after three days of immersion shows the diffusion of electrolyte across the organic material. During this stage, the Nyquist representation shows one semicircle which is usually called time constant (τ), and is given by:

$$\tau = RC \quad (19)$$

Where, R is the resistance and C is the capacitance of the system. This time constant, τ_c is related to the properties of the organic coating:

$$\tau_c = R_c C_c \quad (20)$$

From the Bode diagram, the slope of the impedance magnitude decreases at low frequency (below 1 Hz) and the phase angle decreases as the frequency decreases. This is a results of diffusion of ionic species across the organic coating that develops a resistive behavior inside the material.

The second stage starts after 10 days of immersion and corresponds to the development of a charge transfer process at the steel substrate. The Nyquist representation shows two time constants; the time constant at high frequency (10^4 - 10^3 Hz) corresponds to the dielectric properties of the organic coating (τ_c) and the time constant at low frequency (0.1 Hz), τ_m is associated to the interfacial electrochemical reactions at the metallic substrate:

$$\tau_m = R_{ct} C_{dl} \quad (21)$$

The Bode representation confirms the existence of the two time constants by the appearance of two maximum points in the phase angle curve.

Finally, the third stage is observed after 200 days of immersion and corresponds to the formation of corrosion products at the steel surface that induces a diffusion-controlled process (i.e., the rate of the oxygen diffusion towards the metallic substrate become slower than the rate of the charge transfer process). This diffusion process is clearly identified in the low frequency range of the Nyquist representation by the presence of a straight line with a slope of 45° .

The EIS spectra that describe the different stages of coating degradation due to the exposure to a corrosive medium can be fitted by using the electrical equivalent circuits shown in Figure 11.

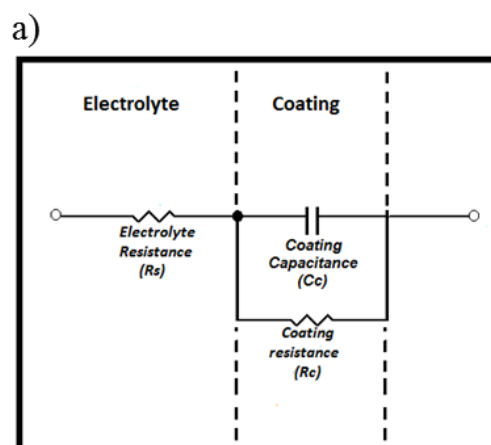


Figure 11. Equivalent electrical circuits to describe the stages in the degradation mechanism of polymer-coated steel substrates under exposure to corrosive media: a) diffusion of electrolyte throughout the coating, b) charge transfer process, and c) diffusion-controlled process.

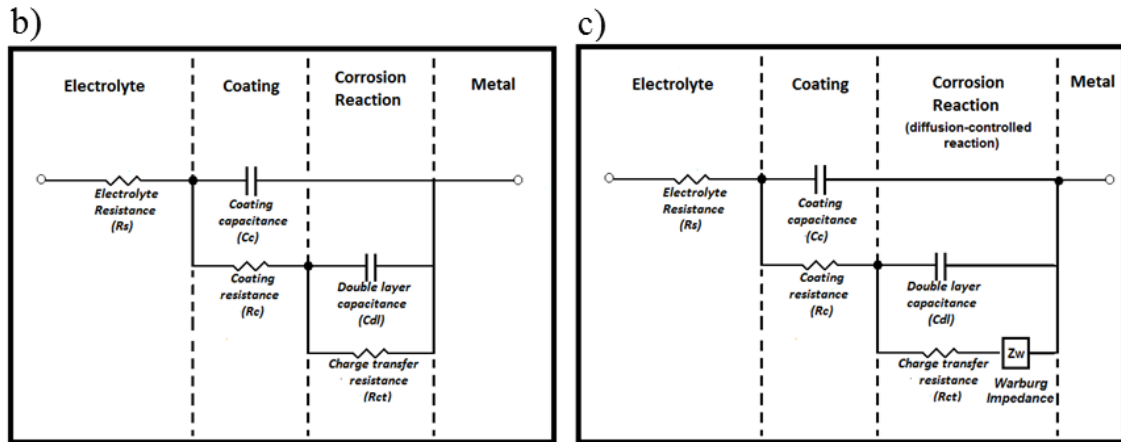


Figure 11. Continued

The physical interpretation of these equivalent circuits to describe the degradation of an organic coating has been well-documented [60, 66, 67]; R_s represents the resistance of the electrolyte, which is given by:

$$R_s = \rho_s \frac{l}{A} = \frac{1}{\kappa_s} * \frac{l}{A} \quad (22)$$

Where ρ corresponds to the resistivity of the electrolyte, l is the length, A is the area, and κ is the conductivity of the electrolyte, which is the inverse of the resistivity.

The electrical elements R_c and C_c are associated to intrinsic properties of the organic coating. The physical interpretation of these coating properties is established by considering the coating system as a capacitor, in which one of the conducting plates is formed by the electrolyte solution, the other conducting plate is formed by the metallic substrate and the dielectric material corresponds the coating itself. With this analogy, R_c represents the coating resistance (resistance of the dielectric material) which is related to the number of pores or ionic conductive paths across the material and it is a measure of

the degree of coating degradation due to the diffusion of electrolyte through the film [60]. C_c corresponds to the coating capacitance which is given by:

$$C_c = \frac{\epsilon_0 \epsilon A}{d} \quad (23)$$

Where, ϵ_0 is the permittivity of free space (8.85×10^{-14} F/cm), ϵ corresponds to the dielectric constant of the coating, A is the surface area of the metallic substrate, and d corresponds to the thickness of the coating. C_c represents a measure of the amount of water that diffuses through the coating and coating delamination [60].

The elements R_{ct} and C_{dl} are related to electrochemical reactions that occur at the metallic substrate. Once the electrolyte reaches the metal surface, a distribution of charged species is developed forming the so-called electrical double layer (edl) [68, 69], which is composed by a first layer of adsorbed species (water molecules and ionic species) at the metal surface, a second layer comprises non-adsorbed ions that are attracted to the metal by coulombic forces, and a diffuse layer in which ions are randomly oriented due to thermal motions. This electrical double layer can be also described as a capacitor in which R_{ct} represents the resistance to charge transfer processes through the edl and C_{dl} corresponds to the double layer capacitance that represents a measure of the electroactive area that is available for the charge transfer process [60, 68].

Finally, Z_W corresponds to the Warburg impedance that describes the diffusion of oxygen through iron corrosion products formed at the coating/steel interface.

CHAPTER II

EXPERIMENTAL DESIGN*

The research project was divided in two main parts; the first part focused on the influence of zinc content on the corrosion protection mechanism of carbon nanotubes/zinc rich epoxy primers on carbon steel under exposure to a simulated concrete pore solution; and the second part focused on the influence of the chloride ion concentration on the corrosion performance of carbon nanotubes/zinc rich epoxy primers on carbon steel exposed to chloride-contaminated solutions. The mechanisms of corrosion protection investigated in the first part of this study were defined based on electrochemical techniques such as open circuit potential (OCP), electrochemical impedance spectroscopy (EIS) and, localized electrochemical impedance spectroscopy (LEIS). The electrochemical findings were supported with morphology analysis using scanning electron microscopy (SEM) coupled with energy dispersive X-ray spectroscopy (EDS) and surface characterization using X-ray photoelectron spectroscopy (XPS). For the second part of this study, the same electrochemical techniques were used; in addition, accelerated corrosion tests were carried out to determine the extent of the

* Part of this chapter is reprinted from Corrosion Science, vol. 109, Y Cubides, H. Castaneda, Corrosion protection mechanisms of carbon nanotube and zinc-rich epoxy primers on carbon steel in simulated concrete pore solutions in the presence of chloride ions, 145-161, Copyright (2016), with permission from Elsevier.

corrosion damage in the different coating systems. The materials and methods for both parts are described as follows:

Experimental procedure to study the influence of zinc content on the corrosion protection mechanism of carbon nanotubes/zinc rich epoxy primers on carbon steel under exposure to a simulated concrete pore solution

Electrolyte solution

The electrolyte used simulates a concrete pore solution contaminated by chloride ions. Table 2 shows the chemical concentration of each of the species in this solution. Sodium chloride (NaCl) was added to investigate the influence of chloride ions on the corrosion degradation process. All the chemicals compounds were of analytical grade and water was deionized with a high purity. The resulting electrolyte had a chloride to hydroxide ratio of 1, corresponding to a sodium chloride concentration of 0.1 M and a pH of 12.87. This chloride to hydroxide ratio ($[\text{Cl}^-]/[\text{OH}^-]$) was higher than the critical chloride concentration reported for concrete structures, which has been established as around 0.6 [70-72]. All testing procedures (except for localized electrochemical impedance spectroscopy) were performed by using this electrolyte solution.

The simulated concrete pore solution was chosen based on previously studies [73-78]. It is important to clarify that this solution does not include all chemical species contained in real cement concrete pore solutions such as fly ash, silica fume, gypsum, etc. However, sodium hydroxide (NaOH), potassium hydroxide (KOH), and calcium hydroxide ($\text{Ca}(\text{OH})_2$) represent the major chemical species that allow to study, in a

controlled environment, the electronic properties of the passive film formed at the carbon steel surface [78].

Table 2. Chemical composition of simulated concrete pore solution with a chloride-to-hydroxide ratio of 1.

	[KOH]	[NaOH]	[Ca(OH) ₂]	[NaCl]	pH
Molarity (M)	0.08	0.02	0.001	0.1	12.87

Coating samples

Carbon nanotubes/zinc-rich epoxy primers were all provided by Tesla NanoCoatings. The coating formulation corresponds to a solvent-based two component epoxy-polyamide primer that incorporates sacrificial zinc dust in spherical configuration together with multi-wall carbon nanotubes. To prepare the zinc-rich coating formulations, epoxy resin (Tesla ® P1150ASAS) was mechanically mixed with a fixed composition of <1 wt% of multi-wall carbon nanotubes and solvent (tert-butyl acetate). After CNTs were completely dissolved in the epoxy resin, different weight percentages of zinc particles were added gradually to the mixture while stirring at room temperature. Finally, a stoichiometric amount of hardener (Tesla ® P1150BSAS) with a weight ratio (epoxy resin: hardener) of 2:1, was added to the mixture and sonicated for 5 min. The different coating formulations are listed in Table 3. The prepared coatings were air sprayed on AISI 1008 carbon steel (UNS G10080) with a chemical composition (maximum nominal composition in wt%) of 0.60% Mn, 0.15% C, 0.030% P, 0.035% S

and balance Fe. The dimensions of the substrate panels were 152 x 76 x 1 mm. Prior to the application of coatings, steel panels were sandblasted followed by degreasing with acetone and drying at room temperature. The coating systems were allowed to cure for 6 hours at 60 °C and then, they were kept at room temperature for seven days before exposure to the electrolyte solution. Exposure was done using a glass tube fixed on the coating surface by an O-ring and a metal clamp that exposed a surface area of 4.67 cm². A dry film thickness of 4 mils approximately was measured by an Elcometer 456 coating thickness gauge.

Table 3. Specifications of the different coating systems.

Coating	Zinc (wt%)	Tesla ® P1150ASAS (Epoxy resin, solvent, multiwall carbon nanotubes <1%) (wt%)	Tesla ® P1150BSAS (Polyamide, solvent, ethylacetate) (wt%)	Dry film thickness (µm)
CNT-60ZRP	60	26.7	13.3	101.6 ± 18.2
CNT-70ZRP	70	20.0	10.0	101.6 ± 10.6
CNT-80ZRP	80	13.4	6.6	101.6 ± 14.2
CNT-90ZRP	90	6.7	3.3	101.6 ± 6.6

Electrochemical measurements

Electrochemical measurements were conducted using a Biologic SP-200 Research Grade Potentiostat/Galvanostat/FRA. A conventional three-electrode cell was used at room temperature. The coated samples served as the working electrodes, a saturated calomel electrode (SCE) was used as the reference electrode, and a Pt/Nb mesh

electrode of 2 cm diameter was the counter electrode. The electrochemical testing procedure included measurements of open circuit potential (OCP) and electrochemical impedance spectroscopy (EIS) over a period of 150 days. Open circuit potential was measured for 10 minutes following impedance measurements in a frequency range of 100 kHz to 10 mHz at 6 points/decade with a sinusoidal amplitude of 10 mV. All electrochemical impedance spectroscopy measurements were performed at open circuit potential. The impedance results were fitted with equivalent electrical circuits using the Z Fit tool of the EC-lab software. All electrochemical tests were performed in duplicate to guarantee reproducibility of the OCP and EIS measurements.

Local electrochemical impedance spectroscopy (LEIS)

LEIS measurements were performed to study the cathodic protection properties of CNT-ZRPs. An artificial defect of 4 mm x 1 mm was made on a coated sample of 1 cm², which was then electrically connected using a conductive silver paint to a metal sample embedded in epoxy resin. The edges of the coated sample were isolated with silicone glue and then, it was allowed to dry for one day. This setup was required due to the configuration of the VersaSCAN L-Cell. The LEIS measurements were performed on a VersaSTAT 3F Potentiostat coupled to a VersaSCAN electrometer and controlled by VersaSCAN software.

A five-electrode cell was used with a saturated calomel electrode as the reference electrode, a platinum wire as the counter electrode, the coated sample as the working electrode, and a LEIS probe as a dual-element probe that scans the local impedance in a defined surface area. A 0.005 M NaCl solution was used to guarantee low electrical

conductivity that ensure accuracy of the LEIS results [79, 80]. The size of the scanned area (length x width) was 6.75 x 4 mm. The LEIS measurements were carried out with a potential amplitude of 10 mV and at a single frequency of 10 Hz.

Morphology characterization

Morphology configuration of the different CNT-ZRP formulations were characterized by SEM coupled to EDS. Coated samples with a 1 cm² surface area were immersed in a simulated concrete pore solution with a [Cl⁻]/[OH⁻] ratio of 1. The samples were removed following immersion for 5, 20, 50, and 90 days. For the cross-section images, the exposed coated samples were embedded in epoxy resin and cut perpendicular to the exposed area. The epoxy resin was used to reduce the alteration or damage of the coated samples during the cutting process. Samples were rapidly dried with air and then maintained in a desiccator to avoid additional degradation on the carbon steel surface. The cross section and surface morphologies of the samples were examined before and after immersion with a HITACHI® TM3000 Tabletop Microscope SEM. Elemental content in the different samples was determined by EDS.

X-ray photoelectron spectroscopy (XPS)

The surface chemical compositions of the coated samples were analyzed by X-ray photoelectron spectroscopy (XPS) on an Omicron XPS/UPS system with an Argus detector using a Mg K α X-ray source (1253.6 eV). The spectrometer was equipped with an electron flood source (CN 10 scientaomicron) to provide charge neutralization to the coated samples and an argon ion sputter gun (NGI3000 LK Technologies) for surface cleaning. The hemispherical analyzer was operated in a fixed analyzer transmission

(FAT) mode with a pass energy of 100 eV for the survey spectra and 20 eV for the high-resolution spectra. Binding energies for XPS spectra were calibrated with reference to the C 1s adventitious carbon peak (285 eV). Identification of chemical species in high-resolution spectra was defined based on literature data. CasaXPS software was used for peak fitting and quantification of atomic compositions by using a Gaussian-Lorentzian procedure and a Shirley type for the background subtraction. For the peak fitting of the high-resolution spectra, position constraints were added based on reported literature values, and the equality of full-width at half-maximum (FWHM) of a peak was considered for all peaks within each core level.

Experimental procedure to study the influence of chloride concentration on the corrosion performance of carbon nanotubes/zinc rich epoxy primers on carbon steel under exposure to simulated concrete pore environments

Electrolyte solution

For the second part of the research project, simulated concrete pore solutions with different chloride concentrations were considered. Three additional chloride concentrations were investigated: blank solution (simulated pore solution without chloride ions), solution with a $[\text{Cl}^-]/[\text{OH}^-]$ ratio of 0.1, and solution with a $[\text{Cl}^-]/[\text{OH}^-]$ ratio of 10. Table 4 shows the chemical composition of the different electrolyte solutions.

Table 4. Chemical composition of simulated concrete pore solutions with different $[\text{Cl}^-]/[\text{OH}^-]$ ratios.

$[\text{Cl}^-]/[\text{OH}^-]$ ratio	KOH (M)	NaOH (M)	$\text{Ca}(\text{OH})_2$ (M)	NaCl (M)	pH
Blank	0.08	0.02	0.001	0	12.98
0.1	0.08	0.02	0.001	0.01	12.95
10	0.08	0.02	0.001	1.02	12.57

Coating samples

The coating formulations for the second part of the research project were the same as the ones used for the first part. It is important to mention that the coating samples of each specific formulation that were exposed to the different electrolytes were prepared in a single batch to guarantee consistent results in terms of chemical composition of the coating systems.

Electrochemical measurements

The electrochemical measurements for the second part of the research project were conducted exactly the same as it was described in the first part.

Fog chamber measurements

A different set of coated samples were placed in a salt spray chamber following the ASTM B117 standard. Intact and scribed samples were considered for this study. Before panels were introduced to the spray chamber, the backs and edges were covered with adhesive tape to isolate the exposed area. The samples were exposed for 30 days and photographs were taken after 3 days, 7 days, and 30 days of exposure to visually inspect

the degradation of the coating systems. In order to guarantee the reproducibility of the results, three samples for each formulation were tested.

Morphology studies

The morphology of the coating systems after being exposed for 150 days to the electrolyte solutions for 150 days was inspected with a high-resolution scanning electron microscopy (Tescan LYRA-3 Model GMH Focused Ion Beam Microscope) at an accelerating voltage of 10.0 kV and under secondary electron mode (SE). In addition, line scan analyses were performed using energy-dispersive X-ray spectroscopy (Standard EDS Microanalysis System with X- MaxN 50).

CHAPTER III

INFLUENCE OF ZINC CONTENT ON THE CORROSION PROTECTION MECHANISM OF CARBON NANOTUBES/ZINC RICH EPOXY PRIMERS ON CARBON STEEL UNDER EXPOSURE TO A SIMULATED CONCRETE PORE SOLUTION*

Open circuit potential (OCP)

Also called “rest potential”, OCP is the potential of a working electrode compared to a reference electrode when the net current that is flowing along the system is equal to zero. The OCP values indicate, among other parameters, the thermodynamic stability that is used as a criterion for cathodic protection; for reinforced concrete structures, the potential criterion for cathodic protection has been bounded with minimum and maximum values. Some authors have reported a maximum value of -720 mV vs. Ag/AgCl/0.5 M KCl (-0.763 V vs. SCE), which represents the potential at which cathodic protection is no longer effective [81, 82]. In addition, a minimum value of -1100 mV vs. Ag/AgCl/0.5 M KCl (-1.143 V vs. SCE) has been reported in association with a hydrogen evolution process [81, 82]. Figure 12 shows the evolution of the open circuit potential (OCP) for CNT-ZRPs at different zinc contents immersed in the

* Part of this chapter is reprinted from Corrosion Science, vol. 109, Y Cubides, H. Castaneda, Corrosion protection mechanisms of carbon nanotube and zinc-rich epoxy primers on carbon steel in simulated concrete pore solutions in the presence of chloride ions, 145-161, Copyright (2016), with permission from Elsevier.

simulated concrete pore solution for 150 days. Figure 12 shows that OCP values for carbon nanotube/zinc-rich epoxy primer with 60 wt% Zn (CNT-60ZRP) were more positive than the cathodic protection limit, which means that no sacrificial protection was provided to the metal substrate. Following the protection mechanism of CNT-60ZRP, the OCP magnitudes suggest a barrier-type corrosion protection to the carbon steel surface in which the zinc particles were mostly isolated by the epoxy matrix.

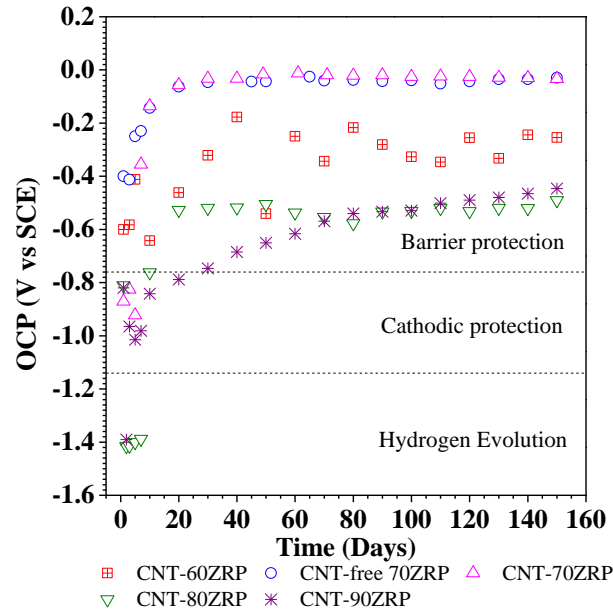


Figure 12. OCP evolution for CNT-ZRPs with different zinc contents immersed in a simulated concrete pore solution with a $[Cl^-]/[OH^-]$ ratio of 1 during 150 days.

In contrast to the case of 60 wt% Zn (CNT-60ZRP), Figure 12 shows that the OCP values for carbon nanotube/zinc-rich epoxy primer with 70 wt% Zn (CNT-70ZRP) were located in the cathodic protection region during the first five days of immersion,

suggesting the presence of cathodic protection and/or zinc dissolution processes. Following five days of immersion, OCP values for CNT-70ZRP shifted rapidly to a more positive magnitude and reached a value close to -0.02 V vs. SCE, which remained constant until the end of the immersion test. To investigate the influence of CNTs in the zinc-rich epoxy primer, OCP values for zinc-rich epoxy primer with 70 wt% zinc and without the presence of carbon nanotubes (CNT-free 70ZRP) are also reported. Figure 12 shows that the potential values for this formulation lie above the cathodic protection region. These results indicate that CNTs improved the electronic connection between the zinc particles allowing to provide cathodic protection to the metallic substrate at least during the first few days of immersion.

Carbon nanotube/zinc-rich epoxy primers with 80 wt% Zn and 90 wt% Zn (CNT-80ZRP and CNT-90ZRP) also exhibited OCP values within the cathodic protection region that remained for longer immersion time. Formulations with higher zinc concentration provided higher galvanic function due to the zinc content and CNTs that can help to improve the electronic contact between the zinc particles and the carbon steel surface. For CNT-80ZRP, Figure 12 shows that the potential decreased rapidly during the first few days of immersion due to electrochemical reactions between the zinc particles and the electrolyte. Abreu et al. [83] defined this period as an activation stage in which native zinc oxide reacts with chloride ions and increases the zinc active area, leading to better electronic connection between the zinc particles and the carbon steel surface.

It is important to notice that between three and seven days of immersion when zinc particles were mostly activated by the electrolyte, the OCP values were more negative than the magnitude for cathodic protection. This suggests that hydrogen reduction was feasible at the metal substrate. After seven days of immersion, the OCP increased into the cathodic protection region, leading to suppression of the hydrogen evolution reaction and the presence of zinc corrosion processes in combination with oxygen reduction reaction. In the same period, the zinc-to-iron area ratio decreased due to the zinc dissolution. Finally, the potential shifted to values above the cathodic protection region and had almost constant magnitude for the rest of the exposure time. This might indicate the presence of a protective layer that isolates the carbon steel surface from the aggressive environment.

For sample CNT-90ZRP, the OCP also decreased below the cathodic protection threshold. As mentioned, this behavior is associated with the hydrogen reduction reaction and available active sites. However, unlike CNT-80ZRP, the potential was below the minimum limit on only the second day of immersion and then shifted to the cathodic protection region. In addition, cathodic protection persisted for a longer time compared to CNT-80ZRP due to the higher amount of electronic pathways that interconnect the zinc particles with the carbon steel surface.

Electrochemical impedance spectroscopy (EIS)

CNT-60ZRP

Figure 13 shows the impedance spectra for CNT-60ZRP at different immersion times. This formulation exhibited almost capacitive behavior during the entire

immersion test with high impedance values at 0.01 Hz (10^9 – 10^{10} ohm-cm²), which means that good barrier protection was provided by the coating system and charge transfer processes did not occur on the carbon steel substrate. This behavior can be attributed to the presence of the epoxy binder with relatively low porosity where zinc particles were highly wetted by the epoxy resin. The anticorrosive properties of these coatings can also be attributed to the presence of CNTs, which can fill in micropores and flaws inside the epoxy binder [23, 24]. Additionally, Jeon et al. [23] reported that CNTs act as adhesion promoters between the epoxy coating and the carbon steel surface, leading to higher resistance to coating delamination and blister formation.

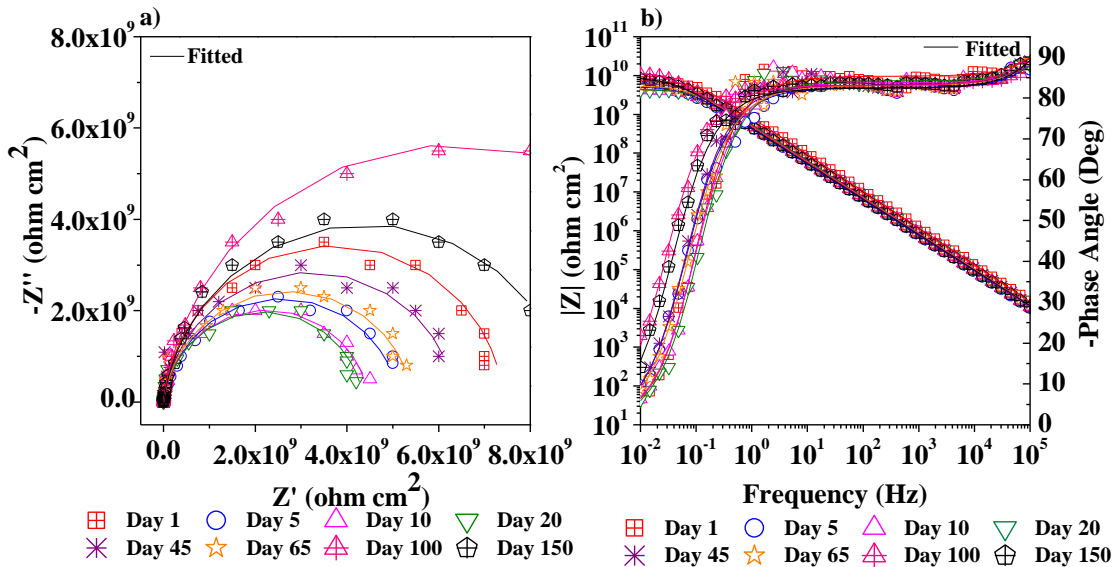


Figure 13. Electrochemical impedance spectra of CNT-60ZRP immersed in a simulated concrete pore solution with a $[Cl^-]/[OH^-]$ ratio of 1 during 150 days: a) Nyquist diagram and b) Bode diagram.

CNT-70ZRP

The impedance spectra for the CNT-70ZRP sample are shown in Figure 14. These results showed capacitive behavior at the initial time, following resistive behavior after the first day of immersion. One possible explanation can be associated to an increase in the porosity of the epoxy binder due to the higher amount of zinc particles. Thus, it could be possible that the amount of CNTs was not sufficient to fill in the majority of pores and therefore, diffusion of electrolyte was observed after a few days of immersion.

Based on the impedance spectra, four different stages were identified during the entire immersion time. The first stage corresponds to the intact condition of the material that was observed only during the first day of immersion. Following this stage, diffusion of electrolyte took place inside the epoxy binder in the second stage. The Nyquist curve showed only one capacitive loop, and the Bode plot exhibited high impedance magnitudes at 0.01 Hz (around 1×10^8 ohm-cm²) that were close to the values reported for organic coatings that provide only barrier protection [66]. Marchebois et al. [52] attributed this capacitive loop in zinc rich epoxy primers with the respective zinc content, to a mixed impedance response considering: the barrier effect of the epoxy binder, contact impedances between the zinc particles due to the presence of zinc oxide that electrically insulates the zinc particles, and electrochemical reactions taking place at the surface of the zinc particles (zinc oxidation and oxygen reduction reaction). They also reported that at the beginning of the immersion time, the influence of the zinc particles in the impedance response was dominated by contact impedances, but the

faradaic processes at the zinc particles became more relevant after several days of immersion [52].

A third stage was identified by the appearance of a second time constant (or loop in the Nyquist representation) at low frequency after 20 days of exposure. This behavior can be explained by the presence of charge transfer processes (zinc dissolution) at the surface of the zinc particles and/or at the metal substrate interface. This is in agreement with the mechanism reported by Marchebois et al. [39].

Finally, the last stage was identified following 100 days of immersion in which a plateau behavior was observed at low frequency (0.1 Hz-1 Hz) in the Bode diagram, and a straight line emerges in the complex representation. This behavior has been associated with a mass transfer mechanism as the control-dominant process within the zinc corrosion products located at the carbon steel surface [52]. Additionally, based on the highly anodic potential of CNT-70ZRP observed during this stage, it is suggested that the diffusion-like behavior at low frequency might be associated to formation of an oxide passive layer on the carbon steel surface due to the high pH of the electrolyte.

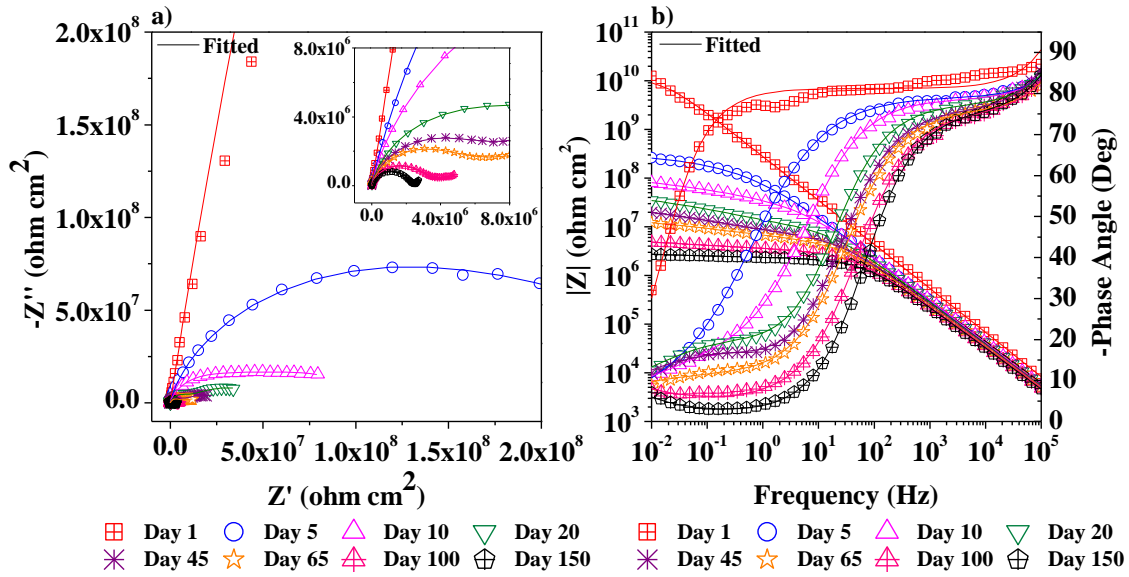


Figure 14. Electrochemical impedance spectra of CNT-70ZRP immersed in a simulated concrete pore solution with a $[Cl^-]/[OH^-]$ ratio of 1 during 150 days: a) Nyquist diagram, and b) Bode diagram.

CNT-80ZRP

Figure 15 shows the impedance spectra for CNT-80ZRP. Following the first day of immersion, the Bode plot (Figure 15b) shows a step-down change in the impedance magnitude at the lowest frequency (0.01 Hz), with a significant decrease between 10^3 and 10^4 ohm cm^2 . This behavior can be associated with a capillary transport mechanism due to high porosity of the coating, which enables high galvanic influence by the zinc particles [84]. However, following 10 days of immersion, the impedance magnitude at 0.01 Hz started to increase due to presence of zinc corrosion products that were formed during the cathodic protection process. This trend was observed during the remaining immersion time, which may indicate that a stable zinc oxide/zinc hydroxide layer was being formed.

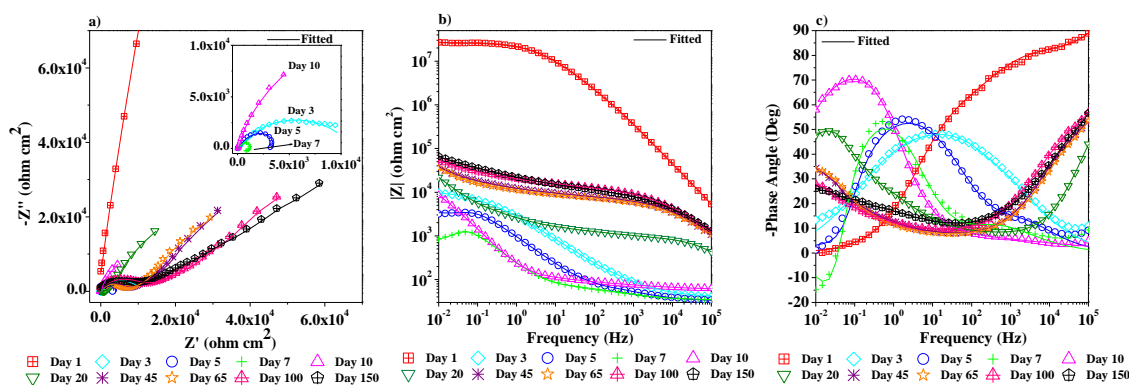


Figure 15. Electrochemical impedance spectra of CNT-80ZRP immersed in a simulated concrete pore solution with a $[Cl^-]/[OH^-]$ ratio of 1 during 150 days: a) Nyquist diagram, b) modulus of impedance, and c) phase angle.

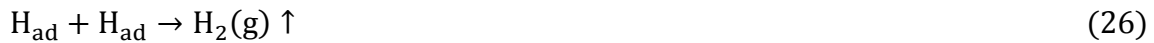
The corrosion degradation mechanism for this formulation was defined in terms of four stages. In the first stage, the complex representation (Figure 15a) produces one semicircle during the first three days of immersion. This can be associated with the mentioned mixed impedance response in which, dielectric properties of the binder, contact impedances, and activation of the zinc particles contribute to the global impedance response.

In the second stage, after five days of immersion, there was a noticeable change in the Nyquist representation (Figure 15a) due to the appearance of two capacitive loops from high to medium frequencies and an inductive loop at the lowest frequencies. This trend was not observed in previous studies on zinc-rich epoxy primers in seawater or 3.5 wt% NaCl solutions [10, 84-86]. However, during this exposure time, the OCP evolution shows that hydrogen reduction reaction could have occurred at the carbon steel surface due to the highly alkaline environment. Therefore, a mechanism involving the hydrogen evolution should be considered.

Alonso et al. [87] studied the risk of hydrogen embrittlement in galvanized reinforcing steel exposed to alkaline solutions. They reported that between pH 12.5 and 13.5, zinc oxidation takes place in the presence of hydrogen evolution according to the following reaction:



where the hydrogen evolution proceeds in the following sequence of reactions:



From this mechanism, it can be suggested that the capacitive loop at the highest frequencies represents the dielectric properties of the epoxy binder, the capacitive loop observed from high to medium frequencies describes the zinc dissolution process accompanied by the hydrogen reduction reaction (reaction 24), and the inductive loop at the lowest frequencies can be associated with adsorption of hydrogen in the metallic substrate (reaction 25). Based on the OCP results, hydrogen evolution reaction was observed for seven days of immersion, and then, the potential increased above of the threshold magnitude into the cathodic protection region. This behavior agrees with the signal change in the Nyquist representation for 10 days of exposure, where the inductive loop disappeared and another capacitive loop started to develop at the highest frequencies.

This behavior represents the third stage in the corrosion degradation mechanism of this coating system. Cathodic protection was active in this stage, meaning that zinc dissolution occurred on the zinc particle surfaces while oxygen reduction reaction took

place at the carbon steel surface. In addition to the capacitive loops representing the barrier properties of the coating, and the galvanic function provided by the zinc particles, the capacitive loop that started to develop at the highest frequency was related to the formation of a layer of zinc corrosion products due to the cathodic protection process.

Finally, in the fourth stage, two semicircles were observed at medium to high frequencies with one large semicircle at the lowest frequency following 20 days of exposure, when cathodic protection was no longer effective. As mentioned, the semicircle at the highest frequency was associated with the formation of a protective layer that provided an extra barrier to subsequent permeation of oxygen and ionic species. This semicircle increased over time, which could be related to continued growth of the protective layer. The loop at middle frequencies represents the barrier properties of the coating, which also increased over time due to the protective layer of zinc corrosion products that it was primarily formed at the coating-electrolyte interface. Finally, the third time constant at low frequency was related to a self-corrosion process of the zinc particles that were not involved in the cathodic protection process. In this process, both zinc dissolution and oxygen reduction reaction occurred on the zinc particle surfaces.

CNT-90ZRP

Figure 16 shows the impedance results for CNT-90ZRP at different exposure times in the simulated concrete pore solution. The evolution of the impedance spectrum for CNT-90ZRP was similar to that of the CNT-80ZRP sample. Nevertheless, several differences from the previous formulation were noticed; these differences are worth to

be mentioned. An activation stage was not detected; this activation refers to the first stage of the corrosion degradation mechanism for CNT-80ZRP in which the resistance of the epoxy binder and contact impedances were dominant. This can be attributed to the excessive porosity of the epoxy binder due to high amount of zinc particles, which allowed for instant diffusion of electrolyte and therefore, faster activation of the zinc particles that probably occurred within the first few hours after immersion.

The impedance signal associated with the hydrogen evolution reaction was only observed during the second day of immersion (i.e., the capacitive loops from high to medium frequencies and the inductive loop at the lowest frequencies). This is also in agreement with the OCP values in which the open circuit potential was below the minimum value for cathodic protection during only the second day of exposure. This means that the interruption of the hydrogen evolution reaction was faster compared to the sample containing 80 wt% zinc. Additionally, the cathodic protection stage (third stage of the corrosion degradation mechanism for CNT-80ZRP) remained for longer time compared to the previous coating, which is expected due to higher amount of zinc particles in the epoxy binder. This higher zinc content increases the likelihood of forming more electronic pathways, either by direct contact between zinc particles or interconnection of zinc particles by CNTs, which allow higher electron transfer between zinc particles and the carbon steel surface. The impedance response in the fourth stage, showing three capacitive loops that correspond to the protective layer of zinc corrosion products, barrier properties of the epoxy binder, and electrochemical reactions on the zinc particle surfaces, were also observed for CNT-90ZRP, indicating that the

predominant corrosion protection mechanism corresponds to cathodic protection provided to the metallic substrate.

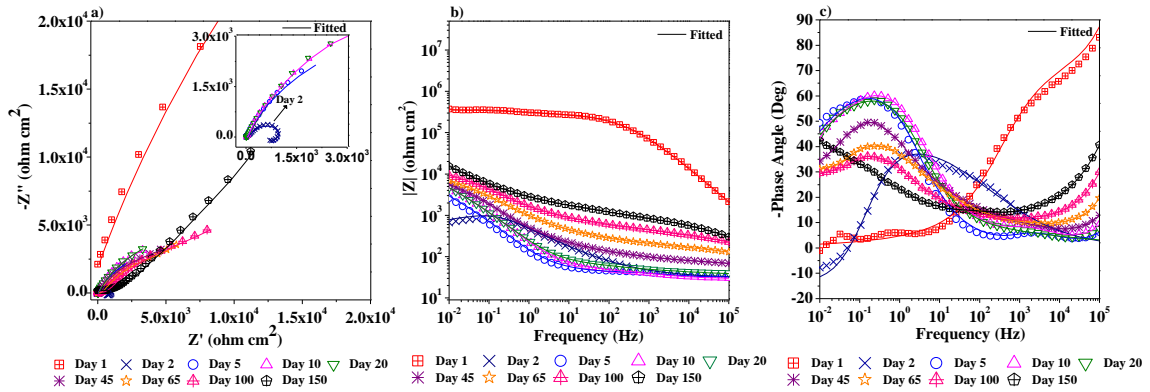


Figure 16. Electrochemical impedance spectra of CNT-90ZRP immersed in a simulated concrete pore solution with a $[Cl^-]/[OH^-]$ ratio of 1 during 150 days: a) Nyquist diagram, b) modulus of impedance, and c) phase angle.

Equivalent electrical circuits

Equivalent circuits were used to reproduce the EIS signal of the different coating systems. Figure 17 shows the equivalent circuit used for CNT-60ZRP, in this circuit, R_s corresponds to the resistance of the electrolyte, C_c represents the coating capacitance, and R_c describes the corrosion resistance of the zinc-rich epoxy material. This equivalent circuit was used for CNT-60ZRP during the entire immersion period, since high impedance magnitudes at 0.01 Hz were observed and only one time constant was identified in the entire frequency range, suggesting a good barrier protection provided by this coating system. A constant phase element (CPE) was used instead of capacitance in

order to consider the deviation of the coating systems from ideal capacitive behavior.

The impedance for the CPE (Z_{CPE}) has been defined as follows:

$$Z_{CPE} = \frac{1}{Y_0(j\omega)^\alpha} \quad (26)$$

Where Y_0 corresponds to the admittance, α represents an empirical exponent associated to the constant phase element, j is the imaginary number, and ω is the angular frequency.

The effective capacitance C_{eff} is associated with the CPE and was calculated based on the expression reported by Orazem et al [65]:

$$C_{eff} = Y_0^{1/\alpha} R_c^{(1-\alpha)/\alpha} \quad (27)$$

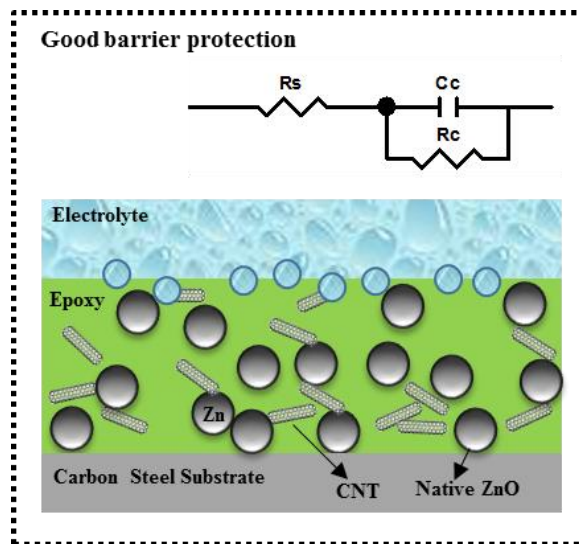


Figure 17. Equivalent electrical circuit describing the impedance spectra of CNT-60ZRP immersed in a simulated concrete pore solution with a $[Cl^-]/[OH^-]$ ratio of 1 for 150 days.

Figure 18 shows high coating resistance (R_c) values for CNT-60ZRP close to 10^{10} ohm cm^2 , with no significant change in its magnitude during the entire exposure time. In addition, it can be also notice that the $C_{c,\text{eff}}$ values for the CNT-60ZRP sample did not change considerably during the complete immersion time. Since the magnitudes of R_c and $C_{c,\text{eff}}$ are related to the coating porosity and the diffusion of electrolyte inside the coating [66, 88], these results suggest that the CNT-60ZRP system remained almost intact during the entire immersion time.

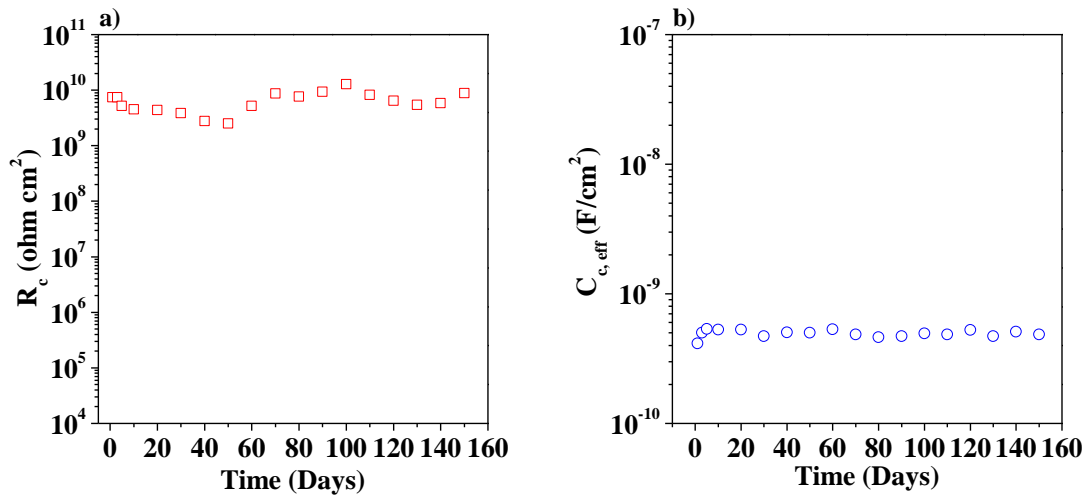


Figure 18. Equivalent circuit elements for CNT-60ZRP immersed in a simulated concrete pore solution with a $[\text{Cl}^-]/[\text{OH}^-]$ ratio of 1 for 150 days: a) coating resistance, and b) coating capacitance.

Figure 19 shows electrical equivalent circuits describing the impedance spectra of CNT-70ZRP. The equivalent circuit shown in Figure 19a was used to describe the almost intact condition during the first day of immersion. This equivalent circuit is

similar to the one used for CNT-60ZRP. Figure 19b shows the equivalent circuit that describes the diffusion of electrolyte through the epoxy material and the activation of the zinc particles by the electrolyte solution. R_c and C_c combine the barrier properties of the epoxy matrix with influence of contact impedances between the zinc particles, and $R_{ct,1}$ and $C_{dl,1}$ are associated to faradaic processes between zinc particles and electrolyte. The equivalent circuit in Figure 19c describes the stage in which a second time constant at low frequency was observed in the impedance spectra. $R_{ct,2}$ and $C_{dl,2}$ correspond to the charge transfer resistance and the double layer capacitance associated to electrochemical processes such as dissolution of the zinc particles that did not contribute to the cathodic protection process or interaction between the electrolyte and the carbon steel substrate. Finally, the equivalent circuit shown in Figure 19d describes the last stage of the mechanism of corrosion protection of this coating system, in which the impedance magnitude at 0.01 Hz remained constant and a diffusion-like behavior was identified in the Nyquist representation. This behavior was associated with the formation of zinc corrosion products that provided additional barrier protection to the carbon steel surface and the formation of a passive layer at the carbon steel surface due to the high pH of the electrolyte solution. A Warburg element (W_s) was included in Figure 19d describing the mass transport process occurring at the carbon steel/coating interface.

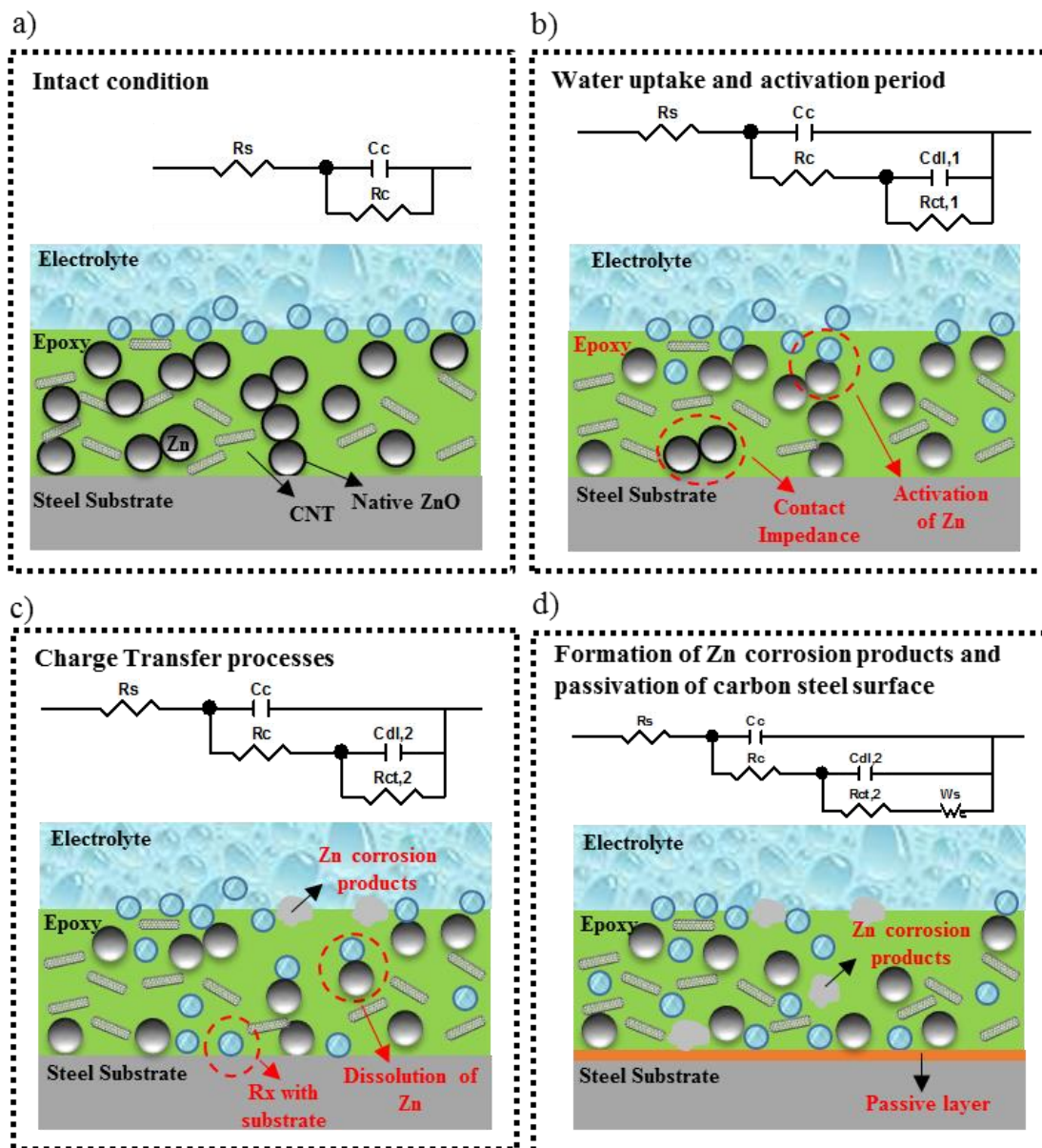


Figure 19. Equivalent electrical circuits describing the impedance spectra of CNT-70ZRP immersed in simulated concrete pore solution with a $[Cl^-]/[OH^-]$ ratio of 1 for 150 days.

Figure 20a shows that R_c continuously decreased during the first three stages owing to the diffusion of electrolyte through the epoxy material that modified the

dielectric properties of the coating and reduced the contact impedances between the zinc particles. During the last stage, R_c remained almost constant due to the formation of zinc corrosion products that slowed down the additional permeation of water and ionic species, or passivation of the carbon steel surface by the alkaline environment that provides an additional barrier layer to protect the metal substrate. The $C_{c,eff}$ values shown in Figure 20b slightly increased during the first few days of immersion due to diffusion of electrolyte that increased the dielectric constant of the coating system (proportional to its capacitance), and then, they remained almost constant due to saturation of the epoxy material with the electrolyte. These coating capacitance values were slightly higher than the corresponding values for CNT-60ZRP. This behavior is expected since the higher zinc content in CNT-70ZRP increased the porosity of the epoxy binder allowing higher penetration of electrolyte through the coating system that increased its dielectric constant and hence, its capacitance.

Figure 20c shows the evolution of charge transfer resistance in CNT-70ZRP. R_{ct} decreased during the second stage due to electrochemical reactions between the zinc particles and the electrolyte providing cathodic protection to the metal substrate. These R_{ct} values also decreased during the third stage due to dissolution of the zinc particles that did not contribute to the cathodic protection process and/or charge transfer processes at the metal substrate. Finally, R_{ct} values remained almost constant in the last stage owing to the formation of zinc corrosion products and passivation of the carbon steel surface. These charge transfer resistance values are complemented with the capacitance values reported in Figure 20d. It can be seen that C_{dl} values increased during the second

stage due to activation of the zinc particles by the electrolyte solution that increased the zinc active area that was available to provide cathodic protection. C_{dl} values also increased during the third stage owing to electrochemical reactions between the carbon steel substrate and the electrolyte that increased the active area of the metal substrate. In contrast, C_{dl} values decreased during the last stage due to formation of a passive oxide layer at the metal surface and zinc corrosion products that decreased the available area for charge transfer processes.

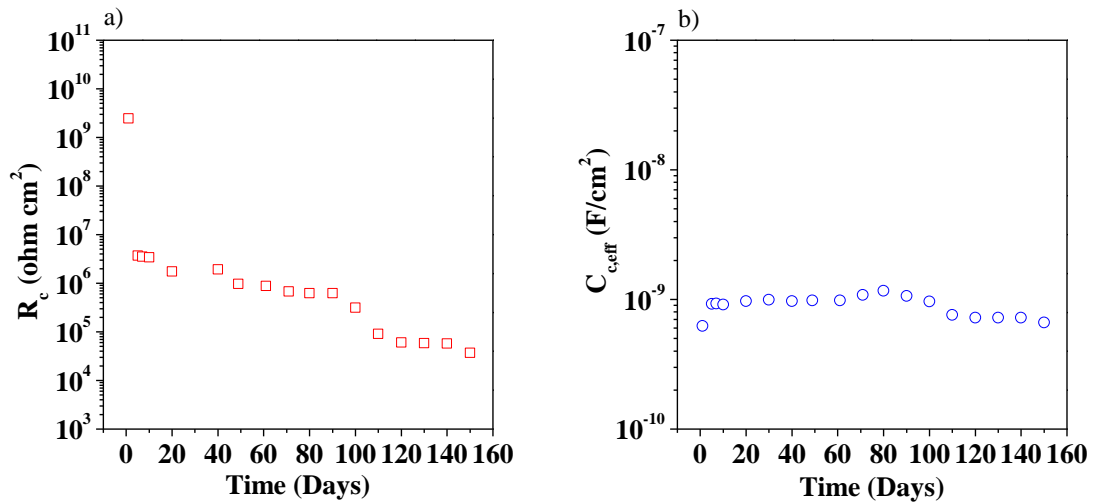


Figure 20. Equivalent circuit elements for CNT-70ZRP immersed in a simulated concrete pore solution with a [Cl⁻]/[OH⁻] ratio of 1 for 150 days: a) coating resistance, b) coating capacitance, c) charge transfer resistance, and d) double layer capacitance.

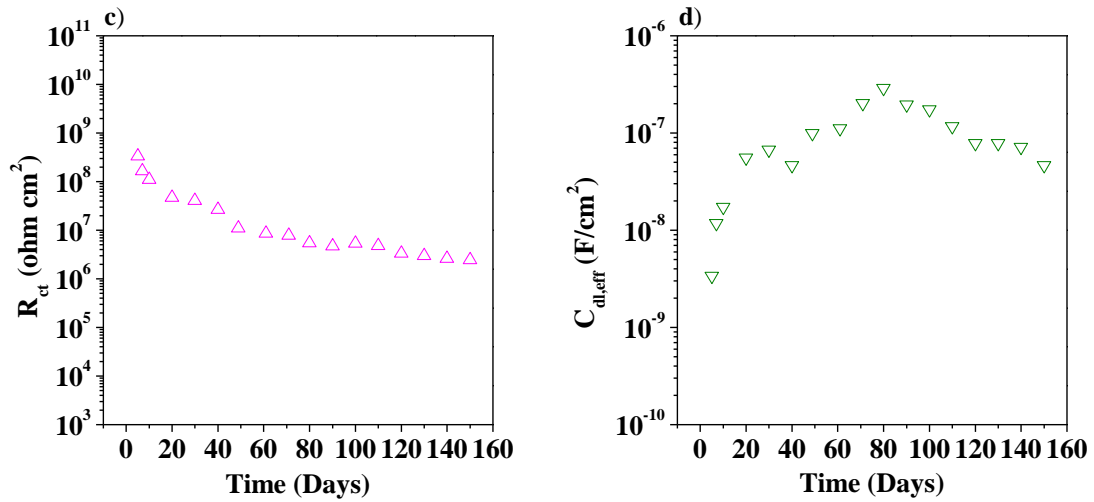


Figure 20. Continued

Figure 21 shows the equivalent circuits proposed for CNT-80ZRP and CNT-90ZRP. The equivalent circuit in Figure 21a describes the activation stage of the zinc particles. R_s represents the electrolyte resistance, while C_c and R_c describe the capacitance and the resistance of the epoxy binder including the contact impedances due to the presence of native zinc oxide on the zinc particle surfaces. $C_{dl,1}$ and $R_{ct,1}$ represent faradaic processes between the zinc particles and the ionic species. The equivalent circuit in Figure 21b describes the cathodic protection in the presence of hydrogen evolution reaction associated with adsorption of hydrogen on the metal substrate. $C_{dl,2}$ and $R_{ct,2}$ represent the zinc dissolution process in the presence of hydrogen evolution, and L and R_L describe the inductance and the resistance associated with the adsorption process of hydrogen on the carbon steel surface. The cathodic protection mechanism involving zinc dissolution in the presence of oxygen reduction reaction can

be described by the equivalent circuit shown in Figure 21c, where $C_{dl,3}$ and $R_{ct,3}$ are associated with the electrochemical process of zinc dissolution on the zinc particle surfaces and oxygen reduction on the carbon steel surface. C_{ox} and R_{ox} are related to the formation of zinc corrosion products on the coating/electrolyte interface. Finally, the equivalent circuit in Figure 21d represents the barrier protection period in which a layer of zinc corrosion products is formed at the top of the coating surface and cathodic protection is no longer effective. $C_{dl,4}$ and $R_{ct,4}$ represent the zinc dissolution processes in the presence of oxygen reduction reaction both taking place on the zinc particle surfaces. This process might be controlled by mass transfer through the zinc corrosion products formed on the surface of the particles, hence, a Warburg impedance was added to account for radial diffusion of ionic species through these corrosion products.

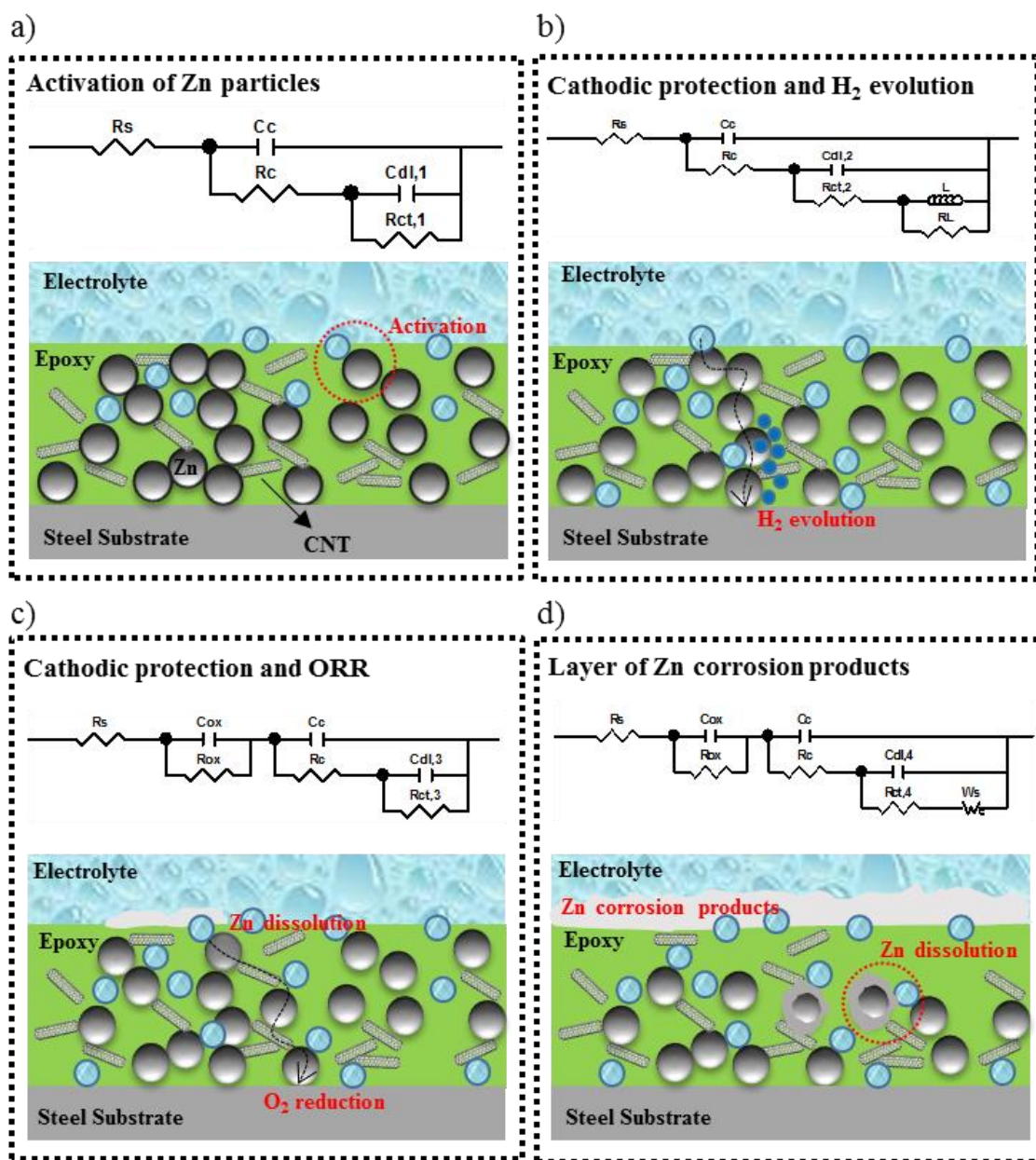


Figure 21. Equivalent electrical circuits describing the impedance spectra of CNT-80ZRP and CNT-90ZRP immersed in a simulated concrete pore solution with a $[Cl^-]/[OH^-]$ ratio of 1 for 150 days.

Figure 22a shows the evolution of different equivalent circuit elements for CNT-80ZRP. These results show that R_c decreased during the first two stages identified from

the EIS spectra that corresponds to the activation of the zinc particles and the cathodic protection process in the presence of the hydrogen evolution reaction. This trend was expected since rapid diffusion of electrolyte across the coating system caused activation of zinc particles (due to dissolution of native zinc oxide by the electrolyte) which increased the electrical conductivity of the epoxy coating. R_{ct} also decreased due to faradaic processes between zinc particles and ionic species that increased the zinc-to-steel area ratio, which means that more zinc active area was created for the cathodic protection process.

During the cathodic protection process in presence of oxygen evolution reaction (third stage), R_c increased drastically due to formation of zinc corrosion products on the coating surface that prevented additional permeation of electrolyte. R_{ct} also increased due to loss of electronic connection between the zinc particles, which decreased the galvanic function provided by the zinc particles in direct contact with them and with the carbon steel surface. During the last stage, in which zinc particles no longer provided cathodic protection, R_{ct} , R_c , and R_{ox} remained almost constant due to formation of a layer of zinc corrosion products on the coating surface, which slowed down the corrosion degradation process.

Similar behavior was observed for CNT-90ZRP, as shown in Figure 22b. Nevertheless, it can be seen that the cathodic protection period was extended compared to CNT-80ZRP sample due to the higher amount of zinc particles. In addition, unlike the R_{ct} evolution for CNT-80ZRP, the R_{ct} values for CNT-90ZRP increased during the last stage even though the cathodic protection process was no longer active. This behavior

can be explained by the higher influence of dissolution processes of the zinc particles in the presence of oxygen reduction reaction taking place on the surface of the zinc particles.

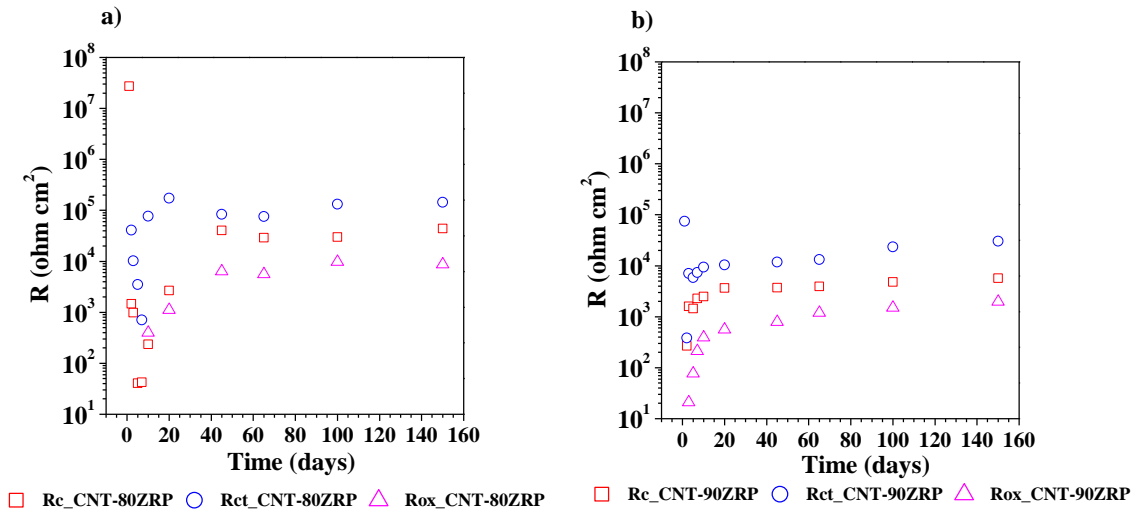


Figure 22. Equivalent circuit elements for CNT-80ZRP and CNT-90ZRP immersed in a simulated concrete pore solution with a $[\text{Cl}^-]/[\text{OH}^-]$ ratio of 1 for 150 days: a) CNT-80ZRP, and b) CNT-90ZRP .

Coating resistance values were used to compare the differences between the CNT-ZRP systems and the result of this comparison are shown in Figure 23. Three noticeable electrochemical behaviors are observed: A pure barrier protection mechanism (CNT-60ZRP), a mixed corrosion protection mechanism (CNT-70ZRP), and a cathodic protection mechanism (CNT-80ZRP and CNT-90ZRP).

The impedance signal for CNT-60ZRP describes a pure barrier protection, where R_c evolution exhibited high values during the entire exposure time. The impedance

behavior can be explained by the low porosity of the epoxy binder and the influence of the CNTs as pore fillers.

There is no predominant mechanism for CNT-70ZRP and a mixed corrosion protection was observed. The mixed response is attributed to the presence of: a) barrier protection provided by the epoxy binder, and b) cathodic protection (or self-dissolution of zinc) provided by the zinc particles. R_c values decreased during 100 days of immersion due to diffusion of electrolyte and zinc particle dissolution. After 100 days of immersion, R_c remained constant due to the presence of zinc corrosion products in the epoxy coating. In Figure 23, R_c values for CNT-free 70ZRP are also reported along with the results for CNT-70ZRP; these values in absence of CNTs were significantly lower than when CNTs were added. This behavior suggests that CNTs improved the overall anticorrosive performance of the zinc rich-epoxy primer.

The impedance signal for CNT-80ZRP and CNT-90ZRP describes a predominant cathodic protection mechanism caused by the high concentration of zinc particles embedded in the epoxy. The low R_c values observed during the first few days of immersion are caused by the high galvanic action produced by the elevated concentration of zinc particles which, also induced the formation of a protective layer that provided extra protection to the carbon steel surface, manifested in a subsequent increase in the R_c values. CNT-90 ZRP exhibited lower R_c values compared to CNT-80ZRP due to higher amount of zinc particles that increased the porosity of the epoxy coating leading to higher diffusion of the electrolyte and lower corrosion resistance of the material. Additionally, higher amount of zinc particles increased the electronic

conductivity of the coating system that facilitated the charge transfer processes between them and with the carbon steel surface. These findings could be related to results reported by Shreepathi et al. [89], who studied the influence of zinc content on corrosion protection mechanisms of zinc-rich epoxy coatings in 3.5% NaCl. They found that coatings with 40 wt% Zn provide excellent barrier protection, while coatings with 80 wt% Zn and 90 wt% Zn offer sacrificial protection. In addition, they also reported that intermediate zinc contents (60 wt% Zn and 70 wt% Zn) did not provide clear evidence of dominance by one of these specific control actions.

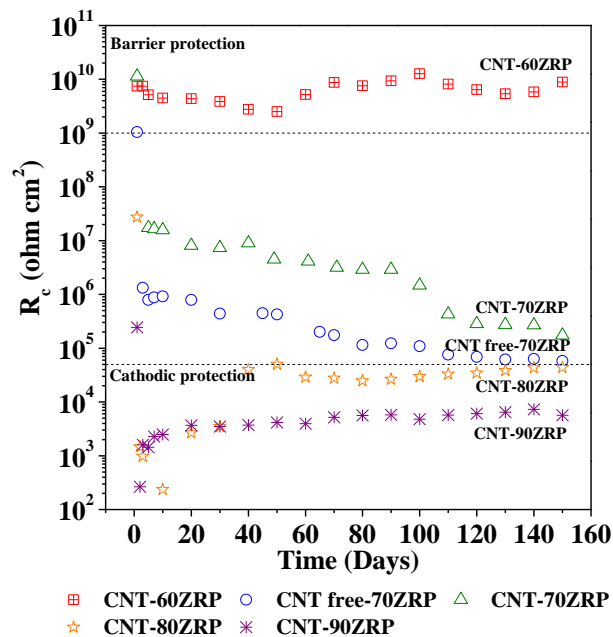


Figure 23. Evolution of coating resistance (R_c) for the different CNT-ZRP systems immersed in a simulated concrete pore solution with a $[Cl^-]/[OH^-]$ ratio of 1 for 150 days.

Local electrochemical impedance spectroscopy (LEIS)

Since cathodic protection was provided by CNT-80ZRP and CNT-90ZRP, localized electrochemical impedance spectroscopy measurements were performed on a scratched CNT-90ZRP sample to investigate the electrochemical performance of the coating sample when damage is induced and the carbon steel surface is completely exposed to a 0.005 M NaCl solution. Figure 24a shows the LEIS spectra for CNT-90ZRP at different immersion times. This figure shows that the local impedance spectra in the scratched area was slightly lower than in the coated areas in the first five hours of exposure. An iron dissolution process was associated with this behavior since red spots were found after the exposure time. However, the local impedance in the damaged area was higher compared to the intact areas after 10 hours of exposure. This can be explained by the cathodic protection provided by the zinc particles in the epoxy binder in which zinc dissolution occurs on the intact coating, while oxygen reduction reaction occurs in the scratched area.

It is important to mention that the zinc particles were not only embedded in the epoxy but also surrounded by a zinc oxide layer, as it can be observed in the SEM images; therefore, the activation of the zinc particles as cathodic protection providers was delayed compared to the dissolution of the steel which occurs almost instantaneously. Once the zinc particles are activated and providing cathodic protection, the prior steel dissolution cannot be reverted. This is the reason why, even though the zinc particles were providing cathodic protection to the carbon steel surface after 10 hour of immersion, iron corrosion products were still found on the scratched area. It is also

important to mention that the extent of iron corrosion products on the defect was considerably lower than that of the zinc corrosion products.

Finally, after 35 hours of immersion, the local impedance between the intact and damaged areas were similar to each other. This means that zinc corrosion products were formed on the scratched area, which provided a temporary blockage for further corrosion degradation processes on the carbon steel surface; these Zn corrosion products can be observed in the optical and 3D images (Figure 24b).

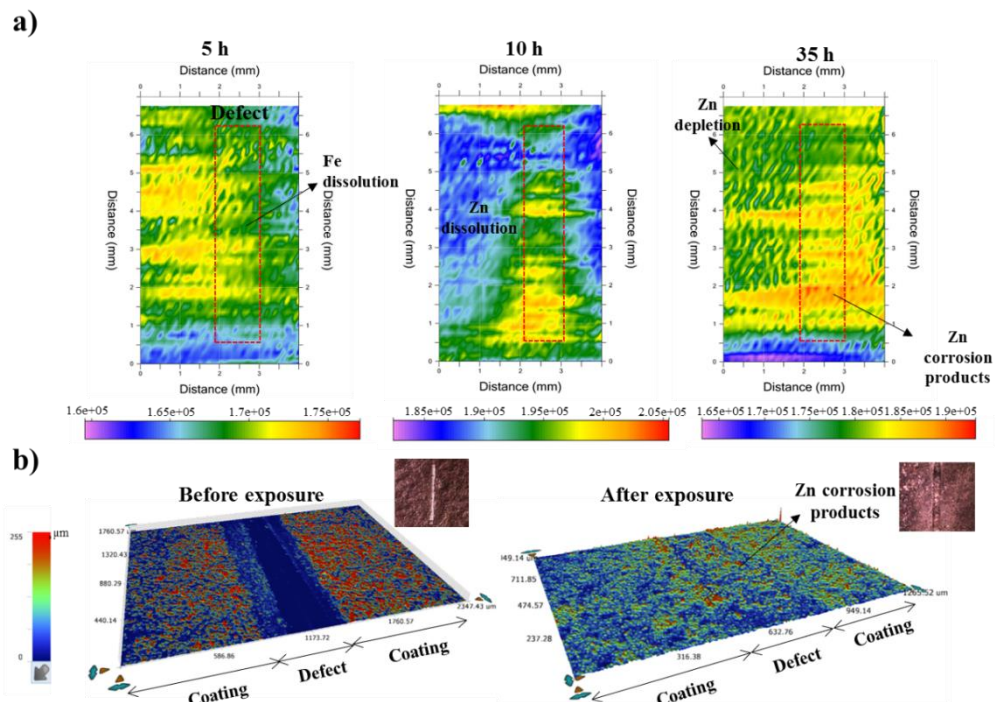


Figure 24. Local electrochemical impedance spectroscopy (LEIS) results for a scratched CNT-90ZRP sample immersed in 0.005M NaCl during 48 hours. a) LEIS spectra at 5h, 10h, and 35h after immersion b) 3D microscope images of the sample before and after exposure.

Morphology characterization

Figure 25 shows cross-section and surface-view SEM images for CNT-60ZRP before and after immersion for 90 days in the electrolyte solution. The cross-section images (Figure 25a and Figure 25b) show that there was no significant change of the coating system during 90 days of exposure. This indicates that CNT-60ZRP provided a predominant barrier corrosion protection. It is evident from the images that there was no attack on the carbon steel surface. Figure 25c shows the coating surface of CNT-60ZRP after 90 days of exposure. The coating surface showed the presence of precipitates. EDS analysis was performed in region 1, and the results are reported in Table 5. The results show that this region contains mostly oxygen and calcium, which means that calcium hydroxide ($\text{Ca}(\text{OH})_2$) was precipitated from the simulated concrete pore solution. No sign of zinc corrosion products was detected, proving that zinc particles were completely isolated by the epoxy resin.

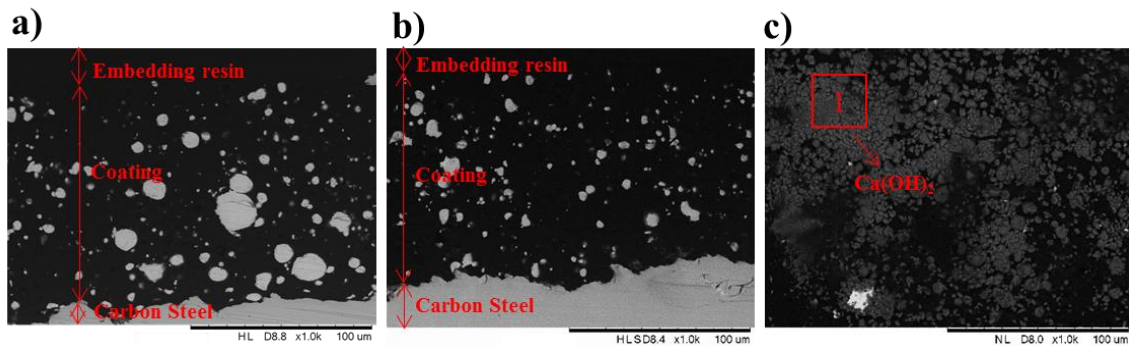


Figure 25. Cross-section and coating surface images for CNT-60ZRP exposed to the simulated concrete pore solution: a) cross-section of the intact coating, b) cross-section of the coating exposed for 90 days, and c) surface-view of the coating exposed for 90 days.

Table 5. EDS results (atomic percent) at indicated locations in the SEM images for the different CNT-ZRP systems immersed in the simulated concrete pore solution.

Coating	Day	Region	Zn	Fe	O	Cl	Na	Ca	K
CNT-60ZRP	90	1	1.15	-	74.52	0.28	1.12	22.62	0.31
		1	15.53	0.79	61.74	0.22	21.23	0.04	0.45
CNT-70ZRP	90	2	37.31	-	46.90	8.34	7.42	0.03	0
		3	29.70	-	52.43	0.54	15.90	0.00	1.43
CNT-free 70ZRP	90	1	3.21	-	71.39	1.21	6.68	16.39	1.12
		2	4.77	76.27	12.48	2.10	3.77	0.17	0.44
		1	64.91	-	10.1	0.79	24.15	0	0.05
CNT-80ZRP	90	2	31.19	-	42.32	8.89	17.51	0.09	0
		3	28.59	-	54.37	1.97	13.71	1.15	0.22
		4	30.27	-	59.91	0.53	8.26	0.48	0.55
CNT-90ZRP	90	5	37.02	-	42.62	0.45	18.04	0.66	1.22
		1	25.5	-	58.11	2.62	13.77	0	0
		2	54.02	-	27.53	0.96	17.44	0.05	0
CNT-90ZRP	90	3	29.68	-	51.34	6.89	11.67	0.24	0.19
		4	39.64	-	39.58	0.7	18.56	0.37	1.16
		5	33.42	-	48.93	1.01	15.75	0	0.89

Figure 26 shows morphology images of CNT-70ZRP and CNT-free 70ZRP at different immersion times. Figure 26a shows the cross-section image of the intact CNT-70ZRP in which it can be noticed that zinc particles were not in direct contact with each other. After 5 days of immersion (Figure 26b), the zinc oxide was removed from the surface of the zinc particles due to interaction with the electrolyte, which means that activation of the zinc particles occurred during this immersion period. Following 90 days of immersion, the cross-section image (Figure 26c) shows that zinc corrosion products accumulated in the epoxy binder and at the carbon steel surface.

Table 5 shows the elemental composition of regions 1 and 2 in Figure 26c. Zinc and oxygen were the primary elements in these regions, suggesting that zinc oxides/hydroxides were formed from electrochemical reactions between the zinc particles and the electrolyte (cathodic protection and zinc dissolution processes). The zinc corrosion products on the carbon steel surface can be responsible for the diffusion-like behavior observed in last stage and the stabilization of the R_c values after 100 days of immersion. Unfortunately, it was not possible detecting the presence of a passive oxide layer at the carbon steel substrate due to the poor resolution of the instrument.

The coating surface image (Figure 26d) following 90 days of immersion shows that zinc corrosion products were also formed at the coating surface. Table 5 shows their atomic composition, which was mainly oxygen and zinc. This also suggests the formation of zinc oxide/zinc hydroxide corrosion products. No iron corrosion products were observed at the carbon steel surface following 90 days of exposure. Therefore, from electrochemical and morphology analysis, it can be concluded that CNT-70ZRP has an efficient balance between physical barrier and cathodic protection.

SEM images are also reported for CNT-free 70ZRP. Figure 26e shows the coating surface after 90 days of exposure. The EDS results in Table 5 show that region 1 corresponds only to precipitates of calcium hydroxide, but there is no evidence of zinc corrosion products. Figure 26f shows the cross-section image for this formulation after 90 days of immersion. Zinc corrosion products were not found, but there was a high amount of iron corrosion products at the carbon steel surface. Table 5 reveals the elemental composition of region 2 and shows high atomic composition of iron and

oxygen. These results demonstrate that CNTs had a positive effect on the anticorrosive performance of zinc-rich epoxy primers since they could improve the barrier properties of the epoxy binder. They could also enhance the electrical conductivity in the epoxy coating and allow the zinc particles to provide sacrificial action to the metallic substrate.

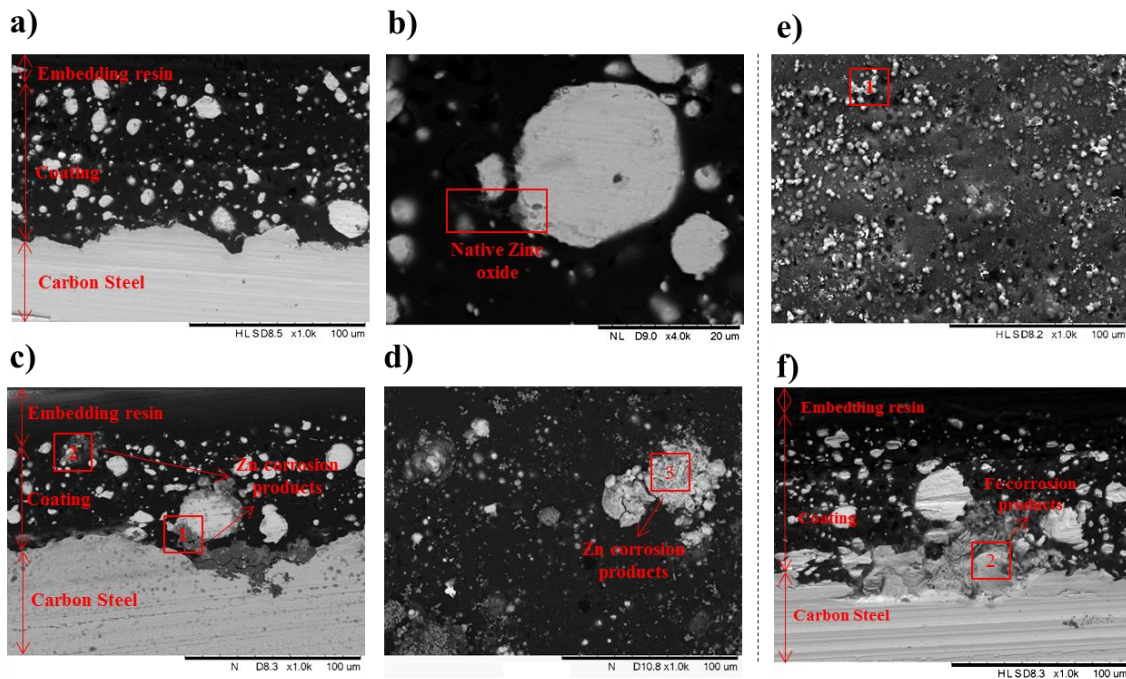


Figure 26. Cross-section and coating surface images for CNT-70ZRP exposed to the simulated concrete pore solution at different immersion times: a) cross-section of intact coating, b) cross-section after 5 days of immersion, c) cross-section after 90 days of immersion, d) surface-view after 90 days of immersion, e) surface-view of CNT-free 70ZRP after 90 days of immersion, and f) cross-section of CNT-free 70ZRP after 90 days of immersion.

SEM images for CNT-80ZRP are presented in Figure 27. The intact coating image (Figure 27a) shows higher accumulation of zinc particles in the epoxy binder compared to the previous formulations; however, some of them were not in direct

contact with each other. This suggests that there was a limited electrical connection between the zinc particles and the carbon steel surface. Figure 27b shows that large regions with empty spaces were created in the epoxy binder following 20 days of immersion. This behavior can be explained by the cathodic protection process in which zinc dissolution takes place at the zinc particle surfaces while hydrogen evolution or oxygen reduction reaction occur at the metal substrate.

In addition, it can be noticed the presence of a layer of zinc corrosion products formed at the coating surface. Abreu et al. [84] reported that this layer is formed as a consequence of the galvanic corrosion process in which the OH^- ions produced at the carbon steel surface due to reduction reaction and Zn^{2+} ions from zinc dissolution diffuse to balance the total charge in the epoxy coating. They then precipitate and form a barrier layer of zinc corrosion products at the coating/electrolyte interface.

CNTs could improve the effectiveness of the cathodic protection process by increasing the electrical contact between the zinc particles and the metal substrate. During the exposure time, the layer of zinc corrosion products became thicker. Following 90 days of immersion (Figure 27c), the layer reached an average thickness of 20 μm . In addition to the barrier layer at the coating surface, zinc corrosion products were also formed on the zinc particle surfaces. This indicates self-corrosion processes of the zinc particles that were not involved in the galvanic function.

The top-view image of CNT-80ZRP exposed for 90 days (Figure 27d) shows that the coating surface was completely covered by zinc corrosion products. Table 5 shows atomic compositions of different morphologies identified from SEM images after 90

days of exposure. These results show that region 1 was enriched with zinc while region 2 was balanced between zinc and oxygen. This demonstrates the self-dissolution process of the zinc particles in the presence of oxygen reduction reaction, which induces the formation of zinc corrosion products at the surface of the zinc particles. Additionally, different Zn/O ratios were found in regions 3, 4, and 5, suggesting that the barrier layer was a combination of different zinc corrosion products.

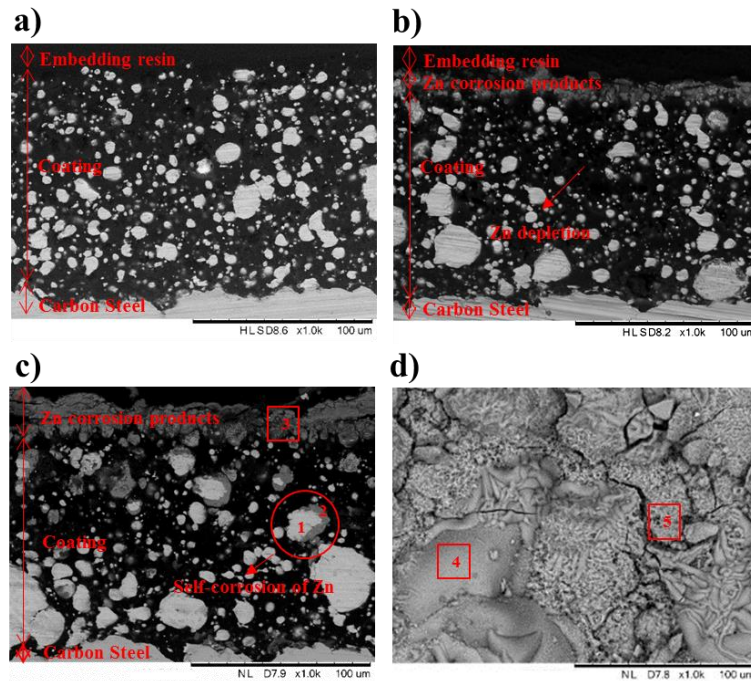


Figure 27. Cross-section and coating surface images for CNT-80ZRP exposed to the simulated concrete pore solution at different immersion times: a) cross-section of intact coating, b) cross-section after 20 days of immersion, c) cross-section after 90 days of immersion, and d) surface-view after 90 days of immersion.

As mentioned in the analysis of the impedance spectra, the corrosion process for CNT-90ZRP was similar to the one for CNT-80ZRP. This is in agreement with the

evolution in SEM images shown in Figure 28 and the EDS results reported in Table 5. Cross-section and surface-view coating micrographs showed almost the same morphology at different exposure times as the one observed for CNT-80ZRP, however, it is evident that after 90 days of immersion, the layer of zinc corrosion products is thicker than the one formed in the CNT-80ZRP coating system.

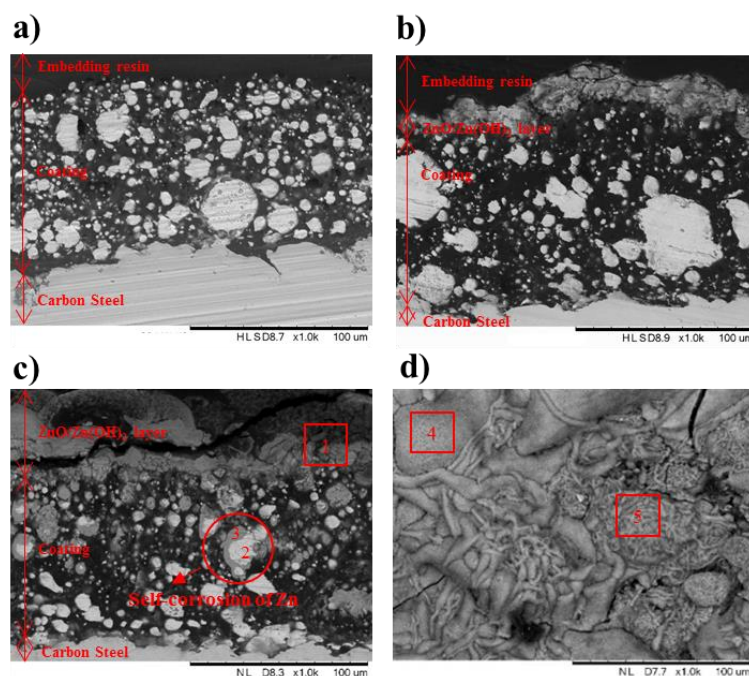


Figure 28. Cross-section and coating surface images for CNT-90ZRP exposed to the simulated concrete pore solution at different immersion times: a) cross-section of intact coating, b) cross-section after 20 days of immersion, c) cross-section after 90 days of immersion, and d) surface-view after 90 days of immersion.

X-ray photoelectron spectroscopy (XPS)

XPS analysis was performed to identify the elemental and chemical composition at the coating surface for different formulations before and after immersion in the

simulated concrete pore solution. The results indicate the presence of zinc corrosion products at the coating surface and their corresponding chemical nature. The survey spectrum provided a qualitative description of the elements at the coating surface. The corresponding high-resolution spectra for Zn 2p_{3/2}, C 1s, and O 1s allowed for identification of the chemical states and quantification of their compositions.

Table 6. Chemical compositions for the different CNT-ZRPs based on high-resolution spectra for C 1s, O 1s, and Zn 2p_{3/2}.

photoelectron peak	Specie	Binding Energy	CNT-60ZRP		CNT-70ZRP		CNT-80ZRP		CNT-90ZRP	
			Atomic composition (%)		Atomic composition (%)		Atomic composition (%)		Atomic composition (%)	
			Intact coating	Exposed coating	Intact coating	Exposed coating	Intact coating	Exposed coating	Intact coating	Exposed coating
C 1s	C-C/C-H	285	76.67	37.02	69.76	33.80	76.88	34.6	24.48	19.87
	C-O	286.5	16.55	39.24	23.89	37.18	17.21	10.22	31.59	23.78
	C=O	287.91	6.78	18.27	6.35	17.60	5.91	18.18	27.97	29.94
	COO	288.8		5.46		8.77		21.39	15.96	19.41
	hydrozincite	290.97				2.66		15.62		6.99
O 1s	C-O	533.34	63.6	57.41	67.88	25.94	63.99	25.24	67.32	36.17
	C=O	534.77	36.4	13.01	32.12	27.87	36.01	25.31	32.67	12.96
	COO	532		29.58		12.34		2.29		0.92
	ZnO	529.92				12.66		21.95		20.48
	Zn(OH) ₂	531.7				7.83		8.19		11.17
Zn 2p _{3/2}	hydrozincite	531.4				13.36		7.62		18.30
	Zn	1019.3				8.53		13.39		14.89
	ZnO	1020.1				16.03		26.65		20.07
	Zn(OH) ₂	1023.9				38.03		30.84		28.94
	hydrozincite	1022.04				37.41		17.01		36.09

Figure 29 shows the XPS spectra for CNT-60ZRP before and after immersion. The survey spectrum (Figure 29a) shows the presence of oxygen, carbon, and nitrogen

for both the intact and the exposed samples. No zinc was found, which is in agreement with the SEM results. Figure 29b shows the C 1s core level photoemission spectrum of CNT-60ZRP before immersion. The peak at the binding energy of 285 eV was attributed to C-C/C-H bonds, the contribution at 286.5 eV was assigned to C-O/C-N bonds, and the peak at 287.91 eV was associated with C=O bonds [90-93]. The corresponding peaks for C-O and C=O bonds were also detected in the O 1s core level (not shown here) at 533.34 eV and 534.77 eV, respectively [93-95]. These functional groups and their corresponding atomic compositions (Table 6) describe the presence of a conventional epoxy coating.

Figure 29c shows the core level spectrum for C 1s after 90 days of exposure. Significant change was observed in the atomic composition of the outermost layer of the epoxy binder. In addition to the functional groups identified for the intact coating, a new peak was recognized at 288.8 eV in the C 1s core level attributed to carboxyl groups [92]. Table 6 shows a high increase in the atomic composition of C-O groups. This behavior can be explained by strong hydrogen bonding interactions between the water molecules and certain hydroxyl and amine groups of the epoxy polymer [96].

Mijovic et al. [97] reported that a water molecule can form hydrogen bonds with hydroxyl, ether, and tertiary amines of the epoxy network. It can also form hydrogen bonds between water molecules previously bound to the polymer, leading to the formation of dimers, trimers, or even water clusters. EIS measurements showed excellent charge transfer resistance and SEM images did not show significant degradation in the epoxy binder. However, the surface of the epoxy coating was highly

altered by the direct contact with the electrolyte. This behavior is in agreement with results by Li et al. [96], who reported that water binds with the hydrophilic groups of the epoxy polymer before diffusing into the free volume of micropores of the epoxy matrix.

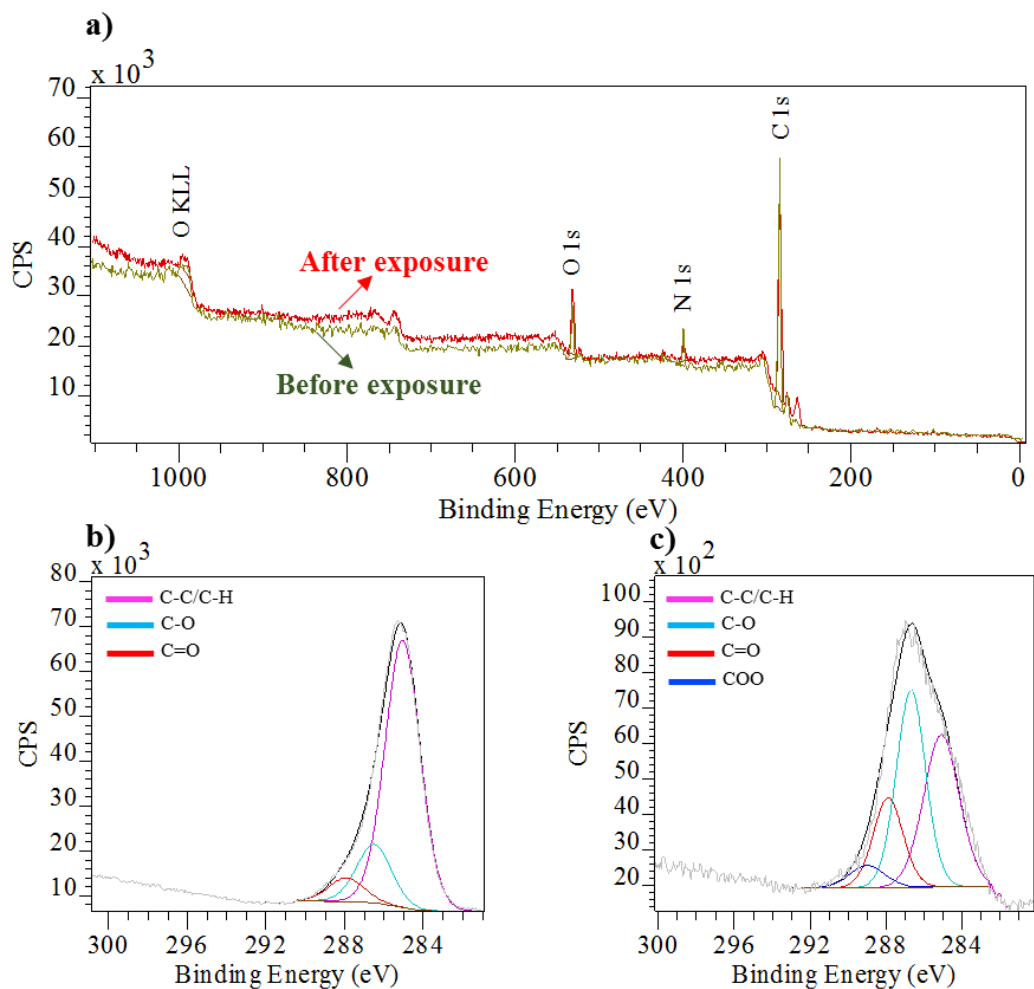
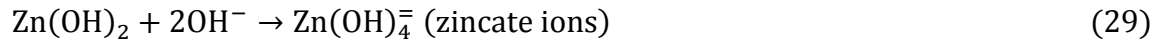


Figure 29. XPS spectra for CNT-60ZRP before and after exposure to SCP during 90 days: a) survey spectrum, b) C 1s high-resolution spectrum before immersion, and c) C 1s high-resolution spectrum after immersion.

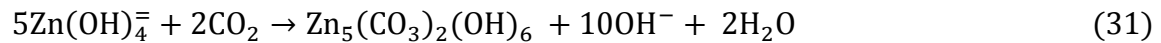
XPS spectra are also reported for CNT-70ZRP. The survey spectra (Figure 30a) show that the surface of the intact coating consisted predominantly of C, O, and N. The coating exposed for 90 days to the electrolyte solution showed the presence of Zn, O, and C, which is expected due to the formation of zinc corrosion products at the coating surface observed in SEM images. Notably, chloride ions were not found at the film surface, which is also in accordance with the EDS results in Table 5. This behavior can be explained by the alkaline pH of the simulated concrete pore solution. In these conditions, zinc corrosion products containing chlorine such as simonkolleite ($\text{Zn}_5(\text{OH})_8\text{Cl}_2$) or zinc chloride (ZnCl_2) are not thermodynamically stable (see Figure 30b).

Based on the C 1s high-resolution spectra (Figure 30c), an additional inner peak at 290.97 eV was assigned to the presence of hydrozincite ($\text{Zn}_5(\text{CO}_3)_2(\text{OH})_6$) [98, 99]. The O 1s core level (Figure 30d) was deconvoluted with three additional contributions compared to the O 1s core level for CNT-60ZRP. A peak at 530 eV was attributed to zinc oxide (ZnO), one at 532 eV was assigned to the presence of zinc hydroxide, and one at 531.4 eV was related to hydrozincite [98, 99]. These peaks were also identified in the Zn 2p_{3/2} core level (Figure 30e): zinc oxide (ZnO) at 1020.65 eV, zinc hydroxide ($\text{Zn}(\text{OH})_2$) at 1023.97 eV, hydrozincite ($\text{Zn}_5(\text{CO}_3)_2(\text{OH})_6$) at 1022.46 eV, and an additional peak at 1019.29 eV assigned to metallic zinc [98, 99]. Based on these identified chemical species, the mechanism of zinc dissolution in alkaline medium can be described as follows [100]:





Initially, zinc hydroxide is formed due to dissolution of the zinc particles. Afterwards, zincate ions can be produced owing to the alkaline pH of the simulated concrete pore solution. Finally, these zincate ions can undergo an additional conversion to zinc oxide. Further transformation occurs due to the presence of carbon dioxide, which can be absorbed or dissolved from the environment into the electrolyte and lead to the formation of hydrozincite ($\text{Zn}_5(\text{CO}_3)_2(\text{OH})_6$) by the following reaction [100]:



Hydrozincite could also be formed during the storage time of the sample before performing XPS analysis. This results from direct interaction of the zinc corrosion products with the CO_2 in air [99]:



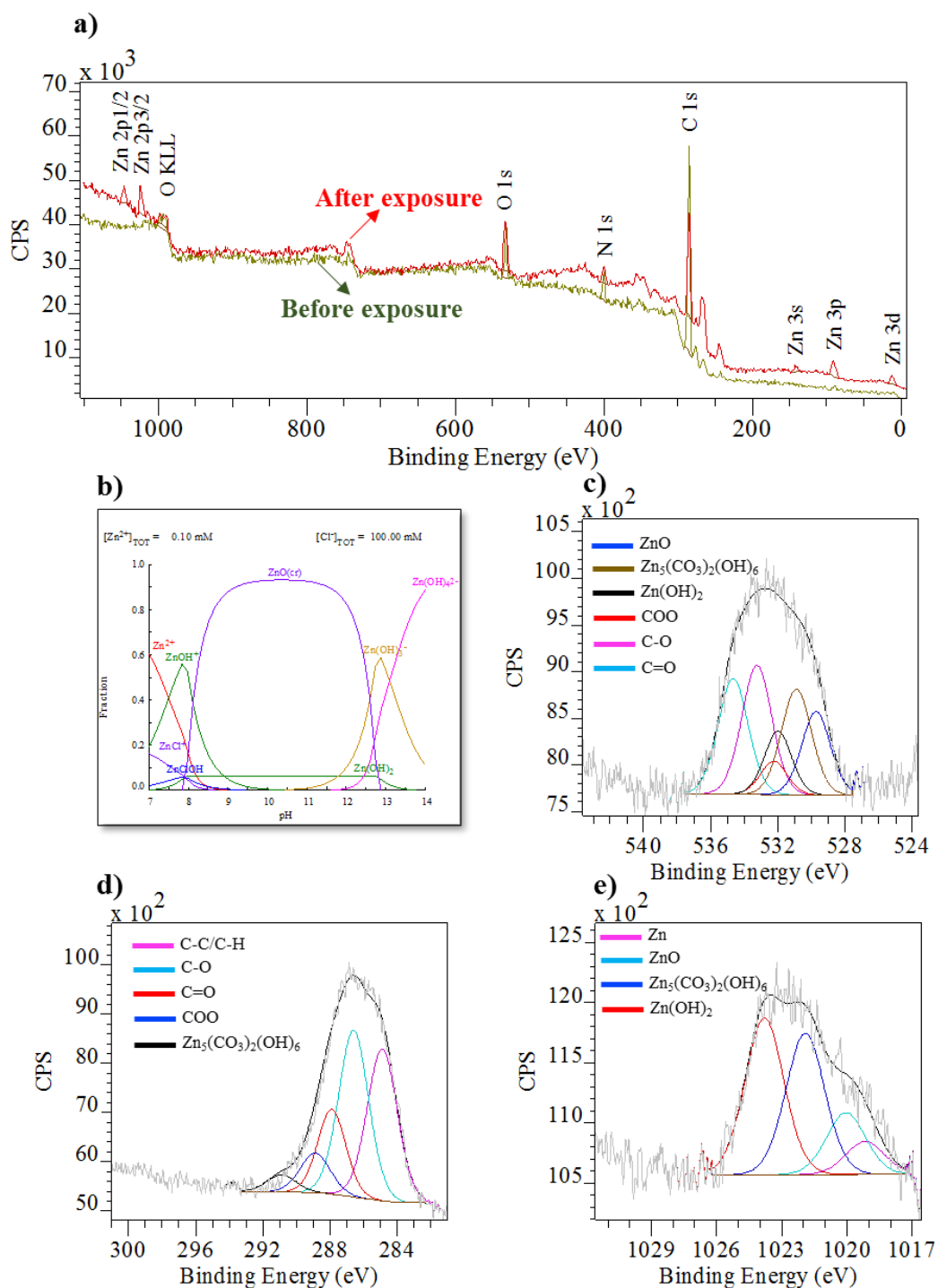


Figure 30. XPS spectra for CNT-70ZRP after exposure to the simulated concrete pore solution during 90 days: a) survey spectrum, b) speciation diagram of Zn, c) C 1s high resolution spectrum, d) C 1s high resolution spectrum, and e) Zn 2p_{3/2} high resolution spectrum.

Figure 31 shows the XPS spectra for CNT-80ZRP. The same species were found as in CNT-70ZRP. However, the distribution of the chemical composition in the O 1s core level shows that the amount of zinc corrosion products increased with respect to the magnitudes for CNT-70ZRP. This behavior is expected based on the SEM images, in which a well-defined layer of zinc corrosion products was formed on the surface of CNT-80ZRP. In contrast, no layer was observed for CNT-70ZRP, and there were only a few agglomerates of zinc corrosion products. The higher amount of zinc corrosion products on the surface of the coating demonstrates the high galvanic process provided by the zinc particles.

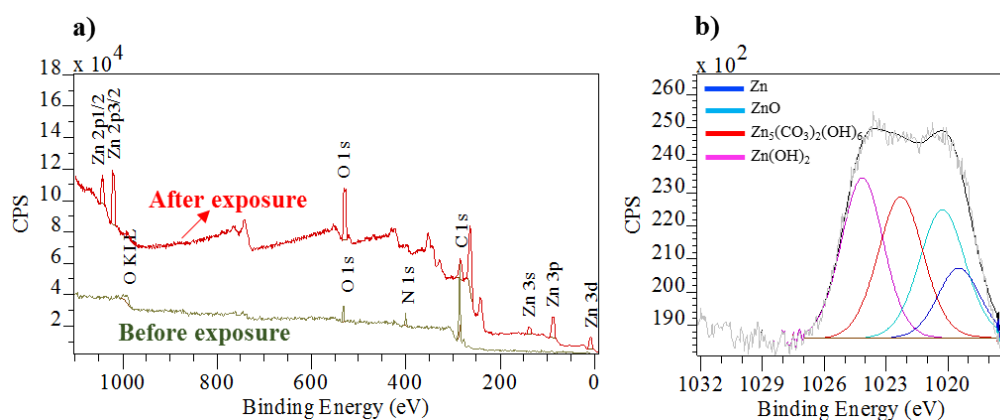


Figure 31. XPS spectra for CNT-80ZRP after exposure to simulated concrete solution during 90 days: a) survey spectrum, and b) Zn 2p_{3/2} high-resolution spectrum.

In the same way, the concentration of zinc corrosion products for CNT-90ZRP was higher than for CNT-80ZRP due to the extended cathodic protection. This allows higher accumulation of zinc corrosion products on the surface of the epoxy coating;

which is clearly shown in Figure 32a, where the percentage of zinc corrosion products on the O 1s core level increases with the amount of zinc particles introduced to the epoxy binder. A higher amount of zinc corrosion products was formed with increased zinc particle concentration. However, Figure 32b shows that as the amount of zinc particles increased in the epoxy binder, a higher content of metallic zinc was found at the coating surface; this means that some zinc particles did not contribute to the cathodic protection process.

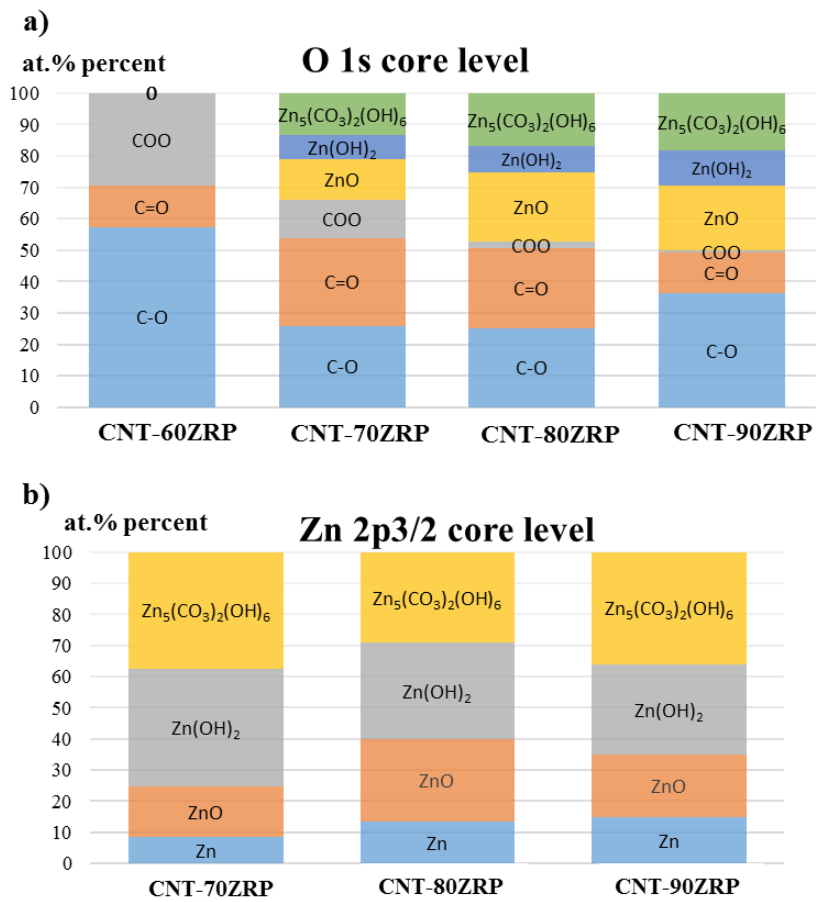


Figure 32. Chemical compositions for the different CNT-ZRP formulations based on high-resolution spectra for a) O 1s, and b) Zn 2p3/2.

CHAPTER IV
INFLUENCE OF CHLORIDE CONCENTRATION ON THE CORROSION
PERFORMANCE OF CARBON NANOTUBES/ZINC RICH EPOXY PRIMERS ON
CARBON STEEL UNDER EXPOSURE TO SIMULATED CONCRETE PORE
ENVIRONMENTS

Open circuit potential (OCP)

In order to follow up the changes in potential and elucidate the protection character, evolution of OCP was recorded during 150 days for the CNT-ZRP systems exposed to simulated concrete pore solutions at different chloride-to-hydroxide ratios. The same OCP criteria defined in the previous chapter were used to analyze these results.

CNT-60ZRP

Figure 33 shows the open circuit potential values for CNT-60ZRP immersed in simulated concrete pore solutions with different chloride-to-hydroxide ratios during 150 days. From Figure 33, it can be seen that OCP values for this coating system were above the cathodic protection limit for the entire immersion period. These results suggest that CNT-60ZRP was unable to provide cathodic protection to the carbon steel substrate, even with the CNT's presence in the zinc-rich primer. This behavior can be explained due to the low pigment volume concentration of this material, which is around 25 vol% Zn, making the zinc particles completely embedded in the epoxy primer and highly

separate from each other. Since cathodic protection is effective when zinc particles are in direct contact (or connected through CNTs) with other zinc particles and with the carbon steel substrate, it is expected that at very low zinc content, there are insufficient electronic pathways to drain cathodic protection current to the carbon steel substrate. However, it is important to notice that, even though cathodic protection was not provided to the metallic substrate, the OCP values for CNT-60ZRP were shifted to more positive values during the first 40 days of immersion, after this period, the potential was nearly constant during the remaining immersion time. This trend suggests that CNT-60ZRP provided good barrier protection to the carbon steel substrate due to the highly crosslinked nature of the epoxy polymer. Regarding the chloride-to-hydroxide ratio, the OCP values were similar during the entire exposure, even for the highest chloride-to-hydroxide ratio that corresponds to a sodium chloride concentration higher than 5 wt%, which might indicate that the electrolyte did not reach the carbon steel surface due to the high barrier protection provided by the epoxy matrix.

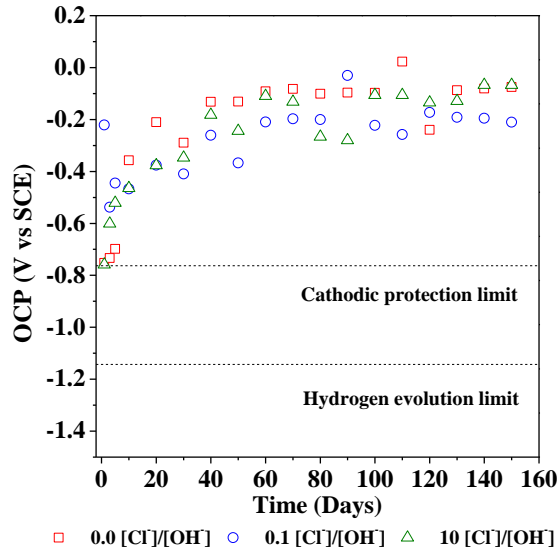


Figure 33. OCP measurements of CNT-60ZRP immersed in simulated concrete pore solutions with different chloride-to-hydroxide ratios for 150 days.

CNT-70ZRP

The OCP values for CNT-70ZRP immersed in the different electrolyte solutions for 150 days are shown in Figure 34. From this figure, it can be observed that the OCP values shifted toward the cathodic protection region during the first two days of immersion. The observed behavior is the activation of the zinc particles by the electrolyte solution; native zinc oxide surrounding the zinc particles reacted with chloride ions allowing the zinc particles to provide cathodic protection to the carbon steel substrate.[84] This reaction increased the zinc-to-iron area ratio, causing the potential to shift toward the cathodic direction. After two days of immersion, the OCP values shifted to anodic potentials due to corrosion of the zinc particles that decreased the zinc active area that was available to provide cathodic protection. Following three days of immersion, the OCP values were no longer in the cathodic protection region and

they shifted to more positive potential values close to -0.03 V vs SCE. After 20 days of immersion, these OCP values stabilized in this passive region and remained in this region for the rest of the immersion time. This trend suggests that; either, zinc corrosion products were formed, thereby protecting the carbon steel surface, or that hydroxide ions coming from the simulated concrete pore solution reached a concentration sufficient to passivate the carbon steel surface.

A particular behavior was observed for the coating system exposed to the simulated concrete pore solution with a chloride-to-hydroxide ratio of 10, in which the OCP shifted again to cathodic potential values after 70 days of immersion. This behavior might be associated to the activation of the carbon steel surface by the excessive amount of chloride ions reaching the metallic substrate. Additionally, high amount of blisters were observed after the sample was removed from the electrolyte, indicating that iron corrosion products were formed underneath the coating and, as a consequence, inducing blister formation and delamination of the coating from the metallic substrate. Since the process of corrosion on reinforcing steel in concrete can be described as a competition between the stabilization and restoration provided by the hydroxide ions and the depassivation of the carbon steel substrate by chloride ions [35], it can be concluded that in CNT-70ZRP samples exposed to chloride-free solutions and the sample exposed to a solution with a chloride-to-hydroxide ratio of 0.1, the influence of hydroxide ions prevailed over the effect of chloride ions. In contrast, in the CNT-70ZRP sample exposed to the simulated concrete pore solution with a chloride-to-hydroxide ratio of 10,

the degradation of the carbon steel surface by chloride ions predominated over the protection provided by the hydroxide ions.

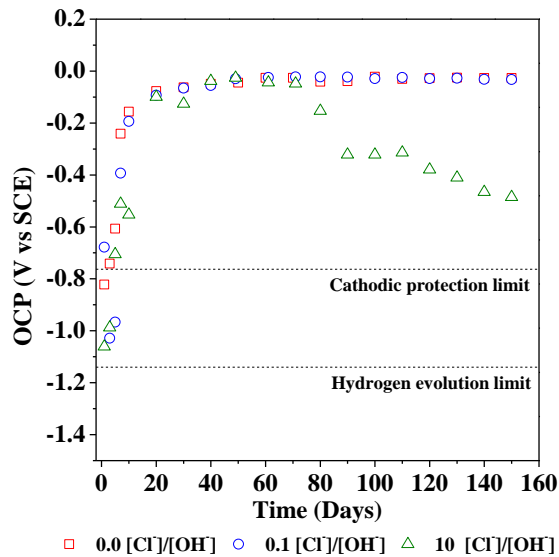


Figure 34. OCP measurements of CNT-70ZRP immersed in simulated concrete pore solutions with different chloride-to-hydroxide ratios for 150 days.

CNT-80ZRP

Figure 35 shows the OCP values for CNT-80ZRP immersed in the different electrolyte solutions for 150 days. From Figure 35, it can be observed that the OCP values decreased during the first seven days for the coating system immersed in the chloride-free solution and during the first three days for the electrolyte solutions with chloride-to-hydroxide ratios of 0.1 and 10. Similar to CNT-70ZRP, this behavior is associated with the activation of the zinc particles by the electrolyte. As can also be seen from Figure 35, the activation of the zinc particles took longer times for the CNT-80ZRP

sample immersed in the blank solution, due to the absence of chloride ions that can react with the zinc oxide covering the zinc particles, which allows the rapid activation of zinc to provide cathodic protection to the carbon steel substrate. Based on the OCP values that were observed between three and seven days of immersion, cathodic protection process with hydrogen evolution might have occurred during this immersion period. However, after seven days of immersion, the OCP values shifted to values within the cathodic protection region, suggesting the end of the hydrogen evolution reaction. The carbon steel substrate was cathodically protected for 10 days when the coating system was immersed in the blank solution and in the electrolyte with low chloride concentration, and for 20 days when the coating system was exposed to the solution with the highest chloride concentration. This behavior shows that CNT-80ZRP samples provided galvanic cathodic protection for longer period of immersion compared to the CNT-70ZRP samples due to the higher zinc content that increases the number of electronic pathways by either, direct contact between zinc particles, or by interconnection of zinc particles with CNTs. After 10 days of immersion, the OCP values for CNT-80ZRP samples exposed to the blank solution and the solution with low chloride concentration shifted to more anodic potentials, and thereafter, they remained almost constant at approximately -0.25 V vs. SCE. This trend might be associated with the formation of zinc corrosion products that prevented corrosion attack to the metallic substrate. In contrast, the OCP values for the CNT-80ZRP sample immersed in the electrolyte solution with high chloride concentration did not shift to more anodic potentials, instead, OCP values remained close to the cathodic protection limit. This

behavior indicates that zinc particles were active during the entire immersion period; however, this trend does not necessarily mean that effective cathodic protection was provided to the carbon steel surface. It is possible that the high chloride concentration can attack the zinc corrosion products formed during the cathodic protection process, and therefore, the protective layer of corrosion products cannot be formed or remain stable. Additionally, chloride ions can react with zinc particles even when they are not providing cathodic protection to the metallic substrate. This is a self-dissolution process of the zinc particles, due to the high concentration of chloride ions, in which zinc dissolution and oxygen reduction reaction occurs on the surface of the zinc particles.

The OCP evolution for CNT-90ZRP in the different electrolytes showed a similar trend as the one reported for CNT-80ZRP. The results are included in Appendix A as supplemental material.

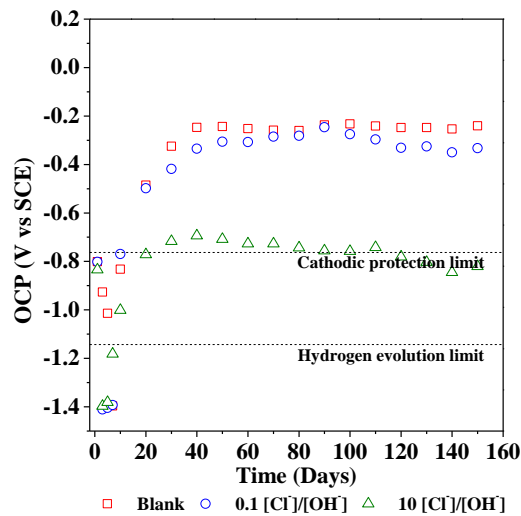


Figure 35. OCP measurements of CNT-80ZRP immersed in simulated concrete pore solution at different chloride-to-hydroxide ratios for 150 days.

Electrochemical impedance spectroscopy (EIS)

EIS was used to investigate the corrosion protection performance of the different coating systems in simulated concrete pore environments, as well as the influence of chloride-to-hydroxide ratio on the corrosion degradation of zinc-rich epoxy primers and carbon steel substrate. Electrochemical parameters such as coating resistance (R_c), coating capacitance (C_c), charge transfer resistance (R_{ct}), double layer capacitance (C_{dl}), and resistance of oxide layers (R_{ox}), were used to study the evolution of the corrosion degradation mechanisms of the different coating systems. As it will be noticed below, these mechanism of coating degradation for the different coating formulations were similar to the corresponding mechanisms reported in the previous chapter.

CNT-60ZRP

Figure 36 shows the EIS spectra for CNT-60ZRP immersed in simulated concrete pore solutions at three different chloride-to-hydroxide ratios for 150 days. As it can be seen in Figure 36, similar impedance spectra were observed for the different chloride-to-hydroxide ratios. The Nyquist representation showed only one time constant, and the Bode diagram exhibited high impedance magnitudes at 0.01 Hz, close to 10^{10} ohm cm^2 . This behavior suggests that good barrier corrosion protection was provided to the metallic substrate which, can be explained by the highly crosslinked epoxy matrix, representing a relatively inert and dielectric material when zinc particles were present in very low concentrations and were therefore, completely embedded in the epoxy primer [101]. In addition, it has been reported that CNTs can play an important role in providing corrosion protection to carbon steel surfaces since they are able to fill in micro-pores and

flaws in the epoxy matrix [102]. Other studies reported that CNTs are also able to fill in micro-holes in the metallic surface, reducing the number of active sites for metal dissolution [103]. It is important to notice that even though the coating system showed high corrosion resistance in the different electrolytes with no sign of corrosion processes at the metallic surface, for the coating sample immersed in the solution with the highest chloride-to-hydroxide ratio, the impedance magnitude at 0.01 Hz shown in Figure 36c decreased slightly faster than that of the coating samples immersed in the blank solution and the electrolyte solution with a chloride-to-hydroxide ratio of 0.1, this behavior might be associated with the degradation of the epoxy matrix by chloride ions [104, 105].

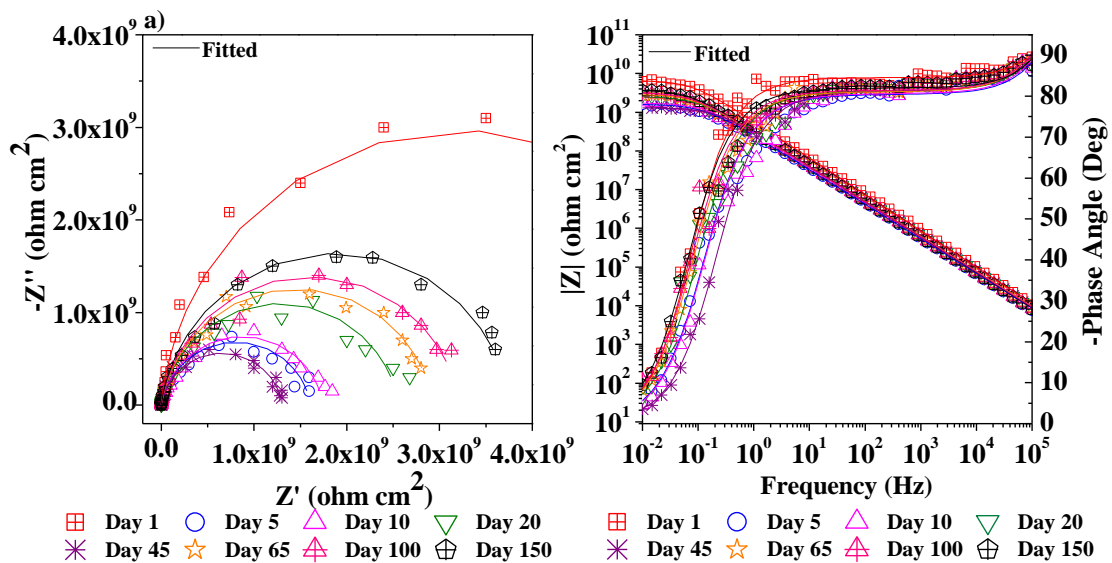


Figure 36. Impedance spectra of CNT-60ZRP immersed in simulated concrete pore solutions with different chloride-to-hydroxide ratios for 150 days: a) blank solution, b) 0.1 $[\text{Cl}^-]/[\text{OH}^-]$, and c) 10 $[\text{Cl}^-]/[\text{OH}^-]$.

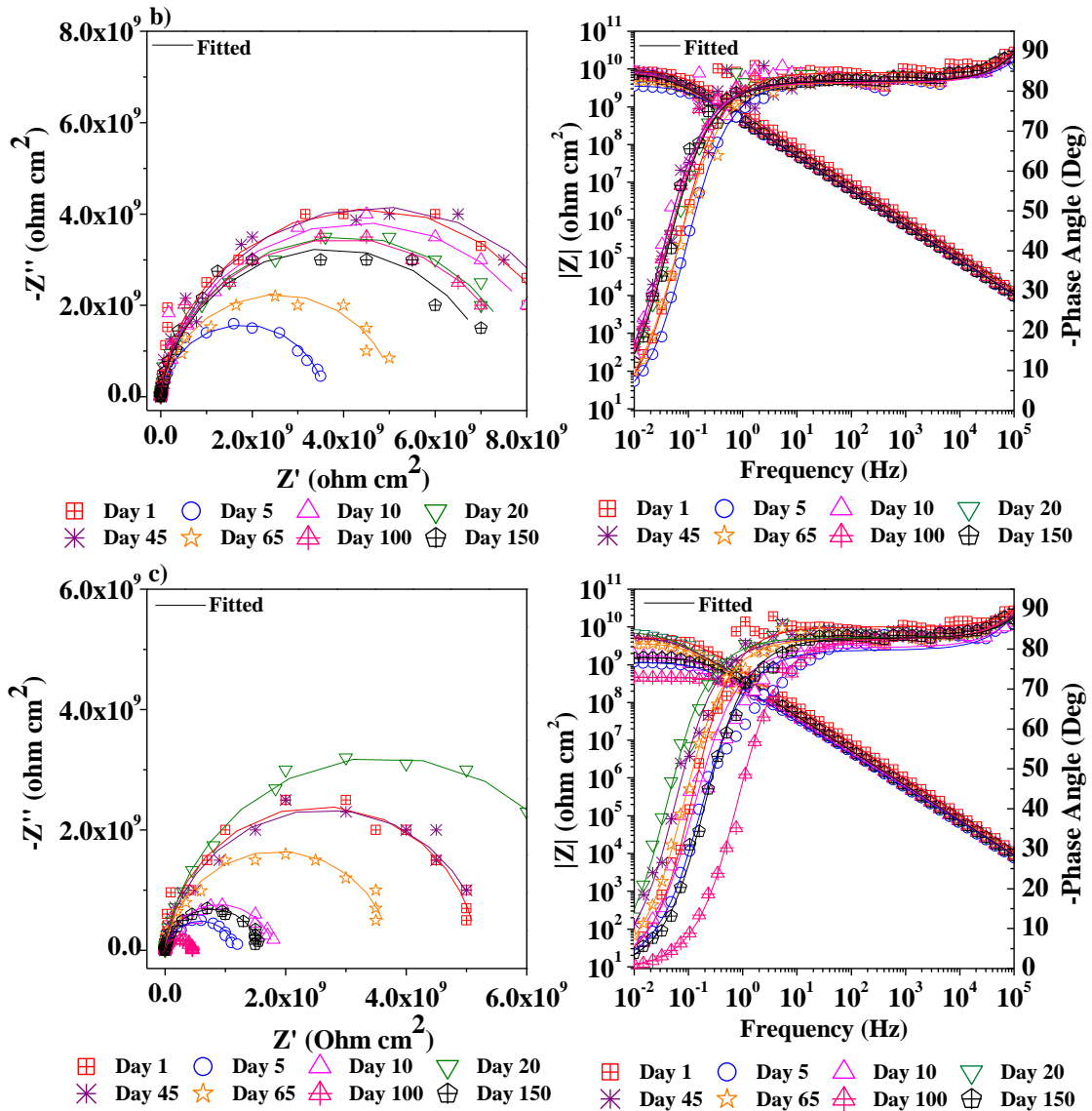


Figure 36. Continued

CNT-70ZRP

Figure 37 shows the Nyquist and Bode representations for CNT-70ZRP immersed in simulated concrete pore solutions at different $[Cl^-]/[OH^-]$ ratios. The impedance spectra at the first day of immersion showed high corrosion resistance of CNT-70ZRP in all the electrolyte solutions, with impedance magnitudes at 0.01 Hz close

to 10^{10} ohm cm^2 . This behavior was due to negligible diffusion of electrolyte through the coating system, which was described by the almost intact condition of the epoxy material.

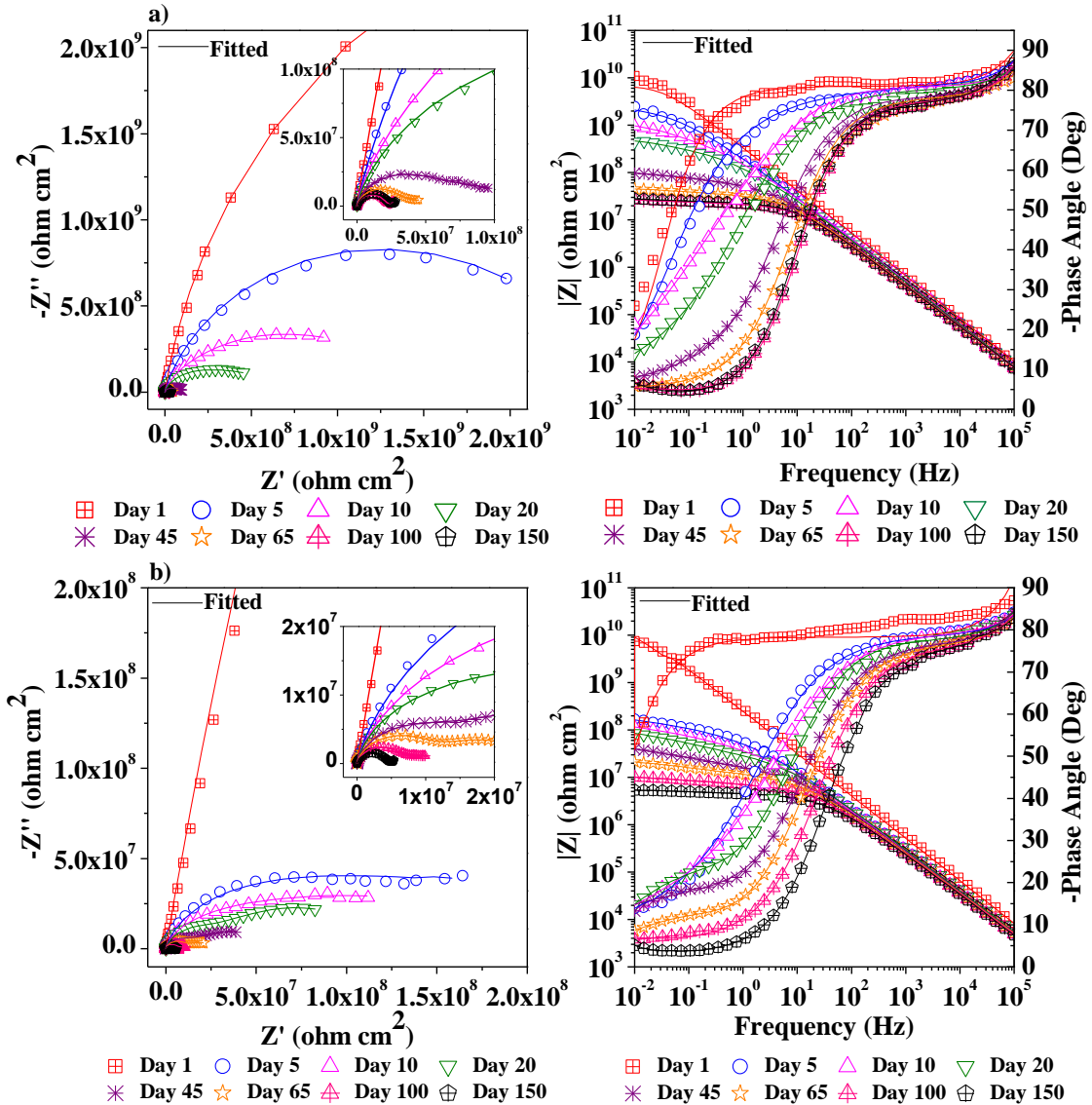


Figure 37. Impedance spectra of CNT-70ZRP immersed in simulated concrete pore solutions with different chloride-to-hydroxide ratios for 150 days: a) blank solution b) 0.1 $[\text{Cl}^-]/[\text{OH}^-]$, and c) 10 $[\text{Cl}^-]/[\text{OH}^-]$.

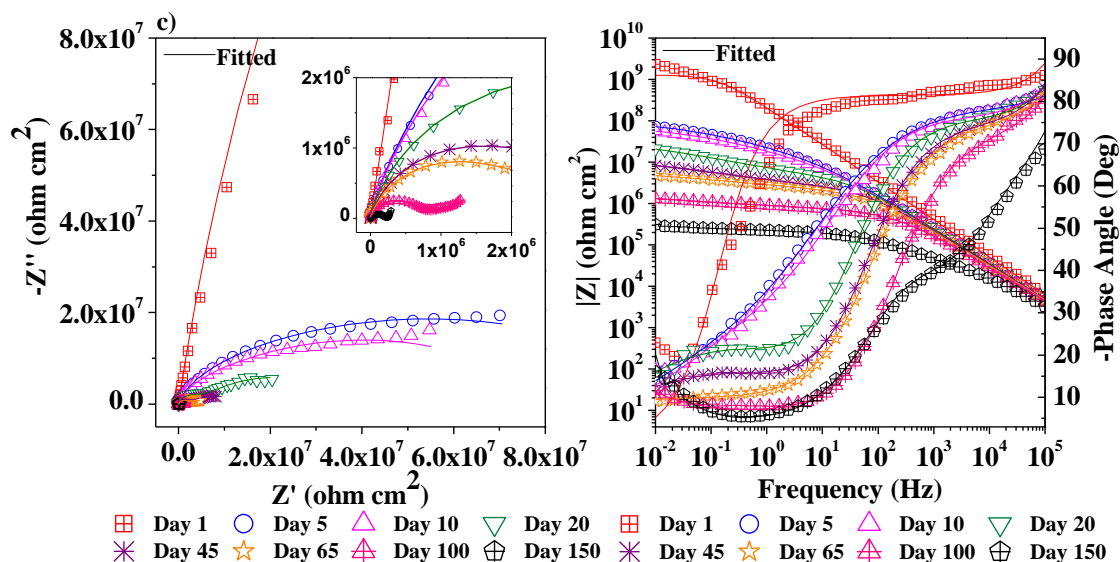


Figure 37. Continued

Following the first day of immersion, the impedance magnitude at 0.01 Hz of CNT-70ZRP in all the different electrolytes significantly decreased owing to diffusion of electrolyte across the coating system. The Nyquist representation showed a depressed capacitive loop that can be associated with the dielectric properties of the zinc-rich epoxy material. However, since cathodic protection was active during the first few days of immersion, some previous works have described that in fact, this capacitive loop could correspond to a mixed impedance response combining the barrier properties of the epoxy matrix, contact impedances between the zinc particles, and electrochemical reactions between the zinc particles and the electrolyte [52, 84]. CNTs could play a role during this period by interconnecting the zinc particles between each other and with the carbon steel substrate, thereby increasing the number of electronic pathways that are available to provide cathodic protection to the metal substrate [20].

The impedance magnitude at 0.01 Hz and the capacitive loop in the Nyquist representation continuously decreased as the immersion time progressed. After 20 days of immersion, another time constant can be recognized at low frequencies (0.1 Hz). Based on the OCP values for this coating formulation, cathodic protection was no longer active after 20 days of immersion; however, zinc particles that did not contribute to the galvanic cathodic protection process could still interact with the electrolyte solution; dissolution of the zinc particles and oxygen reduction reaction both happened at the zinc particle/electrolyte interface. This dissolution process of the zinc particles can explain the appearance of the second time constant at low frequencies. A second interpretation of the presence of this time constant can be associated to electrochemical reactions between the carbon steel substrate and the electrolyte solutions. In this interpretation, the high hydroxide concentration present in the electrolyte solutions reacted with the carbon steel substrate to form a passive oxide layer on the metal surface, similar to the one that is formed in reinforcing steel embedded in concrete. This observation explains the highly anodic potential observed in Figure 34 for CNT-70ZRP immersed in the different electrolytes after 20 days, which is similar to the reported OCP values for passive reinforcing steel in concrete [81].

After 100 days of immersion, a diffusion-like behavior was observed at low frequencies (0.5-0.01 Hz). This behavior has been associated with either, diffusion of reacting chemical species through corrosion products or an oxide passive layer on the carbon steel/coating interface. The presence of corrosion products or an oxide layer at the metallic substrate provides an extra barrier protection to corrosion degradation

processes. This behavior is in agreement with the almost constant impedance magnitude at 0.01 Hz and the highly anodic potential of CNT-70ZRP after 100 days of immersion in the blank solution and in the electrolyte with a chloride-to-hydroxide ratio of 0.1. Therefore, the influence of hydroxide ions in forming an oxide layer at the carbon steel surface was superior compared to the influence of chloride ions in dissolving the metal surface. For the specific coating system immersed in the simulated concrete pore solution with a chloride-to-hydroxide ratio of 10, it can be observed a significant change in the EIS signal and a severe drop in the impedance magnitude at 0.01 Hz due to the high chloride concentration that can compromise the presence of corrosion products formed at the coating-metal interface or it can induce the breakdown of the passive layer. This behavior was in agreement with the OCP measurements reported in Figure 34, in which after 70 days of immersion, the OCP shifted to greater negative potentials that approached those of the OCP values reported for reinforcing steel actively corroded in concrete. This impedance signal can be also attributed to a negative effect of the CNTs when they are exposed to electrolytes with high ionic conductivities (i.e., high concentration of ionic species). In these environments, a high rate of cathodic reaction is prompted to occur, which is completed by the anodic reaction of either one or both metals (i.e., carbon steel surface and zinc particles). Thus, the CNTs become electrodes where extensive iron and zinc dissolution can occur leading to a shortened life time of the coating system [20].

CNT-80ZRP

The impedance spectra for CNT-80ZRP immersed in the different electrolyte solutions for 150 days is shown in Figure 38. From the Bode diagrams, it can be seen that diffusion of the electrolyte occurred right after immersion due to the high porosity of the coating system. The rapid diffusion of electrolyte suggests that the PVC for this specific zinc-rich epoxy primer was higher than the CPVC for this material, leading to a higher number of ionic conductive pathways for electrolyte penetration. Following the first day of immersion, there was a noticeable decrease in the impedance magnitude at 0.01 Hz to impedance values between 10^4 to 10^3 ohm cm^2 . This behavior is attributed to the dissolution of the zinc oxide surrounding the zinc particles; this dissolution re-activated the particles and increased the zinc active area to provide galvanic cathodic protection to the metallic substrate. The complex representation showed one capacitive loop similar to the one for CNT-70ZRP that was associated to the mixed impedance response combining barrier properties of the epoxy matrix, contact impedances between the zinc particles, and faradaic reactions between the zinc particles and the electrolyte solutions. Subsequently to the activation stage, Nyquist representation showed a significant change in the impedance spectra of CNT-80ZRP exposed to the different electrolyte solutions. Two capacitive loops were shown at the high to medium frequencies (0.8-1300 Hz) and one inductive loop was observed at the lowest frequencies (0.02 Hz). Based on the OCP values reported in Figure 35, this period corresponds to the cathodic protection process in the presence of hydrogen evolution reaction. It was suggested that the capacitive loop observed at the highest frequency

(400-1300 Hz) represents the dielectric properties of the zinc-rich epoxy material, the capacitive loop at intermediate frequencies (0.8-1.2 Hz) describes the charge transfer process due to the dissolution of zinc occurring at the zinc particle surface and hydrogen evolution occurring at the carbon steel substrate, and the inductive loop observed in the lowest frequency domain (0.02-0.01 Hz) might be attributed to adsorption of monoatomic hydrogen on the metal surface [87, 106].

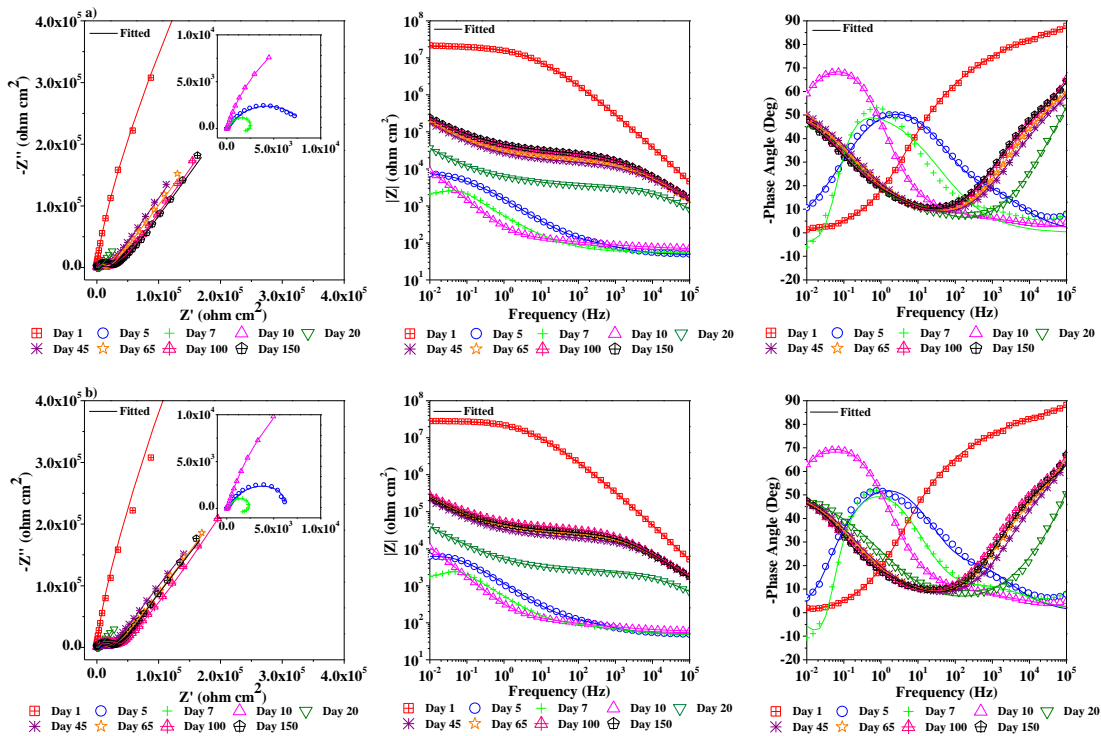


Figure 38. Impedance spectra of CNT-80ZRP immersed in simulated concrete pore solutions with different chloride-to-hydroxide ratios for 150 days: a) blank solution b) 0.1 [Cl⁻]/[OH⁻], and c) 10 [Cl⁻]/[OH⁻].

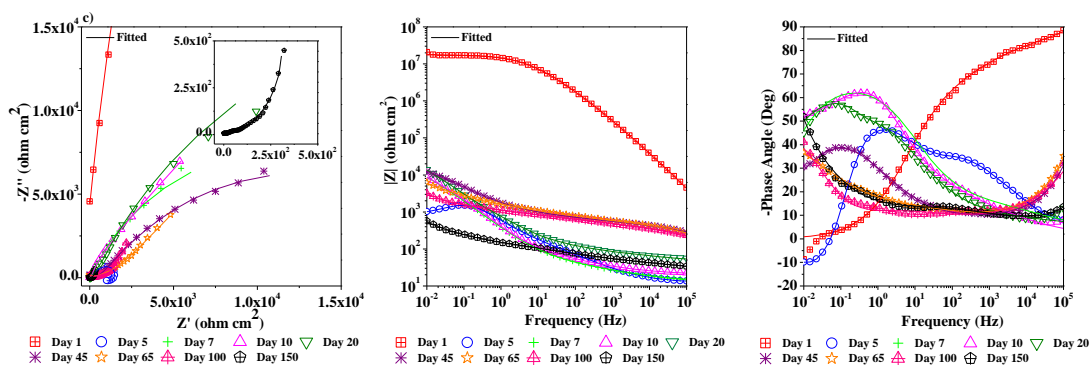


Figure 38. Continued

Following the galvanic cathodic protection process combined with hydrogen evolution reaction, the impedance magnitude at 0.01 Hz increased due to formation of zinc corrosion products that provided additional protection to the carbon steel substrate. Three time constants were defined in the Nyquist representation. The time constant at the lowest frequencies (0.07 Hz) was associated to galvanic cathodic protection process taking place in presence of oxygen reduction reaction, the time constant at the intermediate frequencies (600-1900 Hz) was related to the dielectric properties of the zinc-rich epoxy coating, and the very small time constant at high frequency (20 kHz) was associated to the formation of a layer of zinc corrosion products on top of the coating system surface. The cathodic protection process was effective for 10 days when the coating system was immersed in the blank solution and in the simulated concrete pore solution with a chloride-to-hydroxide ratio of 0.1, while this cathodic protection was extended to 20 days when the coating system was exposed to the electrolyte solution

with the highest chloride-to-hydroxide ratio. This behavior can be explained by the high galvanic activity of the zinc particles in the presence of chloride ions.

Finally, after cathodic protection was no longer active, a significant difference in the impedance magnitude at 0.01 Hz in the Nyquist representation was observed for the coating system immersed in the different electrolyte solutions. For coating system immersed in the blank solution and in the simulated concrete pore solution with a chloride-to-hydroxide ratio of 0.1, the impedance magnitudes at 0.01 Hz increased to values between 10^5 to 10^6 ohm cm^2 owing to the formation of a layer of zinc corrosion products on the coating/electrolyte interface as a result of the effective galvanic cathodic protection provided by the zinc particles. Additionally, these impedance magnitudes remained almost constant as the exposure time progressed, suggesting that the protective layer of zinc corrosion products on top of the coating surface was stable for long-term exposure. From the Nyquist representation and phase angle diagram, three time constants were observed; the time constant at the high frequencies represents the layer of zinc corrosion products formed on the coating surface, the time constant at the intermediate frequencies was describing the electrolyte resistance through the zinc-rich epoxy primer, and the time constant at the low frequency (0.02 Hz) was related to further dissolution of the zinc particles in which both, zinc dissolution and oxygen reduction reaction, took place on the surface of the zinc particles, leading to the formation of zinc corrosion products around their surface. For the situation in which the coating system was immersed in the highest chloride-to-hydroxide ratio, the impedance magnitude at 0.01 Hz only increased to values close to 10^4 ohm cm^2 and after 65 days of immersion it

started to decrease again until reaching impedance values as low as the ones obtained in the activation stage of the zinc particles. This behavior is in agreement with the OCP values for this coating system, in which the potential remained close to the cathodic protection limit, suggesting that zinc particles were reacting during the entire immersion time; the high concentration of chloride ions caused the dissolution of the protective layer comprised by corrosion products formed during the cathodic protection process. Chloride ions could also react with the remaining zinc particles that were not involved in the cathodic protection process leading to significantly lower impedance values at 0.01 Hz compared to the corresponding values obtained in electrolyte solutions with low chloride concentration.

The evolution of the EIS spectra for CNT-90ZRP in the different electrolytes showed a similar trend as the one reported for CNT-80ZRP. The results are included in Appendix A as supplemental material.

Equivalent electrical circuits

The equivalent circuits used to describe the corrosion degradation of the coating systems exposed to the different electrolyte solutions were the same as the equivalent circuits used in the previous chapter.

CNT-60ZRP

Figure 39 shows the R_c and $C_{c,eff}$ values for CNT-60ZRP immersed for 150 days in concrete pore solutions at different chloride-to-hydroxide ratios. The R_c and $C_{c,eff}$ are related to the corrosion-induced deterioration of the coating system that resulted from penetration of water and ionic species from the electrolyte medium [66, 107]. From

Figure 39a, it can be seen that the coating resistance remained almost constant during the entire immersion time, with values between 10^9 and 10^{10} ohm cm^2 , suggesting that good barrier protection was provided to the metallic substrate. Coating resistance for CNT-60ZRP immersed in the electrolyte solution with the highest chloride-to-hydroxide ratio decreased after 90 days of exposure, resulting in values slightly lower than 10^9 ohm cm^2 . This behavior was associated with the degradation of the epoxy matrix during long-term immersion due to an excessive concentration of chloride ions. Figure 39b shows the effective coating capacitance values for the coating system immersed in the different electrolyte solutions, exhibiting values in the order of 10^{-10} F/ cm^2 . The coating capacitance slightly increased during the first few days after immersion, and then it became almost constant during the remaining immersion period. This behavior indicates slow diffusion of electrolyte through the coating system due to high crosslinking of the epoxy material, and the potential influence of CNTs in filling micro-pores and flaws within the coating. It is important to notice that during the first few days of immersion, when the capacitance was increasing due to the permeation of electrolyte across the epoxy material, the coating system immersed in the blank solution showed the highest capacitance values as compared with the electrolyte solutions with chloride ions. This behavior is expected, since diffusion of the electrolyte is hindered when high concentrations of ionic species are present in the electrolyte medium. Furthermore, the ionic radius of chloride (167 pm) is larger than the ionic radius of hydroxide ions (133 pm) and the cations present in the simulated concrete pore solution (Ca^{2+} : 99 pm, K^+ : 102 pm, and Na^+ : 138 pm); therefore, the diffusion rate of the electrolyte decreases as

the concentration of chloride ions increase and increases when hydroxide ions and cations are the main chemical species in the electrolyte solution.

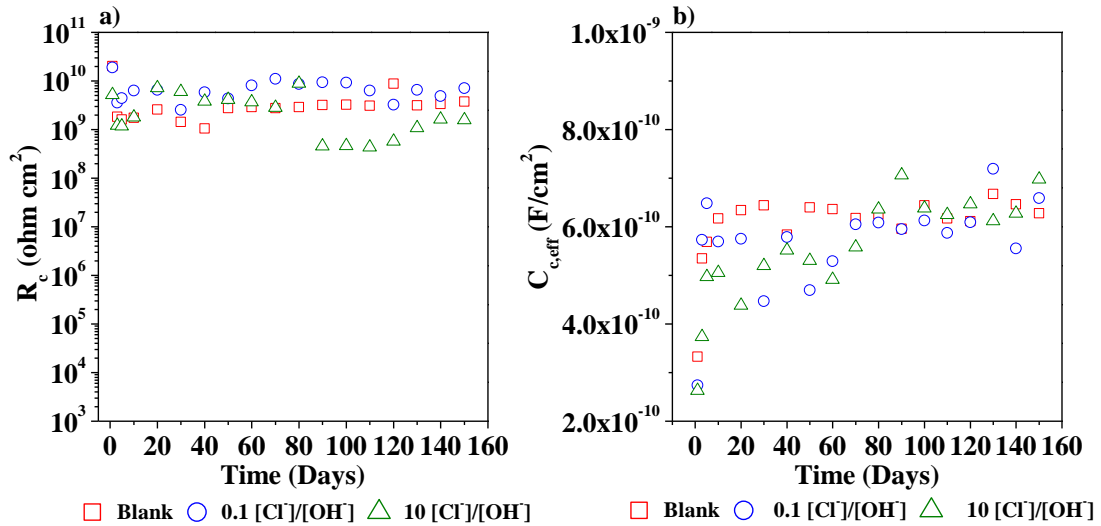


Figure 39. Equivalent circuit elements for CNT-60ZRP immersed in simulated concrete pore solutions with different chloride-to-hydroxide ratios for 150 days: a) coating resistance, and b) coating capacitance.

CNT-70ZRP

Figure 40 shows evolution of the equivalent circuit elements describing the impedance spectra for CNT-70ZRP. Figure 40a shows coating resistance values combining the influence of contact impedances between the zinc particles; R_c rapidly decreased during the first few days of immersion, due to the diffusion of electrolyte through the coating system, causing the activation of zinc particles and decreasing the contact impedances between them. After 20 days of immersion, when cathodic protection was no longer active and a second time constant was recognized in the

Nyquist representation, R_c continuously decreased due to the progressive deterioration of the epoxy material by the electrolyte solutions. Finally, after 100 days of immersion, R_c remained almost constant for the CNT-70ZRP samples immersed in the blank solution and in the solution containing a chloride-to-hydroxide ratio of 0.1. This behavior might be associated with two processes: 1) formation of zinc corrosion products that improved the barrier properties of the epoxy material, or 2) formation of a passive layer on the carbon steel surface, due to high concentration of hydroxide ions in these electrolyte solutions that provided another barrier layer to prevent active dissolution of the metal substrate. In contrast, the coating resistance for CNT-70ZRP sample immersed in the electrolyte solution with the highest chloride concentration, progressively decreased during this period due to blister formation underneath the coating which, caused detachment of the epoxy coating from the metallic substrate. Figure 40b shows the capacitance values associated with barrier properties of CNT-70ZRP. $C_{c,eff}$ increased during the first few days of immersion due to diffusion of electrolyte through the coating system, increasing the dielectric constant of CNT-70ZRP. As progressing the immersion time, the capacitance values of the coating system remained almost constant due to the saturation of the epoxy coating with the electrolyte. The coating system immersed in the highest chloride concentration showed a subsequent increase in the coating capacitance after 100 days of immersion. This trend has been associated to adhesion loss of the epoxy material from the metallic substrate due to blister formation [101].

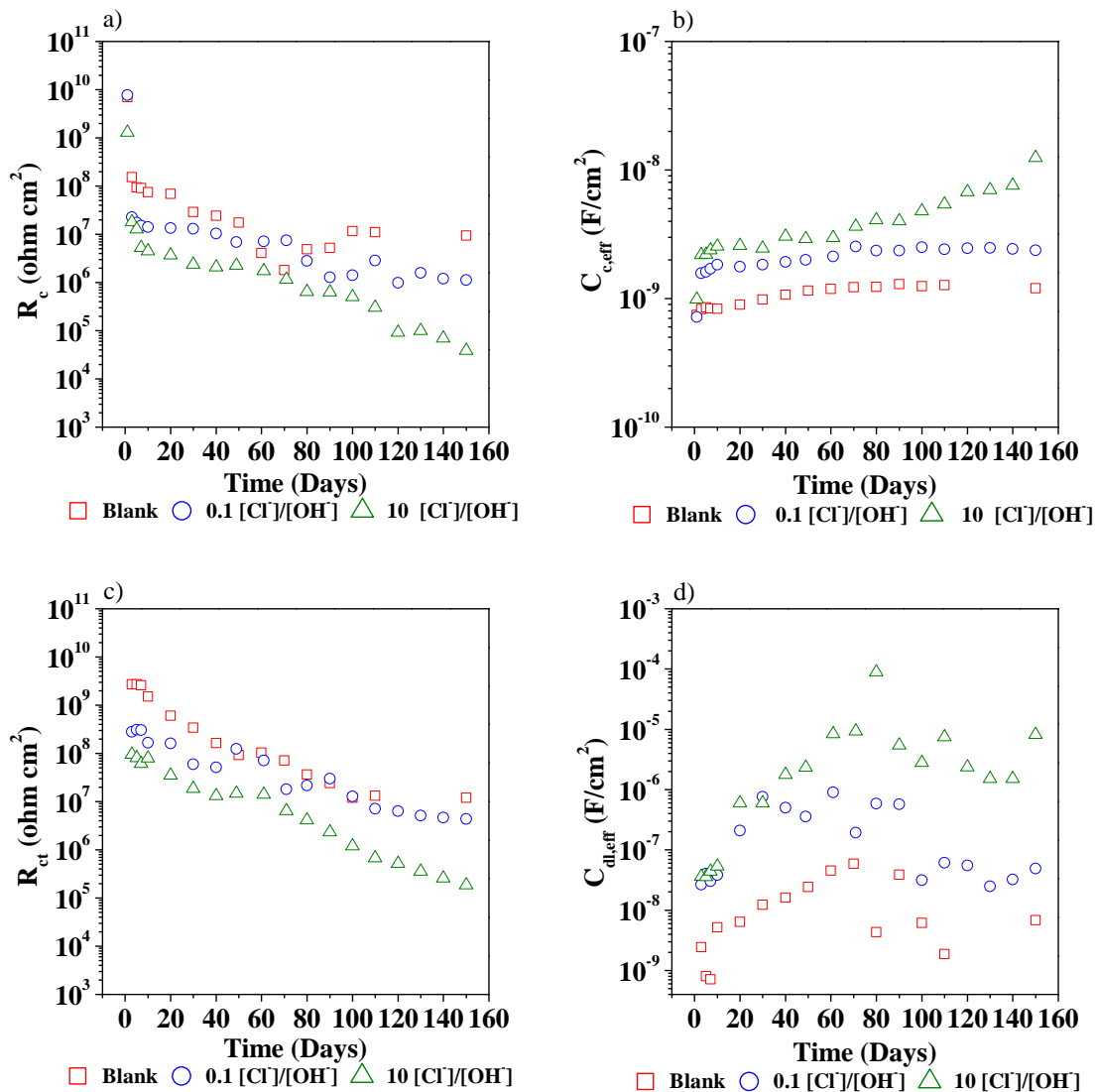


Figure 40. Equivalent circuit elements for CNT-70ZRP immersed in simulated concrete pore solutions with different chloride-to-hydroxide ratios for 150 days: a) coating resistance, b) coating capacitance, c) charge transfer resistance, and d) double layer capacitance.

Figure 40c shows the evolution of the resistance describing the charge transfer processes at either, the zinc/electrolyte interface or the metal substrate; this differentiation is explained as follows. R_{ct} decreased during the activation of the zinc

particles due to electrochemical reactions between these particles and the electrolyte, which increased the zinc active area that was available to provide cathodic protection to the metal substrate. After 20 days of exposure, when a second time constant was recognized at low frequencies, R_{ct} also decreased as immersion time was progressing. It has already been mentioned that two mechanisms might have occurred: 1) dissolution of the zinc particles at the zinc/electrolyte interface, or 2) charge transfer processes between the carbon steel substrate and the electrolyte. During the last period of immersion, R_{ct} remained almost constant for CNT-70ZRP samples immersed in the blank solution and in the solution with low concentration of chloride ions. This behavior can be explained due to formation of corrosion products on the surface of the zinc particles that avoided further dissolution processes or it might be associated to the stability of the passive layer formed at the carbon steel substrate, preventing its active dissolution. For CNT-70ZRP immersed in the electrolyte with the highest chloride concentration, R_{ct} was continuously decreasing even during the last period of immersion time. Two different processes were also proposed to describe this behavior; 1) further dissolution of zinc particles taking place at the zinc/electrolyte interface or 2) breakdown of the passive layer by the high concentration of chloride ions. This suggests that the concentration of chloride ions in this electrolyte solution was higher than the chloride threshold concentration required for breakdown of the passive layer, leading to active dissolution of the carbon steel substrate. Finally, Figure 40d shows the evolution of the double layer capacitance. For CNT-70ZRP samples immersed in blank solution and electrolyte solution with low chloride concentration, $C_{dl,eff}$ slightly increased during 80 days due to

electrochemical reactions between the zinc particles and electrolyte that increased the active area of zinc to enable further dissolution of the zinc particles. After 80 days, $C_{dl,eff}$ decreased due to a reduction in the zinc active area by the formation of zinc corrosion products on the surface of the zinc particles. $C_{dl,eff}$ could also have decreased due to the formation of a passive layer at the metal substrate, which would have reduced the number of active zones available for the dissolution of the metal substrate. For CNT-70ZRP immersed in the highest chloride concentration, $C_{dl,eff}$ was mostly increasing during the entire immersion time, due to the continuous dissolution of the zinc particles and the breakdown of the passive layer creating active zones for iron dissolution.

CNT-80ZRP

Figure 41 shows the evolution of different equivalent circuit elements describing the corrosion degradation mechanism of CNT-80ZRP. Coating resistance values are shown in Figure 41a; it is observed that R_c rapidly decreased during the activation stage and the cathodic protection process in the presence of hydrogen evolution reaction, due to the high diffusivity of electrolyte through the large number of pores inside the epoxy coating. These pores, created by the large PVC of zinc particles, provided effective conductive pathways for ionic transport across the epoxy material. After hydrogen evolution ceased, R_c significantly increased due to the formation of solid corrosion products that sealed the pores of the coating system. After 20 days of exposure, when zinc particles were unable to provide further cathodic protection, a different evolution of R_c was observed for the coating samples immersed in the electrolyte solutions. For the CNT-80ZRP samples immersed in the blank solution and in the electrolyte solution with

low chloride concentration, R_c progressively increased during the remaining exposure time, due to the formation of a protective layer of zinc corrosion products on the coating surface that prevented additional diffusion of the electrolyte. In contrast, for CNT-80ZRP immersed in electrolyte solution with the highest chloride concentration, R_c decreased continuously as immersion time progressed. This behavior is associated with degradation of the epoxy matrix by the high chloride concentration. Figure 41b shows the evolution of coating capacitance for CNT-80ZRP samples immersed in the three different electrolytes solutions. The capacitance values for the coating systems immersed in the blank solution and in the solution with low chloride concentration increased during the first few days, then, these values decreased for the following days, and finally they were nearly constant during the remaining immersion time. This behavior was likely due to the diffusion of electrolyte at the beginning of immersion time, the blockage of coating pores by zinc corrosion products, and the saturation of the coating system with the electrolyte solutions. The coating capacitance of CNT-80ZRP exposed to the highest chloride concentration also increased during the first few days of immersion due to electrolyte penetration, and then it reached a relatively constant value due to the saturation of the epoxy material with the electrolyte. These coating capacitance values were significantly higher than the corresponding capacitance values for coating samples immersed in the blank solution and in the low chloride concentration solution. This behavior confirms the degradation of the epoxy material by the high chloride concentration.

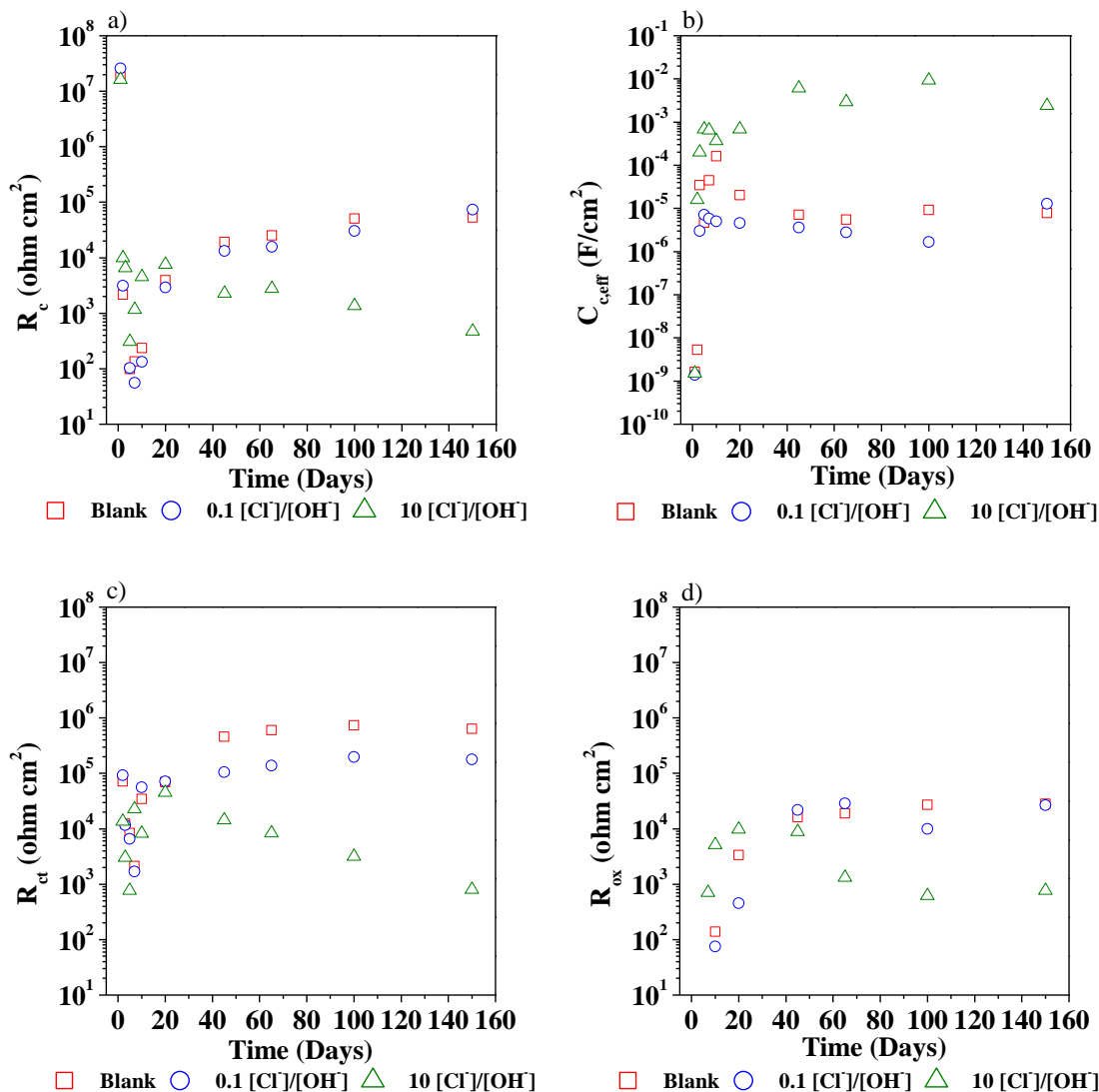


Figure 41. Equivalent circuit elements for CNT-80ZRP immersed in simulated concrete pore solutions with different chloride-to-hydroxide ratios for 150 days: a) coating resistance b) coating capacitance, c) charge transfer resistance, and d) resistance of the oxide layer.

Figure 41c shows the R_{ct} values for CNT-80ZRP immersed in the different electrolyte solutions. Once again, different behavior was observed between the coating samples immersed in the three electrolyte solutions. For CNT-80ZRP samples immersed

in the blank solution and in the electrolyte solution with low chloride concentration, R_{ct} decreased during the activation stage, due to the removal of native zinc oxide covering the zinc particles, increasing the zinc active area and therefore, decreasing the charge transfer resistance associated to zinc dissolution. In addition, R_{ct} also decreased during the sacrificial process in the presence of the hydrogen evolution reaction due to the continuous dissolution of zinc in the absence of the formation of solid corrosion products. During the cathodic protection process in the presence of oxygen reduction reaction, R_{ct} started to increase, due to a reduction in the zinc active area. Later, when cathodic protection was overcome, R_{ct} gradually increased with increasing immersion time, due to the loss of electric contact between the zinc particles and the carbon steel substrate [84]. Finally, during the last period of immersion, R_{ct} remained constant, due to the formation of a layer of zinc corrosion products on the coating surface that prevented additional diffusion of electrolyte and therefore, further dissolution of the zinc particles. For CNT-80ZRP immersed in the electrolyte solution with the highest chloride concentration, a similar behavior was identified in the first 20 days of exposure as was observed for the coating samples immersed in the blank solution and in the simulated concrete pore solution with low chloride concentration. After 20 days of immersion, corresponding to the end of the galvanic cathodic protection, R_{ct} progressively decreased during the remaining immersion time. This behavior was associated with the further dissolution of the zinc particles that did not contribute to the cathodic protection process. Abreu et al.[84] called this process a self-corrosion process, in which zinc was consumed by charge transfer processes occurring on the surface of the zinc particles.

Finally, Figure 41d shows the evolution of the resistance associated with the protective layer of zinc corrosion products formed on the surface of the coating samples; the formation of this layer started during the cathodic protection process in the presence of the oxygen reduction reaction by the combination of charged species. Hydroxide ions formed on the carbon steel substrate and Zn^{2+} ions produced in the coating matrix diffused across the coating, in order to balance the ionic charge; they combined to form insoluble zinc corrosion products on the coating surface [84]. For these reasons, R_{ox} increased during the cathodic protection period due to the development of the protective layer, and then it became almost constant as progressing immersion time suggesting high stability of the protective layer. For the specific situation of CNT-80ZRP immersed in the electrolyte solution with the highest chloride concentration, R_{ox} slightly decreased with time, which can be associated with the re-dissolution of the zinc corrosion products by the large concentration of chloride ions.

Salt spray fog chamber

Salt spray exposure was performed to provide visual assessment of the corrosion protection performance of the coating systems as a function of exposure time [108]. Figure 42 shows photographs of the different coating panels after 720 hours exposure to salt spray fog chamber following ASTM B117 standard. Two conditions were examined in the test chamber: intact surface and scribed surface. From Figure 42, it can be seen that coating systems with an intact surface did not show significant damage after exposure for 30 days to the salt spray fog chamber. However, further visual observations showed some differences in the damage condition of the coating samples. The CNT-

60ZRP panel showed excellent barrier corrosion protection and no corrosion products were observed after exposure. CNT-70ZRP showed little amount of iron corrosion products at the edges of the panel due to inappropriate masking during the sample preparation. Moreover, after 30 days of exposure, the CNT-70ZRP panel showed white corrosion products that resulted from the corrosion processes between the zinc particles and the aggressive environment. Finally, the CNT-80ZRP panel developed high amount of zinc corrosion products that covered the entire exposed area of the panel.

The deterioration process of the coatings was also investigated in scribed surfaces.

Figure 42 showed severe corrosion attack on the CNT-60ZRP panel. Large amounts of iron corrosion products and a lower amounts of zinc corrosion products were formed at the scribed area. This visual observation confirmed that CNT-60ZRP provided excellent barrier protection to the carbon steel substrate but was unable to provide sacrificial protection to the metal substrate. The CNT-70ZRP panel developed a lower amount of iron corrosion products compared to the CNT-60ZRP panel. In addition, the visible amount of zinc corrosion products for CNT-70ZRP was slightly higher than CNT-60ZRP. Based on the surface appearance, it might be suggested that CNT-70ZRP panel was able to provide galvanic cathodic protection to the metallic substrate, at least during the first few days (or hours) of exposure. Finally, the CNT-80ZRP panel showed clear evidence that effective sacrificial protection was provided to protect the carbon steel surface at least during the first seven days of immersion. Nevertheless, the formation of iron corrosion products was observed after 30 days of exposure, which is in agreement with the OCP and EIS measurements that showed that cathodic protection only was

guarantee during the first 20 days of immersion. As a final remark, it should be noticed that even though iron and zinc corrosion products were formed at the scribed areas of all the coating panels, no signs of blister formation, color change, or delamination was identified in any of the exposed panels.

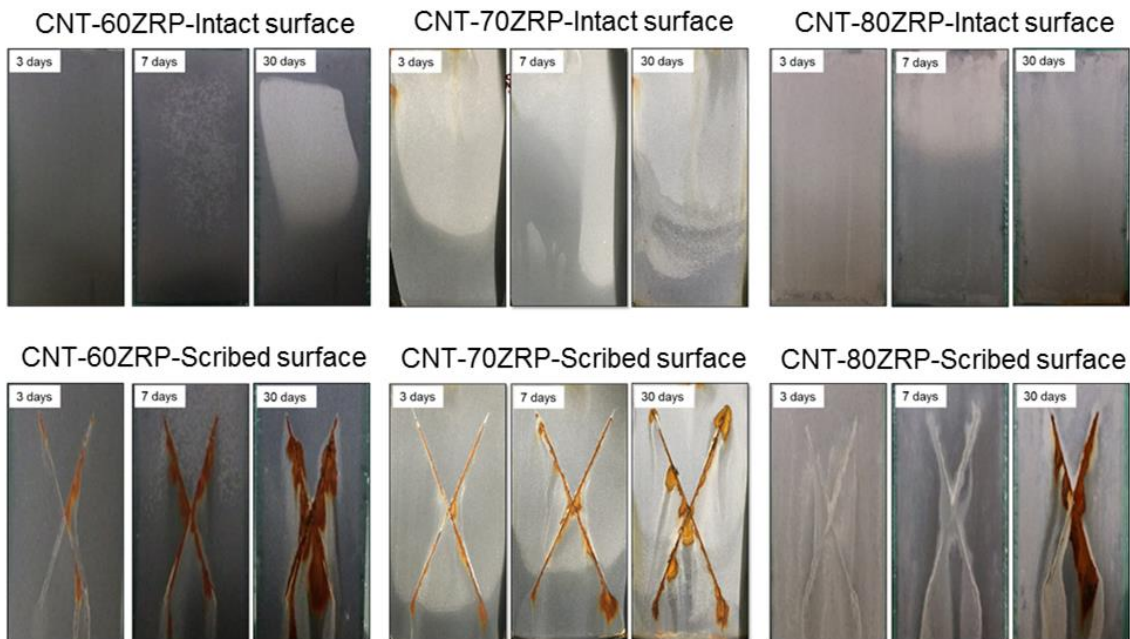


Figure 42. Photographs of CNT-ZRP samples (intact and scribed surface) after different exposure times to salt spray fog chamber.

Morphology studies

Surface appearance of the coating systems after exposure for 150 days to the simulated concrete pore solutions are shown in Figure 43. It can be seen that CNT-60ZRP performed well as a barrier to protect the carbon steel substrate; after 150 days of exposure to the different electrolyte solutions, CNT-60ZRP appeared intact, and no sign

of corrosion products was visually observed on the coating surface. Similar results were observed for the CNT-70ZRP samples immersed in the blank solution and in the solution containing a low chloride concentration. Nevertheless, the coating system immersed in the highly concentrated chloride solution exhibited large number of blisters due to corrosion processes underneath the coating that reduced the adhesion of the coating to the metal substrate. A significant difference in the surface appearance of CNT-80ZRP was observed, compared to the previous coatings. For CNT-80ZRP samples immersed in the blank solution and in the electrolyte with low chloride concentration, a sizeable amount of the coating surface was covered with white corrosion products, owing to the intense sacrificial action provided by the zinc particles. For the coating sample immersed in the solution with high chloride concentration, a lower amount of zinc corrosion products were observed, suggesting re-dissolution or degradation of the zinc corrosion products due to the excessive concentration of chloride ions that were in direct contact with the coating surface. All visual observations were in agreement with the electrochemical measurements.

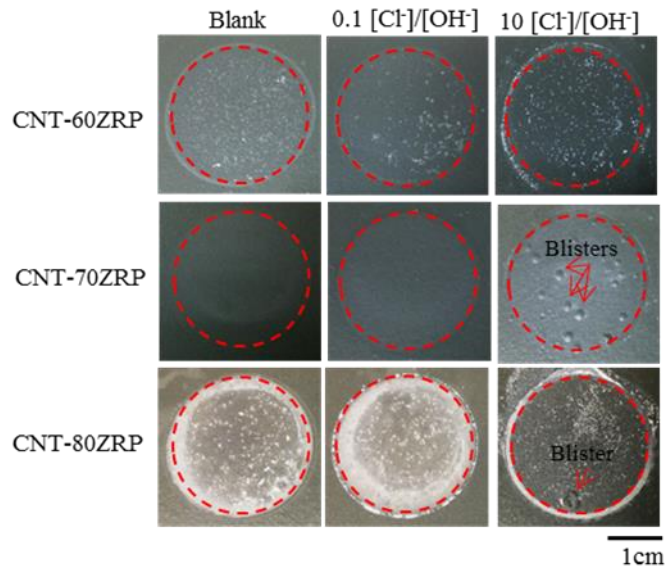


Figure 43. Visual appearances of the surface of CNT-ZRPs after exposure for 150 days to simulated concrete pore solutions with different chloride-to-hydroxide ratios.

SEM micrographs of the surface of CNT-60ZRP after immersion for 150 days in the blank solution are shown in Figure 44. These SEM images show that the zinc particles were highly embedded in the epoxy matrix and they were separated by large distances between each other. This surface morphology confirms the good barrier protection of CNT-60ZRP, which was due to the dense epoxy matrix and the inability of this coating to provide galvanic cathodic protection since zinc particles were highly separated from each other and completely wetted by the epoxy resin.

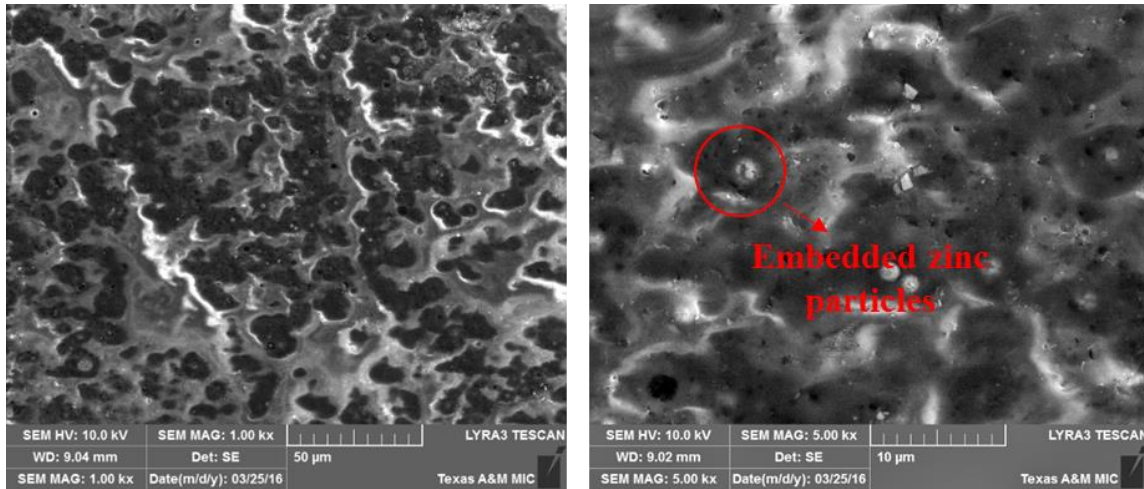


Figure 44. SEM micrographs of CNT-60ZRP after immersion for 150 days in the blank solution.

Figure 45 shows the SEM micrographs of CNT-70ZRP immersed for 150 days in the blank solution and in the electrolyte with high chloride concentration. Figure 45a shows the higher zinc content of CNT-70ZRP compared to CNT-60ZRP. After immersion for 150 days in the electrolyte solution, no sign of corrosion products were found on the coating surface. In addition, it can be recognized that large number of zinc particles did not undergo sacrificial action or zinc dissolution processes. This observation means that not all zinc particles were in direct contact with other zinc particles or interconnected through CNTs, to be able to provide galvanic cathodic protection to the metal substrate. Nevertheless, the electrochemical measurements showed that sacrificial protection was provided during the first few days of immersion, and then a stable barrier protection was provide during the remaining immersion time. Therefore, further studies such as cross-section analysis are needed to investigate if zinc corrosion products were formed inside the coating matrix or at the metal substrate,

additionally, it will be relevant to find out if a passive layer was formed on the carbon steel surface due to the high alkaline environment in the absence of chloride ions.

Figure 45b shows the surface morphology of CNT-70ZRP immersed in the electrolyte solution with the highest chloride concentration. The SEM image on the left showed higher porosity and a less dense epoxy matrix compared to the previous SEM images (left on Figure 16a). Since these SEM images correspond to the same coating formulation and the same SEM magnification, it might be suggested that some sort of degradation occurred for the coating sample exposed to the solution with high levels of chloride ions. The SEM image on the right of Figure 45b captured the presence of CNTs in the coating sample. However, as it can be seen, not all CNTs were able to interconnect with zinc particles.

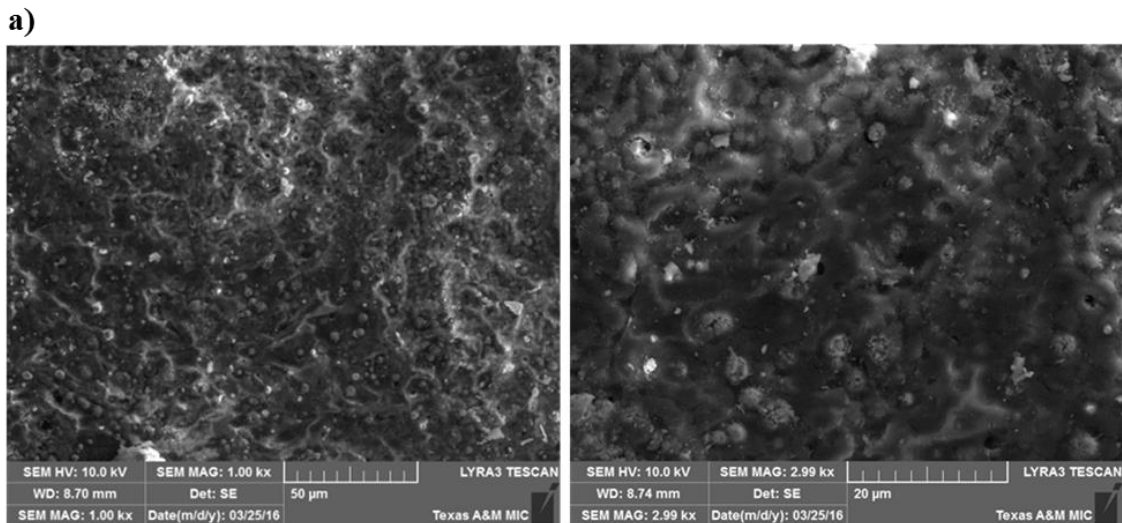


Figure 45. SEM micrographs of CNT-70ZRP after immersion for 150 days in a) blank solution, and b) simulated concrete pore solution with a chloride-hydroxide ratio of 10.

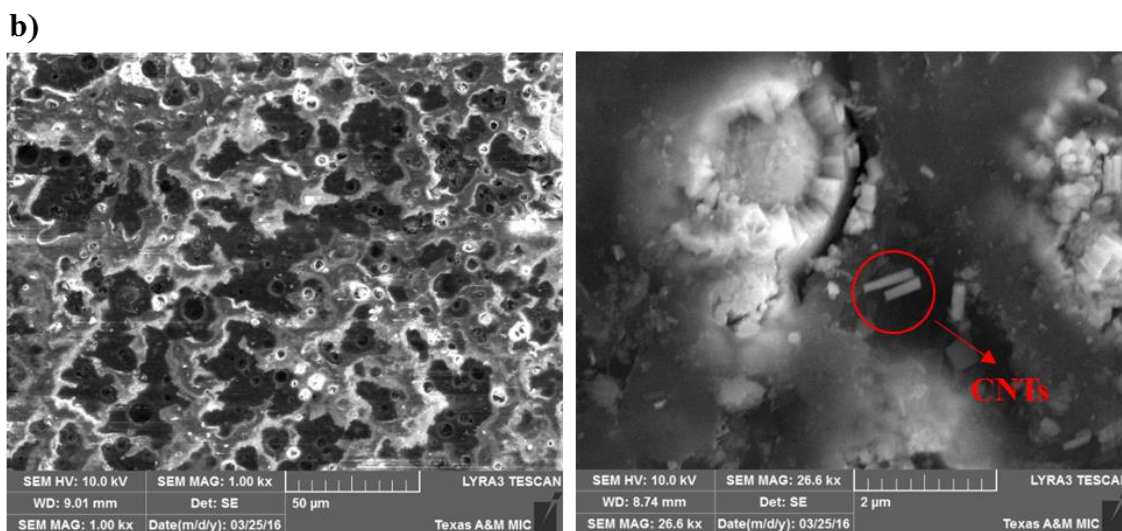


Figure 45. Continued

Figure 46a corresponds to the surface morphology of the CNT-80ZRP sample immersed in the blank solution. As it can be noticed, large amount of zinc corrosion products were covering the majority of the coating surface. This observation confirms that the zinc particles provided efficient galvanic cathodic protection to the carbon steel substrate. On the other hand, Figure 46b corresponding to the CNT-80ZRP sample immersed in the solution with high chloride concentration, showed a lower amount of zinc corrosion products compared to the sample exposed to the blank solution. As it was mentioned in discussion about the surface appearance, this surface morphology might be associated with the re-dissolution of the solid corrosion products by chemical decomposition reactions with chloride ions.

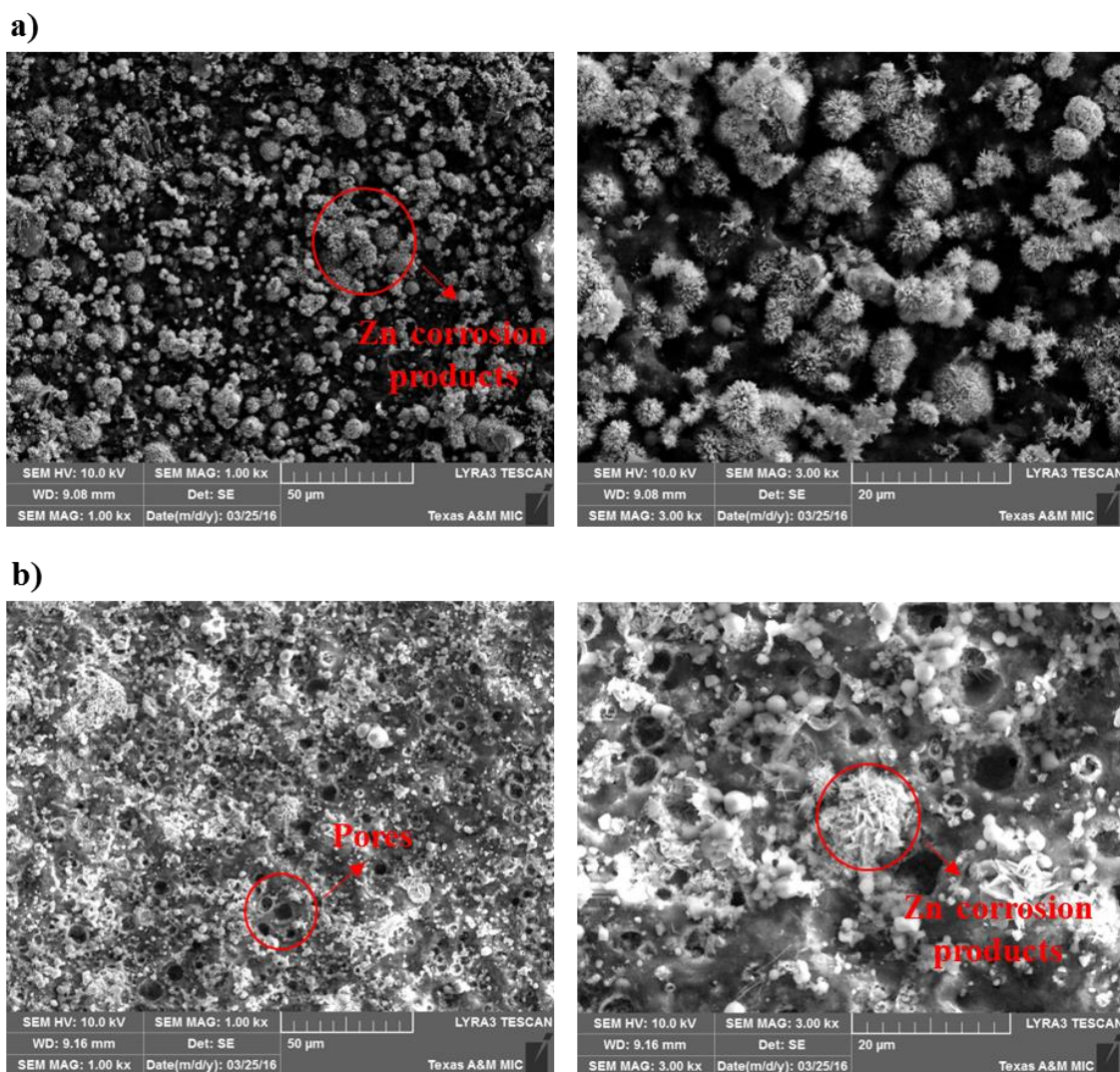


Figure 46. SEM micrographs of CNT-80ZRP after immersion for 150 days in a) blank solution, and b) simulated concrete pore solution with a chloride-hydroxide ratio of 10.

The electrochemical behavior of the CNT-80ZRP sample immersed in the simulated concrete pore solution with a chloride-to-hydroxide ratio of 10 suggests that further dissolution of the zinc particles that did not contribute to the cathodic protection process occurred due to the high chloride concentration diffusing through the epoxy

material. This zinc dissolution process combined with the oxygen reduction reaction occurred on the surface of the zinc particles. To confirm this mechanism, SEM cross-sectional analyses were performed on this sample. Figure 47a shows the cross-section of this coating sample in which the presence of zinc corrosion products on the surface of the zinc particles is clearly observed. A line scan analysis was performed on one of the zinc particles that was covered with zinc corrosion products. Figure 47b shows the EDS spectra for zinc and oxygen along the line scan. From Figure 47b, it can be seen that the dark layer covering the zinc particle contained a lower amount of zinc and higher amount of oxygen in comparison to the composition at the center of the particle, which means that this layer indeed corresponds to zinc corrosion products (mainly oxides, hydroxides, and carbonates) that were formed on the surface of the zinc particles due to dissolution processes on the zinc-electrolyte interface [16, 18, 83, 84].

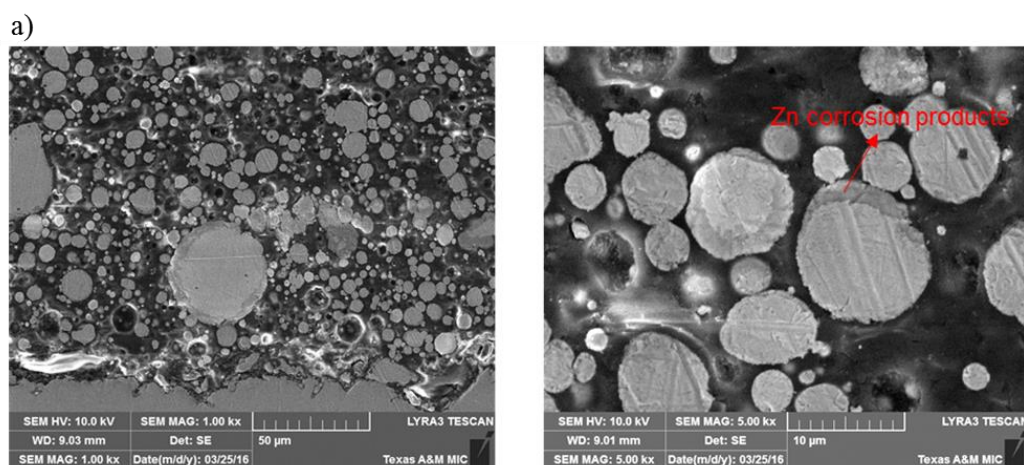


Figure 47. Cross-section analyses of CNT-80ZRP after immersion for 150 days in simulated concrete pore solution with a chloride-to-hydroxide ratio of 10: a) cross-section SEM micrograph b) line scan analyses.

b)

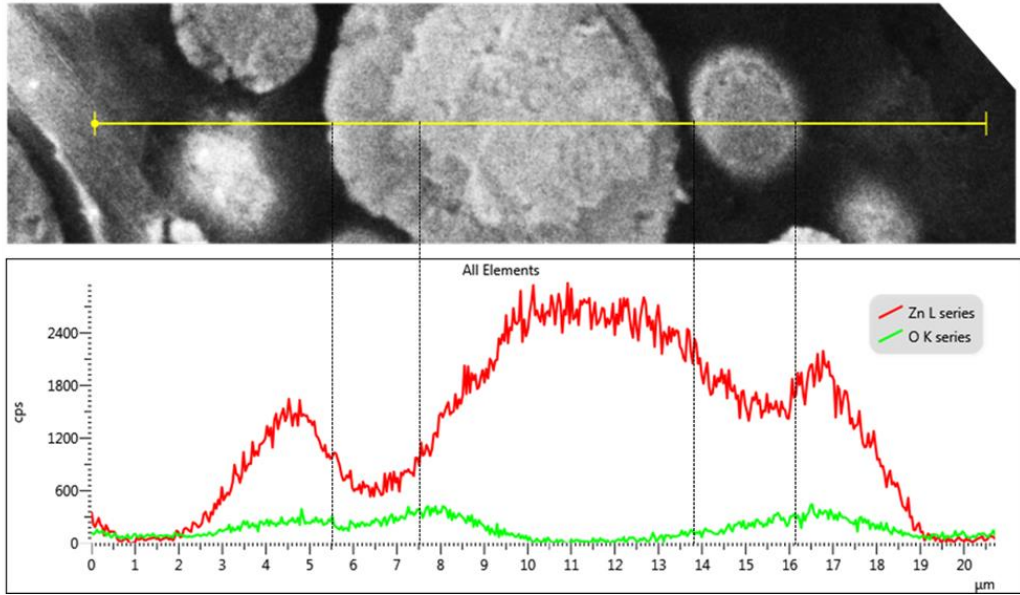


Figure 47. Continued

CHAPTER V

CONCLUSIONS*

The corrosion protection performance of CNT-ZRPs with different zinc contents was investigated at long-term exposure in simulated concrete pore solutions with various chloride-to-hydroxide ratios. Electrochemical measurements, accelerated tests, morphology analyses and surface characterization were performed to investigate the mechanisms of corrosion protection of these coatings. According to these findings, the following conclusions are proposed:

Three different corrosion protection mechanisms were identified: 1) A barrier corrosion protection was provided by CNT-60ZRP, due to the low porosity of the epoxy binder and the likely positive effect of the CNTs who might fill out pores and flaws within the organic coating. 2) A mixed corrosion protection mechanism was identified for CNT-70ZRP, where short-term cathodic protection, barrier protection, and faradaic processes of the zinc particles were identified. 3) A predominant cathodic protection mechanism was observed for CNT-80ZRP and CNT-90ZRP due to the higher amount of zinc particles and presence of CNTs that enhances the electron transfer between zinc particles and the carbon steel surface. The effective cathodic protection provided by

* Part of this chapter is reprinted from Corrosion Science, vol. 109, Y Cubides, H. Castaneda, Corrosion protection mechanisms of carbon nanotube and zinc-rich epoxy primers on carbon steel in simulated concrete pore solutions in the presence of chloride ions, 145-161, Copyright (2016), with permission from Elsevier.

CNT-80ZRP and CNT-90ZRP caused the formation of a protective layer of zinc corrosion products on top of the coating surface. This protective layer was mainly composed of zinc oxide, zinc hydroxide, and hydrozincite.

The corrosion protection performance of a zinc-rich epoxy primer with 70 wt% Zn and without the presence of CNTs did not provide cathodic protection, but there were charge transfer processes involving the carbon steel surface. Therefore, it was concluded that CNTs have a positive effect on the mechanism of corrosion protection of zinc-rich epoxy primers. The CNTs might help in the electronic connection between the zinc particles among themselves and with the carbon steel surface.

The simulated concrete pore solution with a chloride-to-hydroxide ratio of 10 significantly changed the corrosion protection performance of the coating systems. CNT-60ZRP showed, a lower coating resistance due to the degradation of the epoxy matrix by the chloride ions. For CNT-70ZRP, blister formation occurred as a result of the breakdown of the passive layer at the carbon steel substrate and the active dissolution of the metal surface. For CNT-80ZRP, the solid corrosion products formed at the coating surface were dissolved by the high chloride concentration. In addition, zinc particles that did not contribute to the cathodic protection process were further dissolved inside the epoxy matrix.

The three different corrosion protection mechanisms proposed from the electrochemical assessment were verified by visual examination of coating samples exposed to salt spray fog chamber. Additionally, morphology analyses were also in agreement with the electrochemical measurements. From the cross-sectional and surface

images, the author found that the morphology of the CNT-60ZRP did not significant change after exposure to the electrolyte solutions probing its excellent barrier protection. The morphology analyses for CNT-70ZRP showed the presence of zinc corrosion products as a resulted of the cathodic protection process and the self-dissolution process of zinc particles. However, these morphology analyses were unable to confirm the formation of a passive layer at the carbon steel surface. Finally, the morphology images for CNT-80ZRP and CNT-90ZRP samples showed the formation of a layer of zinc corrosion products on the coating surface and the further dissolution of the zinc particles that did not contribute to the sacrificial protection process.

REFERENCES

- [1] W. Morris, M. Vázquez, S.R. De Sánchez, Efficiency of coatings applied on rebars in concrete, *Journal of Materials Science*, 35 (2000) 1885-1890.
- [2] J. Wei, X.X. Fu, J.H. Dong, W. Ke, Corrosion Evolution of Reinforcing Steel in Concrete under Dry/Wet Cyclic Conditions Contaminated with Chloride, *Journal of Materials Science & Technology*, 28 (2012) 905-912.
- [3] C.-Q. Ye, R.-G. Hu, S.-G. Dong, X.-J. Zhang, R.-Q. Hou, R.-G. Du, C.-J. Lin, J.-S. Pan, EIS analysis on chloride-induced corrosion behavior of reinforcement steel in simulated carbonated concrete pore solutions, *Journal of Electroanalytical Chemistry*, 688 (2013) 275-281.
- [4] F. Belaid, G. Arliguie, R. Francois, Corrosion products of galvanized rebars embedded in chloride-contaminated concrete, *Corrosion*, 56 (2000) 960-965.
- [5] S.A. El Haleem, S.A. El Wanees, E.A. El Aal, A. Diab, Environmental factors affecting the corrosion behavior of reinforcing steel II. Role of some anions in the initiation and inhibition of pitting corrosion of steel in Ca (OH) 2 solutions, *corrosion Science*, 52 (2010) 292-302.
- [6] X. Feng, Y. Tang, Y. Zuo, Influence of stress on passive behaviour of steel bars in concrete pore solution, *Corrosion Science*, 53 (2011) 1304-1311.

- [7] M. Moreno, W. Morris, M. Alvarez, G. Duffó, Corrosion of reinforcing steel in simulated concrete pore solutions: effect of carbonation and chloride content, *Corrosion Science*, 46 (2004) 2681-2699.
- [8] X. Shi, N. Xie, K. Fortune, J. Gong, Durability of steel reinforced concrete in chloride environments: An overview, *Construction and Building Materials*, 30 (2012) 125-138.
- [9] S. Ahmad, Reinforcement corrosion in concrete structures, its monitoring and service life prediction—a review, *Cement and Concrete Composites*, 25 (2003) 459-471.
- [10] F. Tang, G. Chen, R.K. Brow, J.S. Volz, M.L. Koenigstein, Corrosion resistance and mechanism of steel rebar coated with three types of enamel, *Corrosion Science*, 59 (2012) 157-168.
- [11] S. Pour-Ali, C. Dehghanian, A. Kosari, Corrosion protection of the reinforcing steels in chloride-laden concrete environment through epoxy/polyaniline–camphorsulfonate nanocomposite coating, *Corrosion Science*, 90 (2015) 239-247.
- [12] R. Selvaraj, M. Selvaraj, S. Iyer, Studies on the evaluation of the performance of organic coatings used for the prevention of corrosion of steel rebars in concrete structures, *Progress in organic coatings*, 64 (2009) 454-459.
- [13] K. Saravanan, S. Sathiyarayanan, S. Muralidharan, S.S. Azim, G. Venkatachari, Performance evaluation of polyaniline pigmented epoxy coating for corrosion protection of steel in concrete environment, *Progress in organic coatings*, 59 (2007) 160-167.

- [14] G. Batis, P. Pantazopoulou, A. Routoulas, Corrosion protection investigation of reinforcement by inorganic coating in the presence of alkanolamine-based inhibitor, *Cement and Concrete Composites*, 25 (2003) 371-377.
- [15] H. Marchebois, M. Keddou, C. Savall, J. Bernard, S. Touzain, Zinc-rich powder coatings characterisation in artificial sea water: EIS analysis of the galvanic action, *Electrochimica Acta*, 49 (2004) 1719-1729.
- [16] K. Schaefer, A. Mischczyk, Improvement of electrochemical action of zinc-rich paints by addition of nanoparticulate zinc, *Corrosion Science*, 66 (2013) 380-391.
- [17] S. Park, M. Shon, Effects of multi-walled carbon nano tubes on corrosion protection of zinc rich epoxy resin coating, *Journal of Industrial and Engineering Chemistry*, 21 (2015) 1258-1264.
- [18] A. Gergely, É. Pfeifer, I. Bertóti, T. Török, E. Kálmán, Corrosion protection of cold-rolled steel by zinc-rich epoxy paint coatings loaded with nano-size alumina supported polypyrrole, *Corrosion Science*, 53 (2011) 3486-3499.
- [19] A. Gergely, I. Bertóti, T. Török, É. Pfeifer, E. Kálmán, Corrosion protection with zinc-rich epoxy paint coatings embedded with various amounts of highly dispersed polypyrrole-deposited alumina monohydrate particles, *Progress in Organic Coatings*, 76 (2013) 17-32.
- [20] A. Gergely, Z. Pászti, J. Mihály, E. Drotár, T. Török, Galvanic function of zinc-rich coatings facilitated by percolating structure of the carbon nanotubes. Part II: Protection properties and mechanism of the hybrid coatings, *Progress in Organic Coatings*, 77 (2014) 412-424.

- [21] P. Hammer, F. dos Santos, B. Cerrutti, S. Pulcinelli, C. Santilli, Carbon nanotube-reinforced siloxane-PMMA hybrid coatings with high corrosion resistance, *Progress in Organic Coatings*, 76 (2013) 601-608.
- [22] P.P. Deshpande, S.S. Vathare, S.T. Vagge, E. Tomšík, J. Stejskal, Conducting polyaniline/multi-wall carbon nanotubes composite paints on low carbon steel for corrosion protection: electrochemical investigations, *Chemical Papers*, 67 (2013) 1072-1078.
- [23] H. Jeon, J. Park, M. Shon, Corrosion protection by epoxy coating containing multi-walled carbon nanotubes, *Journal of Industrial and Engineering Chemistry*, 19 (2013) 849-853.
- [24] X. Chen, C. Chen, H. Xiao, F. Cheng, G. Zhang, G. Yi, Corrosion behavior of carbon nanotubes–Ni composite coating, *Surface and Coatings Technology*, 191 (2005) 351-356.
- [25] L. Yang, F. Liu, E. Han, Effects of P/B on the properties of anticorrosive coatings with different particle size, *Progress in Organic Coatings*, 53 (2005) 91-98.
- [26] M.C. Turhan, Q. Li, H. Jha, R.F. Singer, S. Virtanen, Corrosion behaviour of multiwall carbon nanotube/magnesium composites in 3.5% NaCl, *Electrochimica Acta*, 56 (2011) 7141-7148.
- [27] L. Freire, X.R. Nóvoa, M.F. Montemor, M.J. Carmezim, Study of passive films formed on mild steel in alkaline media by the application of anodic potentials, *Materials Chemistry and Physics*, 114 (2009) 962-972.

- [28] M.i. Nagayama, M. Cohen, The anodic oxidation of iron in a neutral solution I. The nature and composition of the passive film, *Journal of the Electrochemical Society*, 109 (1962) 781-790.
- [29] S.A. El Haleem, E.A. El Aal, S.A. El Wanees, A. Diab, Environmental factors affecting the corrosion behaviour of reinforcing steel: I. The early stage of passive film formation in Ca (OH) 2 solutions, *Corrosion Science*, 52 (2010) 3875-3882.
- [30] L. Bertolini, B. Elsener, P. Pedefferri, E. Redaelli, R.B. Polder, *Corrosion of steel in concrete: prevention, diagnosis, repair*, John Wiley & Sons, 2013.
- [31] M. Sánchez-Moreno, H. Takenouti, J.J. García-Jareño, F. Vicente, C. Alonso, A theoretical approach of impedance spectroscopy during the passivation of steel in alkaline media, *Electrochimica Acta*, 54 (2009) 7222-7226.
- [32] M. Montemor, A. Simoes, M. Ferreira, Chloride-induced corrosion on reinforcing steel: from the fundamentals to the monitoring techniques, *Cement and Concrete Composites*, 25 (2003) 491-502.
- [33] K. Tuutti, *Corrosion of steel in concrete*, Swedish Cement and Concrete Research Institute, Report Fo, 4 (1982) 82.
- [34] H. Böhni, *Corrosion in reinforced concrete structures*. edited by Hans Böhni, Cambridge, England : Woodhead ; Boca Raton : CRC Press, 2005., 2005.
- [35] F. Simescu, H. Idrissi, Corrosion behaviour in alkaline medium of zinc phosphate coated steel obtained by cathodic electrochemical treatment, *Corrosion Science*, 51 (2009) 833-840.

- [36] U. Angst, B. Elsener, C.K. Larsen, Ø. Vennesland, Critical chloride content in reinforced concrete — A review, *Cement and Concrete Research*, 39 (2009) 1122-1138.
- [37] L. Li, A. Sagues, Chloride corrosion threshold of reinforcing steel in alkaline solutions-Open-circuit immersion tests, *Corrosion*, 57 (2001) 19-28.
- [38] H. Yu, K.-T.K. Chiang, L. Yang, Threshold chloride level and characteristics of reinforcement corrosion initiation in simulated concrete pore solutions, *Construction and Building Materials*, 26 (2012) 723-729.
- [39] M. Manera, Ø. Vennesland, L. Bertolini, Chloride threshold for rebar corrosion in concrete with addition of silica fume, *Corrosion Science*, 50 (2008) 554-560.
- [40] P.V. Nygaard, M.R. Geiker, A method for measuring the chloride threshold level required to initiate reinforcement corrosion in concrete, *Materials and Structures*, 38 (2005) 489-494.
- [41] A. Neville, Chloride attack of reinforced concrete: an overview, *Materials and Structures*, 28 (1995) 63-70.
- [42] M. El-Reedy, *Steel-reinforced concrete structures: Assessment and repair of corrosion*, CRC press, 2007.
- [43] S.A. Austin, R. Lyons, M. Ing, Electrochemical behavior of steel-reinforced concrete during accelerated corrosion testing, *Corrosion*, 60 (2004) 203-212.
- [44] L. Freire, M.J. Carmezim, M.G.S. Ferreira, M.F. Montemor, The electrochemical behaviour of stainless steel AISI 304 in alkaline solutions with different pH in the presence of chlorides, *Electrochimica Acta*, 56 (2011) 5280-5289.

- [45] M. Sánchez, J. Gregori, C. Alonso, J.J. García-Jareño, H. Takenouti, F. Vicente, Electrochemical impedance spectroscopy for studying passive layers on steel rebars immersed in alkaline solutions simulating concrete pores, *Electrochimica Acta*, 52 (2007) 7634-7641.
- [46] E. Volpi, A. Olietti, M. Stefanoni, S.P. Trasatti, Electrochemical characterization of mild steel in alkaline solutions simulating concrete environment, *Journal of Electroanalytical Chemistry*, 736 (2015) 38-46.
- [47] X.G. Zhang, *Corrosion and electrochemistry of zinc*, Springer Science & Business Media, 2013.
- [48] S. Arman, B. Ramezanzadeh, S. Farghadani, M. Mehdipour, A. Rajabi, Application of the electrochemical noise to investigate the corrosion resistance of an epoxy zinc-rich coating loaded with lamellar aluminum and micaceous iron oxide particles, *Corrosion Science*, 77 (2013) 118-127.
- [49] A. Meroufel, S. Touzain, EIS characterisation of new zinc-rich powder coatings, *Progress in Organic Coatings*, 59 (2007) 197-205.
- [50] A. Kalendová, D. Veselý, M. Kohl, J. Stejskal, Anticorrosion efficiency of zinc-filled epoxy coatings containing conducting polymers and pigments, *Progress in Organic Coatings*, 78 (2015) 1-20.
- [51] E. Akbarinezhad, M. Ebrahimi, F. Sharif, A. Ghanbarzadeh, Evaluating protection performance of zinc rich epoxy paints modified with polyaniline and polyaniline-clay nanocomposite, *Progress in Organic Coatings*, 77 (2014) 1299-1308.

- [52] H. Marchebois, S. Joiret, C. Savall, J. Bernard, S. Touzain, Characterization of zinc-rich powder coatings by EIS and Raman spectroscopy, *Surface and Coatings Technology*, 157 (2002) 151-161.
- [53] J. Vilche, E. Bucharsky, C. Giudice, Application of EIS and SEM to evaluate the influence of pigment shape and content in ZRP formulations on the corrosion prevention of naval steel, *Corrosion Science*, 44 (2002) 1287-1309.
- [54] B. Ramezanzadeh, S. Arman, M. Mehdipour, Anticorrosion properties of an epoxy zinc-rich composite coating reinforced with zinc, aluminum, and iron oxide pigments, *J Coat Technol Res*, 11 (2014) 727-737.
- [55] A. Meroufel, C. Deslouis, S. Touzain, Electrochemical and anticorrosion performances of zinc-rich and polyaniline powder coatings, *Electrochimica Acta*, 53 (2008) 2331-2338.
- [56] N. Arianpouya, M. Shishesaz, M. Arianpouya, M. Nematollahi, Evaluation of synergistic effect of nanozinc/nanoclay additives on the corrosion performance of zinc-rich polyurethane nanocomposite coatings using electrochemical properties and salt spray testing, *Surface and Coatings Technology*, 216 (2013) 199-206.
- [57] E. Barsoukov, J.R. Macdonald, *Impedance spectroscopy: theory, experiment, and applications*, John Wiley & Sons, 2005.
- [58] V.F. Lvovich, *Impedance spectroscopy: applications to electrochemical and dielectric phenomena*, John Wiley & Sons, 2012.

- [59] X.-Z.R. Yuan, C. Song, H. Wang, J. Zhang, *Electrochemical impedance spectroscopy in PEM fuel cells: fundamentals and applications*, Springer Science & Business Media, 2009.
- [60] A. Amirudin, D. Thieny, *Application of electrochemical impedance spectroscopy to study the degradation of polymer-coated metals*, *Progress in organic coatings*, 26 (1995) 1-28.
- [61] D.D. Macdonald, *Review of mechanistic analysis by electrochemical impedance spectroscopy*, *Electrochimica Acta*, 35 (1990) 1509-1525.
- [62] H. Song, D.D. Macdonald, *Photoelectrochemical Impedance Spectroscopy I. Validation of the Transfer Function by Kramers-Kronig Transformation*, *Journal of The Electrochemical Society*, 138 (1991) 1408-1410.
- [63] M. Orazem, J. Esteban, O. Moghissi, *Practical applications of the Kramers-Kronig relations*, *Corrosion*, 47 (1991) 248-259.
- [64] M.E. Orazem, B. Tribollet, *Electrochemical impedance spectroscopy*, John Wiley & Sons, 2011.
- [65] B. Hirschorn, M.E. Orazem, B. Tribollet, V. Vivier, I. Frateur, M. Musiani, *Determination of effective capacitance and film thickness from constant-phase-element parameters*, *Electrochimica Acta*, 55 (2010) 6218-6227.
- [66] F. Mansfeld, *Use of electrochemical impedance spectroscopy for the study of corrosion protection by polymer coatings*, *Journal of Applied Electrochemistry*, 25 (1995) 187-202.

- [67] G. Walter, A review of impedance plot methods used for corrosion performance analysis of painted metals, *Corrosion Science*, 26 (1986) 681-703.
- [68] E. McCafferty, *Introduction to corrosion science*, Springer Science & Business Media, 2010.
- [69] A.J. Bard, L.R. Faulkner, J. Leddy, C.G. Zoski, *Electrochemical methods: fundamentals and applications*, Wiley New York, 1980.
- [70] D. Hausmann, Steel corrosion in concrete--How does it occur?, *Materials protection*, (1967).
- [71] C. Andrade, C. Page, Pore solution chemistry and corrosion in hydrated cement systems containing chloride salts: a study of cation specific effects, *British Corrosion Journal*, 21 (1986) 49-54.
- [72] M. Hurley, J. Scully, Threshold chloride concentrations of selected corrosion-resistant rebar materials compared to carbon steel, *Corrosion*, 62 (2006) 892-904.
- [73] F. Zhang, J. Pan, C. Lin, Localized corrosion behaviour of reinforcement steel in simulated concrete pore solution, *Corrosion Science*, 51 (2009) 2130-2138.
- [74] J. Singh, D. Singh, The nature of rusts and corrosion characteristics of low alloy and plain carbon steels in three kinds of concrete pore solution with salinity and different pH, *Corrosion Science*, 56 (2012) 129-142.
- [75] K. Andersson, B. Allard, M. Bengtsson, B. Magnusson, Chemical composition of cement pore solutions, *Cement and Concrete Research*, 19 (1989) 327-332.

- [76] P. Ghods, O.B. Isgor, F. Bensebaa, D. Kingston, Angle-resolved XPS study of carbon steel passivity and chloride-induced depassivation in simulated concrete pore solution, *Corrosion Science*, 58 (2012) 159-167.
- [77] A. Moragues, A. Macias, C. Andrade, Equilibria of the chemical composition of the concrete pore solution. Part I: Comparative study of synthetic and extracted solutions, *Cement and Concrete Research*, 17 (1987) 173-182.
- [78] J. Williamson, O.B. Isgor, The effect of simulated concrete pore solution composition and chlorides on the electronic properties of passive films on carbon steel rebar, *Corrosion Science*, (2016).
- [79] M. Mouanga, M. Puiggali, B. Tribollet, V. Vivier, N. Pébère, O. Devos, Galvanic corrosion between zinc and carbon steel investigated by local electrochemical impedance spectroscopy, *Electrochimica Acta*, 88 (2013) 6-14.
- [80] J.-B. Jorcin, H. Krawiec, N. Pébère, V. Vignal, Comparison of local electrochemical impedance measurements derived from bi-electrode and microcapillary techniques, *Electrochimica Acta*, 54 (2009) 5775-5781.
- [81] K. Davies, J. Broomfield, Cathodic protection mechanism and a review of criteria, *Cathodic Protection of Steel in Concrete and Masonry*, 41 (2013).
- [82] G.K. Glass, A.M. Hassanein, N.R. Buenfeld, CP criteria for reinforced concrete in marine exposure zones, *Journal of materials in civil engineering*, 12 (2000) 164-171.
- [83] C.M. Abreu, M. Izquierdo, M. Keddou, X.R. Nóvoa, H. Takenouti, Electrochemical behaviour of zinc-rich epoxy paints in 3% NaCl solution, *Electrochimica Acta*, 41 (1996) 2405-2415.

- [84] C. Abreu, M. Izquierdo, P. Merino, X. Novoa, C. Perez, A new approach to the determination of the cathodic protection period in zinc-rich paints, *Corrosion*, 55 (1999) 1173-1181.
- [85] R. Armas, C. Gervasi, A. Di Sarli, S. Real, J. Vilche, Zinc-rich paints on steels in artificial seawater by electrochemical impedance spectroscopy, *Corrosion*, 48 (1992) 379-383.
- [86] S. Feliú, R. Barajas, J.M. Bastidas, M. Morcillo, Study of protection mechanisms of zinc-rich paints by electrochemical impedance spectroscopy, *ASTM SPECIAL TECHNICAL PUBLICATION*, 1188 (1993) 438-438.
- [87] F. Recio, M. Alonso, L. Gaillet, M. Sánchez, Hydrogen embrittlement risk of high strength galvanized steel in contact with alkaline media, *Corrosion Science*, 53 (2011) 2853-2860.
- [88] S. Shen, Y. Zuo, The improved performance of Mg-rich epoxy primer on AZ91D magnesium alloy by addition of ZnO, *Corrosion Science*, 87 (2014) 167-178.
- [89] S. Shreepathi, P. Bajaj, B. Mallik, Electrochemical impedance spectroscopy investigations of epoxy zinc rich coatings: Role of Zn content on corrosion protection mechanism, *Electrochimica Acta*, 55 (2010) 5129-5134.
- [90] H.A. Al-Turaif, Surface morphology and chemistry of epoxy-based coatings after exposure to ultraviolet radiation, *Progress in Organic Coatings*, 76 (2013) 677-681.
- [91] G. Xiao, M. Delamar, M. Shanahan, Irreversible interactions between water and DGEBA/DDA epoxy resin during hygrothermal aging, *Journal of Applied Polymer Science*, 65 (1997) 449-458.

- [92] H.J. Shin, K.K. Kim, A. Benayad, S.M. Yoon, H.K. Park, I.S. Jung, M.H. Jin, H.K. Jeong, J.M. Kim, J.Y. Choi, Efficient reduction of graphite oxide by sodium borohydride and its effect on electrical conductance, *Advanced Functional Materials*, 19 (2009) 1987-1992.
- [93] K. Li, K. Wang, M.-s. Zhan, W. Xu, The change of thermal–mechanical properties and chemical structure of ambient cured DGEBA/TEPA under accelerated thermo-oxidative aging, *Polymer Degradation and Stability*, 98 (2013) 2340-2346.
- [94] J.-H. Zhou, Z.-J. Sui, J. Zhu, P. Li, D. Chen, Y.-C. Dai, W.-K. Yuan, Characterization of surface oxygen complexes on carbon nanofibers by TPD, XPS and FT-IR, *Carbon*, 45 (2007) 785-796.
- [95] R. Rajagopalan, J.O. Iroh, Characterization of polyaniline–polypyrrole composite coatings on low carbon steel: a XPS and infrared spectroscopy study, *Applied Surface Science*, 218 (2003) 58-69.
- [96] M. Liu, P. Wu, Y. Ding, G. Chen, S. Li, Two-dimensional (2D) ATR-FTIR spectroscopic study on water diffusion in cured epoxy resins, *Macromolecules*, 35 (2002) 5500-5507.
- [97] J. Mijovic, H. Zhang, Local dynamics and molecular origin of polymer network-water interactions as studied by broadband dielectric relaxation spectroscopy, FTIR, and molecular simulations, *Macromolecules*, 36 (2003) 1279-1288.
- [98] E. Diler, S. Rioual, B. Lescop, D. Thierry, B. Rouvellou, Chemistry of corrosion products of Zn and MgZn pure phases under atmospheric conditions, *Corrosion science*, 65 (2012) 178-186.

- [99] J. Duchoslav, R. Steinberger, M. Arndt, T. Keppert, G. Luckeneder, K. Stellnberger, J. Hagler, G. Angeli, C. Riener, D. Stifter, Evolution of the surface chemistry of hot dip galvanized Zn–Mg–Al and Zn coatings on steel during short term exposure to sodium chloride containing environments, *Corrosion Science*, 91 (2015) 311-320.
- [100] R. Ghosh, D.D.N. Singh, Kinetics, mechanism and characterisation of passive film formed on hot dip galvanized coating exposed in simulated concrete pore solution, *Surface and Coatings Technology*, 201 (2007) 7346-7359.
- [101] F. Deflorian, V. Miskovic-Stankovic, P. Bonora, L. Fedrizzi, Degradation of epoxy coatings on phosphatized zinc-electroplated steel, *Corrosion*, 50 (1994) 438-446.
- [102] M. Deyab, Effect of carbon nano-tubes on the corrosion resistance of alkyd coating immersed in sodium chloride solution, *Progress in Organic Coatings*, 85 (2015) 146-150.
- [103] B.M. Praveen, T.V. Venkatesha, Y. Arthoba Naik, K. Prashantha, Corrosion studies of carbon nanotubes–Zn composite coating, *Surface and Coatings Technology*, 201 (2007) 5836-5842.
- [104] G.W. Walter, The application of impedance methods to study the effects of water uptake and chloride ion concentration on the degradation of paint films—I. Attached films, *Corrosion Science*, 32 (1991) 1059-1084.
- [105] G.W. Walter, The application of impedance methods to study the effects of water uptake and chloride ion concentration on the degradation of paint films—II. Free films and attached/free film comparisons, *Corrosion Science*, 32 (1991) 1085-1103.

- [106] M.G. Koul, A. Sheetz, P. Ault, J. Repp, A. Whitfield, Effect of Zn-Rich Coatings on the Corrosion and Cracking Resistance of High-Strength Armor Steel, *Corrosion*, 70 (2013) 337-350.
- [107] A. Marques, A. Simões, EIS and SVET assessment of corrosion resistance of thin Zn-55% Al-rich primers: Effect of immersion and of controlled deformation, *Electrochimica Acta*, 148 (2014) 153-163.
- [108] D. Schmidt, B. Shaw, E. Sikora, W. Shaw, L. Laliberte, Comparison of testing techniques used to analyze the corrosion resistance of sacrificial coating systems, *Corrosion*, 63 (2007) 958-974.

APPENDIX A

SUPPLEMENTAL MATERIAL FOR CHAPTER III

Electrochemical behavior of CNT-90ZRP

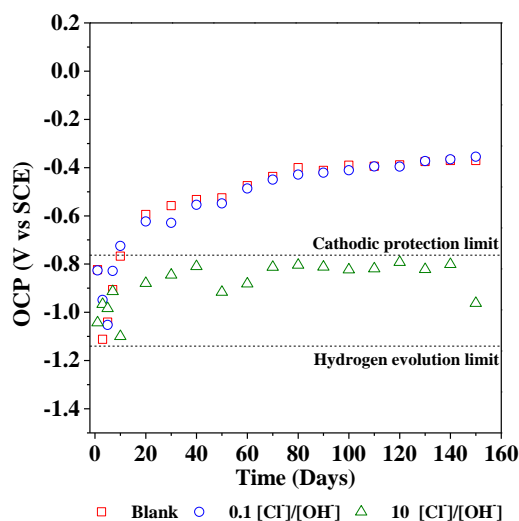


Figure 48. OCP measurements of CNT-90ZRP immersed in simulated concrete pore solution with different chloride-to-hydroxide ratios for 150 days.

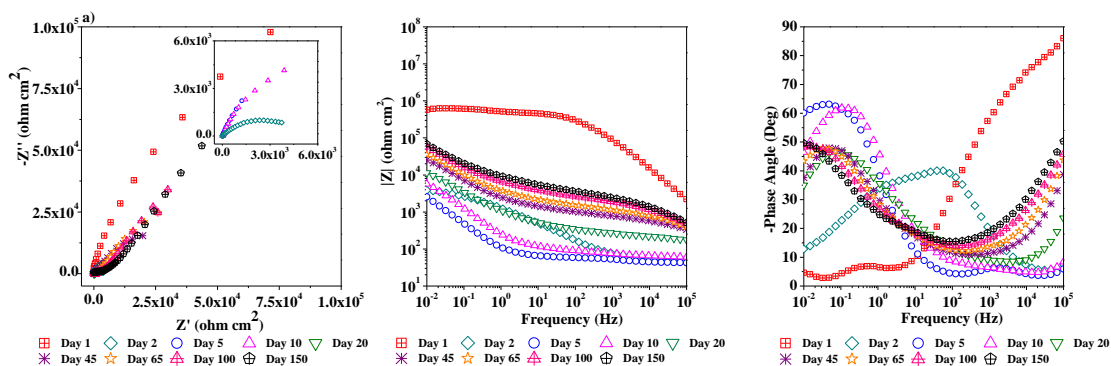


Figure 49. Impedance spectra of CNT-90ZRP immersed in simulated concrete pore solutions with different chloride-to-hydroxide ratios for 150 days: a) blank solution b) 0.1 [Cl⁻]/[OH⁻], and c) 10 [Cl⁻]/[OH⁻].

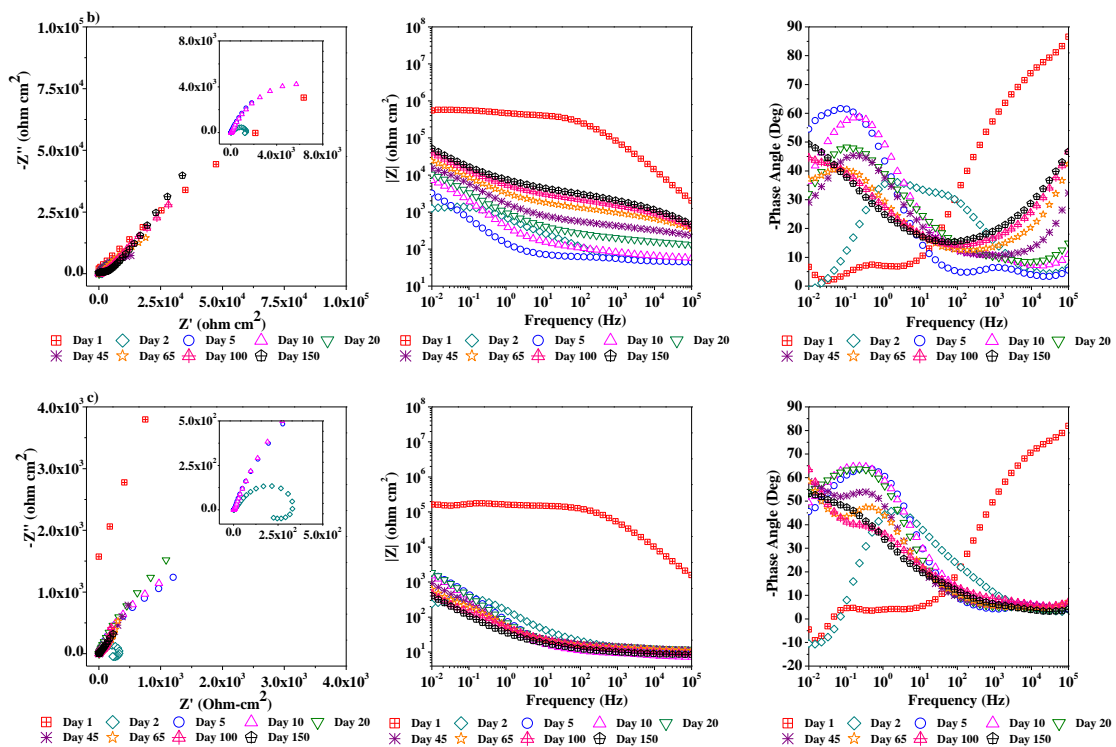


Figure 49. Continued